

**Numerical Simulation of Heat Transfer and Fluid Flow in  
Additively Manufactured Plate-Fin Heat Exchangers  
with Wavy Fins**

Von der Fakultät für Maschinenbau  
der Gottfried Wilhelm Leibniz Universität Hannover

zur Erlangung des akademischen Grades eines  
Doktor- Ingenieur (abgekürzt: Dr.-Ing.)

genehmigte Dissertation

von Frau

M. Sc. -Ing. Huda Jasim Mohammed Al-Azzawi

2021

Supervisors: Prof. Dr.-Ing. Stephan Kabelac

Prof. Dr.-Ing. Ms Birgit Glasmacher

Date of exam: June 23<sup>rd</sup>, 2021

Dedicated in Loving Memory  
to My Parents, who taught me to believe in myself.

## ACKNOWLEDGEMENTS

---

During my work on the present thesis, I have been fortunate to interact with many people who helped me to complete this work.

I would like to take this opportunity to express my deepest gratitude to my supervisor Prof. Stephan Kabelac, who gave me the opportunity to finish my study in the Institute of Thermodynamic. His creative ideas and encouragement have profoundly contributed to the completion of this thesis. I am incredibly grateful for his steadfast guidance and his eternal patience in discussing various aspects of my work at the Institute.

I am so very grateful for my family; for all their encouragement and support and for their unconditional affection throughout this long journey, which made my stay and studies in Germany more enjoyable.

Special thanks to Nadia Jasim Mohammed Al-Azzawi, her son Ahmad and Ibrahim, and her daughter Rania, Nadia, and Rancy Salam Al-Jumaili. The invaluable moral support I received from this group kept me happy and smiling.

I also extend my sincerest thanks to my Iraq-based colleague Ahmed Abbas Zaalán Altamimi, for supporting me during this time.

**Hannover in June 23<sup>rd</sup>, 2021**

## ABSTRACT

---

The heat transfer is considered to be one of the most important industrial processes as seen in all these opulent applications in energy conversion and in chemical industry. This thesis presents a CFD numerical simulation of heat transfer and fluid flow in plate-fin heat exchangers (PFHE) design to predict the fluid friction and heat transfer characteristics, and we investigate in detail the effect of longitudinal heat conduction effects using the open source CFD code OpenFOAM. Numerical tests for both the hot and cold fluid in the laminar flow regime ranging between  $50 \leq Re \leq 2000$  of the Reynolds number with different cases of geometrical parameters of the fin were performed (1, 1.1 and 1.2 mm in fin spacing; 0, 1.5, 2 and 2.5 mm in fin amplitude; 65, 100, 130 and 195 mm in fin length). The results for each case of the wavy fin with variation in fin amplitude are presented by means of a Colburn  $j$  factor and the Fanning friction factor  $f$ . The results reveal that the longitudinal heat conduction in the fins and the plates itself has a significant influence on the heat transfer performance in all cases. The CFD results are compared with available correlations in the literatures for Shah and London [1] and Chennu [2]. We also find that the available correlations for wavy fins are not suitable for the general case of the variable geometrical parameters to predict the heat transfer and pressure drop, particularly when the amplitude of the fins is small. Therefore, we have developed new correlations which extend the application range also for small fin amplitudes. Three models are presented for evaluation the heat transfer coefficient within a given range. A good agreement between the new correlations and analytical and numerical models are shown in this thesis. The CFD data of the single pair of wavy channels in the plate-fin heat exchanger were validated with the experimental data. The heat transfer performance data for both the experimental and CFD numerical results were obtained at the inlet gas temperature, ranging (1023-840 K) for hot gas, and for cold gas ranging between 523-476 K. The experimental and numerical results are validated by the available literatures from Chennau [11], Junqi et al. [13], and new correlations which illustrate a sufficiently good agreement with our results.

Keywords: Plate-Fin Heat Exchanger, Wavy fin, Fin amplitude

## KURZFASSUNG

---

Die Wärmeübertragung gilt als eines der wichtigsten industriellen Verfahren, wie sie bei den vielfältigen Anwendungen in der Energiewandlung und in der chemischen Industrie zu beobachten sind. In dieser Arbeit wird eine numerische CFD-Simulation der Wärmeübertragung und der Strömung in Plattenrippen-Wärmeübertragern (PFHE) vorgestellt, um die Fluidreibung, die Flüssigkeitsreibung und der Wärmeübertragung vorherzusagen. Wir untersuchen detailliert die Auswirkungen von Wärmeleitungseffekten in Längsrichtung mithilfe der Open-Source-CFD Code OpenFOAM. Es wurden numerische Tests sowohl für das heiße als auch für das kalte Fluid im laminaren Strömungsgebiet im Bereich zwischen  $50 \leq Re \leq 2000$  der Reynolds-Zahl mit verschiedenen Fällen geometrischer Parameter der Rippe durchgeführt (1, 1,1 und 1,2 mm Rippenabstand; 0, 1,5, 2 und 2,5 mm Rippenamplitude; 65, 100, 130 und 195 mm Rippenlänge). Die Ergebnisse für jeden Fall der Wellenrippe mit Variation der Lamellenamplitude werden mittels eines Colburn j-Faktors und des Fanning-Reibungsfaktors  $f$  dargestellt. Die Ergebnisse zeigen, dass die Wärmeleitung in Längsrichtung in den Rippen und den Platten selbst in allen Fällen einen signifikanten Einfluss auf die Wärmeübertragungsleistung hat. Die CFD-Ergebnisse werden mit den verfügbaren Korrelationen in der Literatur von Shah und London [1] und Chennu [2] verglichen. Wir stellen auch fest, dass die verfügbaren Korrelationen für Wellenrippen nicht für den allgemeinen Fall der variablen geometrischen Parameter geeignet sind, um die Wärmeübertragung und den Druckabfall vorherzusagen, insbesondere wenn die Amplitude der Lamellen klein ist. Daher haben wir neue Korrelationen entwickelt, die den Anwendungsbereich auch für kleine Lamellenamplituden erweitern. Zur Bewertung des Wärmeübergangskoeffizienten innerhalb eines bestimmten Bereichs werden drei Modelle vorgestellt. Eine gute Übereinstimmung zwischen den neuen Korrelationen und den analytischen und numerischen Modellen wird in dieser Arbeit gezeigt.

Die CFD-Daten des einzelnen Paares von Wellenkanälen im Plattenrippen-Wärmeübertrager wurden mit den experimentellen Daten validiert. Die Wärmeübertragungsleistungsdaten sowohl für die experimentellen als auch für die numerischen CFD-Ergebnisse wurden bei der Gastemperatur am Eingang im Bereich (1023-840 K) für heißes Gas und für kaltes Gas im Bereich zwischen (523-476 K) erhalten. Die experimentellen und numerischen Ergebnisse werden durch die verfügbare Literatur von Chennau [11], Junqi et al. [13] sowie neue Korrelationen verglichen, die eine hinreichend gute Übereinstimmung mit unseren Ergebnissen zeigen.

# CONTENTS

---

Acknowledgements	iii
Abstract	iv
Contents	vi
List of Figures	x
List of Tables	xiii
Nomenclature	xiv

<b>1.</b>	<b>Introduction-Motivation and Scope</b>	<b>1</b>
1.1.	Compact Heat Exchanger (CHE)	3
1.1.1.	Plate-Fin Heat Exchanger	3
1.1.2.	Heat Transfer Surfaces	6
1.1.3.	Applications	6
1.1.4.	Challenges of PFHE in Industrial Application	7
1.2.	Flow arrangement	8
1.2.1.	Cross-Flow	9
1.2.2.	Counter-Flow	10
1.2.3.	Cross-Counter Flow	10
1.3.	Fin Features	11
1.3.1.	Heat Transfer Surfaces Enhancement	11
1.4.	Objectives	12
1.4.1.	Outline of The Thesis	14
<b>2.</b>	<b>OPENFOAM Software</b>	<b>16</b>
2.1.	ParaView	17
2.1.1.	Mesh Generation	17
2.2.	Simulation Controls	19
2.2.1.	Boundaries	20
2.2.2.	Initial Conditions Setup in OPENFOAM	21
2.2.3.	Thermophysical Properties	21
2.2.4.	Control Time Setup	22

2.3.	Types of Turbulence Models	23
2.3.1.	The Physical Modeling	24
2.3.2.	Mathematical Language in OPENFOAM	24
2.4.	Radiation Heat Transfer	25
2.4.1.	Radiation Heat Transfer Solver	26
2.4.2.	Radiation Models	26
2.4.2.1.	No Radiation Model	26
2.4.2.2.	Finite Volume Discrete Ordinates Model	27
2.4.2.3.	P1 Model	27
2.4.2.4.	View Factor Model	27
<b>3.</b>	<b>Literatures Review</b>	<b>30</b>
3.1.	Plate-Fin Heat Exchanger	30
3.2.	PFHE Related Studies	31
3.2.1.	Proposed Correlations Studies	31
3.2.2.	Numerical and Analytical Studies	39
3.2.3.	OPENFOAM Studies	40
3.2.4.	Experimental studies	41
3.3.	Hydraulic Diameter	42
<b>4.</b>	<b>Analytical Modeling Analysis</b>	<b>45</b>
4.1.	Data Reduction	45
4.1.1.	Heat Transfer Performance	48
4.1.2.	Stanton Number and Colburn Factor ( $j$ )	48
4.1.3.	Fanning Friction Factor ( $f$ )	48
4.2.	CFD Simulation Methodology	49
4.2.1.	Setup of Fin Test in OPENFOAM	50
4.3.	Numerical Simulation Analysis	54
4.3.1.	Developing Flow and Fully Developed Regions	54
4.3.2.	Grid Sensitivity	58
4.4.	Models Formulation Approach	60
4.4.1.	Model (1)	61
4.4.2.	Model (2)	63

4.4.2.1.	Energy Balance (Hot Gas)	65
4.4.2.2.	Energy Balance (Cold Gas)	65
4.4.2.3.	Energy Balance Metallic (Plate and Fin)	66
4.4.2.4.	Boundary Conditions	66
4.4.2.5.	Analytical Model Approach	67
4.4.3.	Model (3)	72
4.4.3.1.	Cell Coefficients Calculations	75
4.5.	Results	77
4.5.1.	Thermal Entrance Length	77
4.5.2.	Longitudinal Heat Conduction Effect	82
4.5.3.	Geometrical Parameters Effect	84
4.5.4.	Fin Analysis	88
4.5.5.	Models Validation	94
4.5.6.	Proposed new Correlations	98
<b>5.</b>	<b>Heat Exchanger Design Procedures</b>	<b>104</b>
5.1.	PFHE Geometrical Parameters	104
5.2.	PFHE Design Procedure	105
5.2.1.	Hydraulic Diameter Parameter	105
5.2.2.	Heat Transfer Coefficient	106
5.3.	Geometrical Characteristics of Wavy Fin	107
5.4.	Determination of Heat Transfer	108
5.4.1.	Hot Gas	109
5.4.2.	Cold Gas	110
5.5.	Fin Efficiency	112
5.5.1.	Outlet Temperature and Pressure Estimation	113
<b>6.</b>	<b>Experimental Data Analysis</b>	<b>116</b>
6.1.	Description the Equipment and Instruments	118
6.1.1.	Plate-Fin Heat Exchanger	118
6.1.2.	Compressed Air	119
6.1.3.	Heating Unit	120
6.1.4.	Mass-Flow Measuring	120

6.1.5.	U-Tube Manometer	121
6.1.6.	Thermocouples	121
6.2.	Experimental Data	121
6.2.1.	Effectiveness Differences with Mass-Flow Rate	124
6.2.2.	Variation of Pressure Drop with Mass-Flow Rates	126
6.2.3.	Simulation Results Validation with Experimental	129
6.2.4.	Error Estimation in Heat Transfer	132
<b>7.</b>	<b>Conclusion and Outlook for Future Work</b>	<b>135</b>
7.1.	Conclusions & Remarks	135
7.2.	Scope of Future work	136
	References	139
	Appendix	152
	Appendix A: Coriolis Device Calibration	152
	Appendix B: Polynomls correlations at temperature-dependent properties.	154
	Appendix C: OPENFOAM files.	155

## LIST OF FIGURES

---

<b>Chapter 1</b>	<b>Page No.</b>
Figure 1.1: The history of energy consumption [21]. The global primary energy consumption of fossil and other fuel sources	2
Figure 1.2: Basic structure of plate-fin heat exchanger [69].	5
Figure 1.3: Shows the dimensions for the wavy fin type.	8
Figure 1.4: Cross Flow Arrangement.	9
Figure 1.5: Counter Flow Arrangement.	10
Figure 1.6: Cross-Counter Arrangement.	10
Figure 1.7: Common Ducts Geometries.	12
<b>Chapter 2</b>	
Figure 2.1: Shows the OPENFOAM framework, basic steps of a modelling task.	17
Figure 2.2: A single block.	18
Figure 2.3: Mesh grading along a block edge.	19
Figure 2.4: Shows Bloch for fin channel.	20
<b>Chapter 4</b>	
Figure 4.1: Shows the wavy fin at different fin amplitudes.	46
Figure 4.2: Shows the perspective view of the computational domain with geometrical parameter of the single pair wavy channel.	47
Figure 4.3: Wall temperature distribution.	52
Figure 4.4: Temperature distributions for two fluids in a single channel.	52
Figure 4.5: The experimental data from the current literature is written in table 4.4. The comparison aspect ratio is at 0.25, and for our case at 0.1375.	56
Figure 4.6: Shows the mesh close to the wall.	58
Figure 4.7: Shows the comparison of the two mesh generations by their outlet temperature results, which were obtained from numerical simulations for hot and cold fluids, (a) $Re=50$ , (b) $Re=2000$ .	59

Figure 4.8:	The heat transfer performance in terms of Colburn factor $j$ comparison between two mesh generations.	60
Figure 4.9:	The counter flow arrangement. $\Delta T_1 = (t_{h,in} - t_{c,out})$ and $\Delta T_2 = (t_{h,out} - t_{c,in})$ .	63
Figure 4.10:	A differential control volume element represents the heat conduction, and the heat convection analysis in the counter-flow heat exchanger.	65
Figure 4.11:	The schematic of the metal wall in two channels.	66
Figure 4.12:	Cross-section area for plate and fin thickness.	70
Figure 4.13:	The split of the plate thickness.	71
Figure 4.14:	A differential control volume of solid material in 3D.	73
Figure 4.15:	A differential control volume of wall material in 3D.	74
Figure 4.16:	Shows the local Nusselt number distributions along the flow direction of the channel, depending on our cases as written in Table 4.1 and Model (1).	78
Figure 4.17:	Shows the effectiveness with LHC and without LHC	84
Figure 4.18:	Shows the influence of the geometrical parameter on the heat-transfer performance, (a) at varied fin spacing $s_{fs}$ , (b) at varied fin amplitudes $a_f$ , (c) at varied aspect ratio $a_f = s_{fs}/h_{fs}$ , and (d) at varied fin lengths $L$ .	85
Figure 4.19:	Effectiveness Vs fin amplitude.	88
Figure 4.20:	Local heat transfer coefficients in the fin and plate surfaces at different positions, (a b, c, d) for fin amplitude zero (plain fin), and for fin amplitude 1.5 mm (wavy fin), for both fluids.	89
Figure 4.21:	Mean heat transfer coefficient in the half wave period.	91
Figure 4.22:	Local heat transfer coefficient along the flow direction.	92
Figure 4.23:	Heat transfer performance along the flow direction.	93

Figure 4.24:	Comparison between available literature with the developed models (1, 2, 3), Figures (a, and c) are for plain fin at geometrical parameters ( $a_f=0$ , $s_{fs}=1.1$ mm, and $L_f=130$ mm), and Figures (b, and d) are for wavy fin at geometrical parameters ( $a_f=1.5$ mm, $s_{fs}=1.1$ mm, and $L_f=130$ mm).	95
Figure 4.25:	Comparisons between new correlations with the modified models, at geometrical parameter is $a_f=0$ , $s_{fs}=1.1$ mm, and $L_w=130$ mm.	101
Figure 4.26:	Comparison between all cases and models developed.	101
<b>Chapter 5</b>		
Figure 5.1:	The geometrical parameters for one side of the inlet in the PFHE.	108
<b>Chapter 6</b>		
Figure 6.1:	Schematic diagram of the experimental test rig with measurement position.	116
Figure 6.2:	Photograph of the experimental setup.	118
Figure 6.3:	The image of the plate-fin heat exchanger.	118
Figure 6.4:	Screw compressed air system. [BOGE AIR. boge.com].	119
Figure 6.5:	Heater unit used in the Experimental setup.	120
Figure 6.6:	Mass-flow measuring devices.	120
Figure 6.7:	Effectiveness variation with mass-flow rate	125
Figure 6.8:	Variation pressure drop with mass-flow rate	127
Figure 6.9:	The heat transfer comparison between numerical, experimental, new correlation, and available literatures	130
<b>Chapter 7</b>		
Figure 7.1	The shape of (a) continuous wavy fin; (b) staggered wavy fin;(c) discontinuous wavy fin; (d) perforated wavy fin [54].	137

## LIST OF TABLES

---

<b>Chapter 2</b>		<b>Page No.</b>
Table 2.1:	The relaxation factors for our simulation set-up.	19
<b>Chapter 4</b>		
Table 4.1:	Geometrical parameters cases that are adopted in the present thesis.	50
Table 4.2:	Thermodynamic properties of the working fluid and wall materials with fixed geometrical parameters of wavy fin.	51
Table 4.3:	Simulation results for counter flow heat exchanger of fluids, at geometrical parameters case $a_f=0$ , $s_{fs}=1,1$ mm, $l_w=13$ mm	53
Table 4.4:	Data from developing Laminar is used for our analysis results, the data is presented at fin amplitude $a_f=0$ as rectangular duct shape, and at a different aspect ratio by Shah and London 1978[1].	54
Table 4.5:	The data at developing laminar flow for the rectangular duct when fin amplitude is zero [1].	57
<b>Chapter 5</b>		
Table 5.1:	Dimensions of the heat exchanger.	104
Table 5.2:	The basic dimensions of fins.	105
<b>Chapter 6</b>		
Table 6.1:	The heat exchanger design data with flow arrangement.	119
Table 6.2:	Polynomial physical properties.	119
Table 6.3:	Experimentally observed data at different mass-flow rates for hot and cold air at constant inlet temperature. $T_{hot}=1023$ K, $T_{cold}=523$ K.	123
Table 6.4:	Experimentally observed data at different-mass flow rates for hot and cold air at constant inlet temperature. $T_{hot}=840$ K, $T_{cold}=476$ K.	123
Table 6.5:	Heat transfer coefficient results for the inlet temperature for hot gas $T_{hout}=1023$ K, and for cold gas $T_{cold}=523$ K	132
Table 6.6:	Heat transfer coefficient results for the inlet temperature for hot gas $T_{hout}=840$ K, and for cold gas $T_{cold}=476$ K.	133

# NOMENCLATURE

---

## I Symbols

Symbol	Unit	Meaning
$a_f$	m	Wave amplitude
$A$	m <sup>2</sup>	Heat transfer area
$A_c$	m <sup>2</sup>	Free flow area
$A_{c-p}$	m <sup>2</sup>	Cross-section area of plate
$A_{c-f}$	m <sup>2</sup>	Cross-section area of fin
$A_h$	m <sup>2</sup>	Heat transfer area of hot side
$A_c$	m <sup>2</sup>	Heat transfer area of cold side
$A_w$	m <sup>2</sup>	The plate area
$B$	m	Width of the heat exchanger
$c_p$	J/kg.K	Isobaric specific thermal capacity
$D_h$	m	Hydraulic diameter, $4A/P$
$f$	-	Fanning Frictional Factor, dimensionless
$H$	m	Height of heat exchanger
$h_{fs}$	m	Fin spacing in the height
$j$	-	Colburn $j$ Factor, dimensionless
$k$	-	Conduction parameter
$K$	W/m <sup>2</sup> .K	Overall heat transfer coefficient
$L$	m	Fin length flow, fin passage
$L_{eff}$	m	effective inlet/outlet length
$l_w$	m	Wave length
$l_d$	m	Distributor length
$\dot{m}$	kg/s	Mass flow rate
$p_s$	m	Side plate thickness
$G$	kg/m <sup>2</sup> ·s	Mass flux
NTU	-	Number of heat transfer units
N-layer	-	Number of layers
N-channel	-	Number of channels
$\Delta P$	Pa	Pressure drop

---

$\Delta T$	K	Temperature Difference
$\dot{Q}$	W	Rate of heat transfer
$s_{fs}$	m	Fin spacing in width
$\Delta T_{LM}$	K	Logarithmic mean temperature difference
$u$	m/s	Flow velocity
$\eta_f$	-	Fin efficiency, dimensionless
$\eta_0$	-	Overall fin efficiency
$\mu$	sPa	Dynamic viscosity
$\rho$	kg/m <sup>3</sup>	Density
$\alpha$	W/m <sup>2</sup> .K	Heat transfer coefficient
$\lambda$	W/m.K	Thermal conductivity
R	-	Heat capacity flow rate ratio
$\varepsilon$	-	Effectiveness
$\psi$	-	Fin surface enlargement factor
$\delta_{sp}$	m	Side plate thickness
$\delta_{sb}$	m	Side bar thickness

## **II Index**

fd	Fluid
s	Solid
c	Cold gas
h	Hot gas
p	Plate
in	Inlet
out	Outlet
X	x– coordinate
Y	y– coordinate
Z	z - coordinate
f	Fin
fs	Fin space
w	Wall

m      Metallic

### **III- Dimensionless Numbers**

<b>Abbreviation</b>	<b>definition</b>	<b>Name</b>
Re	$\rho u D_h / \mu$	Reynolds Number
St	$\alpha / u \rho c_p$	Stanton Number
Nu	$\alpha D_h / \lambda$	Nusselt Number
Pr	$\mu c_p / \lambda$	Prandtle Number
Pe	Re. Pr	Péclet number

# 1 INTRODUCTION-MOTIVATION AND SCOPE

---

The negative impact of the world's energy consumption can be reduced through legislation and safety regulations that would become obligations for all industrial countries. These nations must think about manufacturing with an allowable limitation for environmental protection, achievable through the saving of energy. While the idea of this saving has piqued interest, there has been relatively little research into the subject. Heat exchangers are widely used in various industrial, transportation and domestic applications, such as thermal power plants, means of transport, heating and air conditioning systems, electronic equipment and aerospace vehicles. In all of these applications, improvements in the exchanger efficiency can lead to substantial savings in cost, space, energy and materials. Therefore, most of the previous research searches for effective ways to increase the efficiency of heat exchangers.

Compact Heat Exchangers (CHEs) are characterized by compactness, small volume, low weight, high effectiveness and low cost, and they are widely used in gas-gas examples. A compact exchanger is a common device used extensively in a variety of industry applications dependent on its merits, such as automobile, aerospace, chemical industries, air conditioning and power plant etc. The naval and aeronautical applications have high thermal effectiveness because of the fins found on both sides to induce boundary-layer growth based on disturbance of flow and high thermal conductivity, depending on the thickness of the plate.

Many high-performance fin structures have been developed for use in various engineering applications as mentioned above, including wavy fins, offset strip fins, perforated fins, and louvered fins. Previous studies related to the topic of fin structures include a selection of working fluids that have a high-thermal conductivity, and highly effective heat transfer surfaces that are made from high-conductivity materials. The effectiveness of the heat transfer enhancement techniques have been recorded for both single-phase and two-phase heat transfer. For the purpose of this thesis, the single-phase forced convection enhancement techniques have been considered. In most publications, the heat transfer enhancement methods were often reported in publications before they could be grouped as passive or active enhancement methods. The basis of the active heat-transfer enhancement method lies in the utilization of some external power to permit the mixing of working fluids, the rotation of heat transfer surfaces, the vibration of heat transfer surfaces and the working fluids, and the generation of electrostatic fields. Passive methods aim for the enhancement of heat transfer, in addition to achieving higher values of the products of heat transfer coefficients and the heat transfer surface area.

The choice of a passive method depends greatly on the mode of convection heat transfer (whether natural or forced convection) and the working fluids that are used during the heat transfer. Recently, this subject has been placed under high priority as a method to reduce energy consumption and emissions. In the relevant research, the capacity for saving energy was prioritized. One way to improve heat recovery performance through heat transfer enhancement (and thus to achieve the general objective) is observation of the passive or active technique. However, there are major challenges involved, such as the lack of generalized correlations for both heat transfer and pressure drop in plate-fin heat exchangers, and especially for specific enhancement surfaces such as the wavy-fin type.

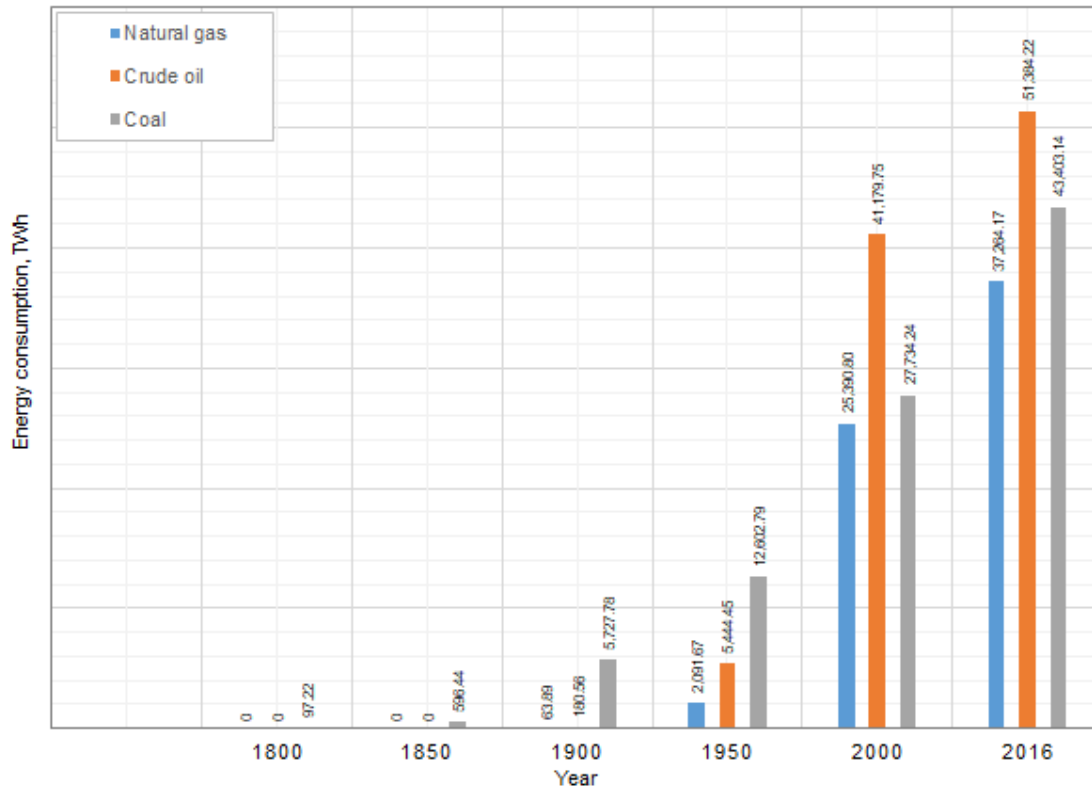


Figure 1.1: The history of energy consumption [21]. The global primary energy consumption of fossil and other fuel sources<sup>1</sup>.

Figure 1.1 summarizes the global energy consumption of fossil fuels (natural gas), crude oil, and coal from 1800 onward.

<sup>1</sup>The energy was measured in terawatt-hours (TWh), 1 TWh=3.6E+15 joules (J), while 1 British Thermal Unit equal to BTU=1055.87 Joules, [21].

Overall, we see that the global consumption of fossil energy has significantly increased. As shown, coal was the first and only fossil source until the 1860s. In 20th century there was a large diversification of fossil energy consumption that resulted in coal declining from 96% of the total production in 1900 to less than 30% in 2000. Today, crude oil has become the largest energy source, and accounts for around 33% of fossil energy, followed by coal and natural gas at 28% and 33%, respectively.

### 1.1. COMPACT HEAT EXCHANGER (CHE)

The process of heat exchange between two fluids with different temperatures and pressures is achieved via separation with a solid parting sheet. The enhancement surfaces can substantially augment the heat load, in order to reduce the heat exchanger size (which will become a typical feature of the compact heat exchanger type) and to reduce the gas-side thermal resistance. A compact heat exchanger is generally identifiable by the distinctly large heat transfer surface. This type of exchanger possesses a high heat-transfer-surface-area to volume ratio. The compact heat exchanger is used in multiple applications because it achieves the highest possible heat-transfer for the smallest amount of required space. Some traditional industries have also turned towards compact heat exchangers, including the chemical process industry, power industry, the food and beverage industry, and multiphase flow (especially in recent years).

#### 1.1.1. PLATE-FIN HEAT EXCHANGER

Shell-and-tube heat exchangers are widely used in many applications compared to the plate-fin heat exchanger (PFHE). PFHEs fall far behind other types of traditional heat exchangers; they are a type of compact heat exchanger that enhances the heat transfer surface area by providing an extended surface (fins). The surface is interfaced between the two fluids. This type of heat exchanger is considered unique because of its construction, with various geometric parameters to compensate for high thermal resistance, particularly if one of the fluids is a gas. Based on these merits, these heat exchangers have been used extensively in low-temperature process systems such as cryogenics, LNG plants, and ethylene plants. The plate-fin heat exchanger's design accounts for hot-flow length, cold-flow length, fin height, fin amplitude, fin length, fin thickness, and number of layers. A mathematical model design of PFHE has to consider the details of the geometry and impose constraints for the fin selection process.

The design methodology was developed based on the plate-fin heat exchanger methodology, fin pattern selection, flow arrangement, and pressure drop constraints. The heat transfer and pressure drop performance are predicted by a Nusselt number and a Fanning friction factor correlation. There are approximately sixty standardized fin parts, such as the plain fin, louvered fin, offset strip fin, and wavy fin, each with specific heat transfer and pressure drop performance. A major challenge in designing the plate-fin heat exchanger was the lack of a standardized fin selection method. PFHEs consist of: a gasket plate; the metal plate of a heat exchanger, used to transfer heat; the plate-fin, including different types of fins that have been characterized by high effectiveness, compactness, and low weight; and a stack of alternate flat plates called ‘parting sheets’ and ‘corrugated fins’, brazed together as a block. Many plates give freedom of flow arrangement to achieve the required heat duty within the specific pressure drop and the fluid flow between the parting sheets [31].

PFHEs have high compactness (up to  $1000\text{--}2500\text{ m}^2/\text{m}^3$ ) and low weight. Some of the commonly used heat exchanger fins are wavy, offset strip, louvered, perforated, and pin fins [23]. A plate-fin heat exchanger has been designed to achieve our objective, which is to maximize the effectiveness value and to minimize the total annual cost. Six design parameters were selected, including fin pitch, fin height, fin offset, length, cold-stream flow length, and the hot-stream flow length. The level of conflict between the fin pitch, fin height, fin offset length, hot-stream flow length, and cold-stream length were found to be important design parameters which cause a conflict between effectiveness and the total annual cost [6]. A new methodology to design a multi-stream plate-fin heat exchanger was proposed to minimize the exchanger volume. The selection of fin types and imposed constraints were considered simultaneously in the design process to regress the Fanning friction factor  $f$  and Colburn  $j$  factor. Some design parameters, such as the hydraulic diameter  $d_h$ , the ratio of secondary surface-area to the total heat transfer area, and the ratio of the total transfer area on one side of exchanger to the volume between plates of that side in  $\text{m}^2/\text{m}^3$  [62].

The separating plates work as the primary heat transfer surfaces with fins intimately bonded to the primary surfaces. Fins act as a secondary surface to increase the heat transfer area and the heat transfer to other fluid through a parting sheet that induces the turbulent flow, to enhance the local convective heat transfer. The fins also have another role as structural supports against the internal pressure difference: The sidebars are used for preventing the fluid from leaking out. Fins and sidebars are brazed with the parting sheets to ensure that the thermal links

have mechanical stability. A wide variety of plate-fin geometries have been used to enhance the heat transfer coefficient, which offers additional space with the advantage of costing less than other types of heat exchangers such as the shell-and-tube heat exchangers. An exchanger consists of alternating layers of fins separated by parting sheets. The edges of each layer are sealed with sidebars which give the unit mechanical strength, preventing fluids from leaking outside of the construction and into the atmosphere. Additionally, the layers are brazed together. Figure 1.2 shows the basic structure of a compact heat exchanger [63]. PFHEs offer several features which can be beneficial over other types of heat exchangers, as summarized in the following:

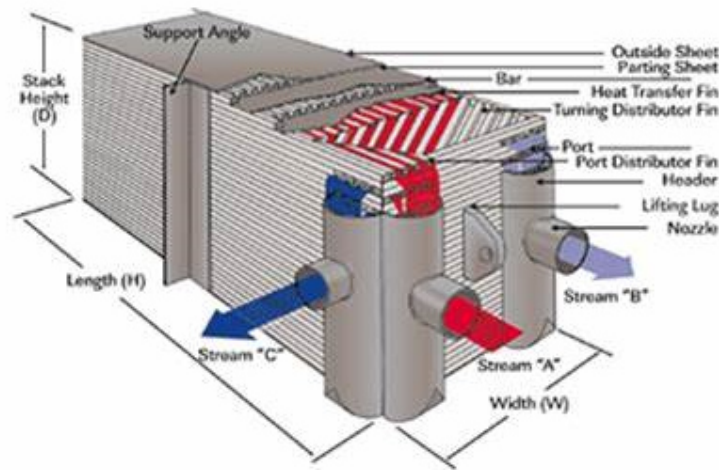


Figure 1.2: Basic structure of a plate-fin heat exchanger [69]

- 1- Compactness: Large heat transfer surface area per unit volume, with small passage size adopted on the fin to enhance heat transfer, producing a high overall heat transfer coefficient.
- 2- Effectiveness: High thermal effectiveness and a close temperature approach (results as low as 3 K temperature difference between single-phase fluid streams, and 1 K between boiling and condensing fluids was common).
- 3- The average temperature: PFHE operates even with low-temperature differences, about 3 K with a single phase.
- 4- Flexibility: Multi-stream operation (up to ten process streams can exchange heat in a single heat exchanger), also used with a wide range of fluids working and different conditions.
- 5- Flow arrangement: True counter-flow operation is possible in a plate-fin heat exchanger

(unlike the shell-and-tube heat exchanger, where the shell-side flow is usually a mixture of cross and counter flow).

PFHEs have different limitations in their applications. Some research doesn't take various parameters into account, and several problems in the application of the plate-fin heat exchangers were not analyzed due to the following:

- 1- Reduced range of the temperature and pressure, especially with the rectangular fin shape which has a low performance in comparison with the geometry of other fins.
- 2- Cleaning problem. It was complicated to reach inside the narrow passages, thus it is limited to non-corrosive fluids in its application.
- 3- Hard to repair the failure or leakage between passages.
- 4- Manufacturability and capital cost are another major hurdle.
- 5- Few researchers have carried out general systematic design methods that simultaneously take into account both the fin selection and thermal design of plate-fin heat exchangers.

### **1.1.2. HEAT TRANSFER SURFACES**

The benefits of using an extended surface for heat transfer have received considerable attention, particularly for gas flow, as the PFHEs are mainly employed for liquid-gas and gas-gas applications. By using fins configured for extended surfaces, we can enhance the heat transfer coefficients, however the pressure-drop penalties are high. The friction factor is increased where the discontinuous type of fin geometry was adopted to interrupt the boundary layers. Friction drag is the friction of a fluid against the surface that it is moving through. It is directly proportional to the area of the surface in contact with the fluid and increases with the square of the velocity [60]. Although friction drag is associated with the high heat transfer coefficient, form drag has no counterpart and represents wasted energy. The form drag can be substantial depending on the quality of the cutting edge. However, machined-formed fins are generally free from this problem.

### **1.1.3. APPLICATIONS**

The applications that use a plate-fin type heat exchanger fall far behind other types of heat exchanger, such as shell and tube heat exchangers, although it is suitable for a wide range of different temperatures and different pressures for gas-gas, gas-liquid and other phases.

The exchangers are used for cryogenic air separation and LPG fractionation are the largest and most complex units, with several meters in length. Brazed aluminum plate-fin exchangers are used in the aerospace industry because of their low weight-to-volume ratio and compactness. They are used mainly in the environment control system of the aircraft, avionics cooling, hydraulic oil cooling and fuel heating. This type of compact heat exchanger has everlasting demand for the automobile and air conditioning industries [63]. Other applications for PFHEs include fuel cell heat recovery plants, pollution control systems, ethylene and propylene production plants, fuel processing and conditioning plants.

#### 1.1.4. CHALLENGES OF PFHE IN INDUSTRIAL APPLICATION

Shell-and-tube heat exchangers are widely used in many applications when compared with plate-fin heat exchangers. In the past, a few researchers were tasked with improving heat transfer and pressure drop in the plate-fin heat exchanger, thus there are many existing variations of data and solutions to address heat transfer problems in different kinds of geometry parameters, which have been reviewed in [1] and [28]. PFHEs fall far behind the traditional shell and tube heat exchanger in industry applications for the following reasons: (1) A lack of understanding of the mechanisms controlling the fluid flow and heat transfer in PFHE utilizing laminar flow regime, which uses the thermal enhancement surfaces (secondary surfaces), such as tabulator strips like wavy fin. Further, a design methodology is lacking for this type of exchanger (2) There are few correlations available to predict the heat transfer and pressure drop, which covers a wide range of geometrical parameters. The available correlations that have been reviewed in the literature for wavy fin-type are not suitable to predict the heat transfer and pressure drop. They are not suitable to use at specific fin amplitudes, when the fin amplitude and the length of the fin are small. It is therefore essential to develop a new correlation which is valid for all engineering designs in the future. (3) The high performance of this type of heat exchanger is the critical component, and their performance is highly sensitive to longitudinal heat conduction. Therefore, in the present thesis, we will investigate the effects of longitudinal heat conduction in the metal wall. A single pair of wavy channels is applied with different geometrical parameters such as fin amplitude  $a_f$ , fin space  $s_{fs}$ , fin height  $h_{fs}$ , fin waviness  $l_w$ , and fin length  $L$ . Figure 1.3 shows the fin types adopted in the current work.

According to the available literature, we can conclude that there is little research available regarding the different types of fins and their performance, particularly regarding the wavy fin. Therefore, in the present thesis, we focus on the wavy fin-type and take many geometrical parameters into account.

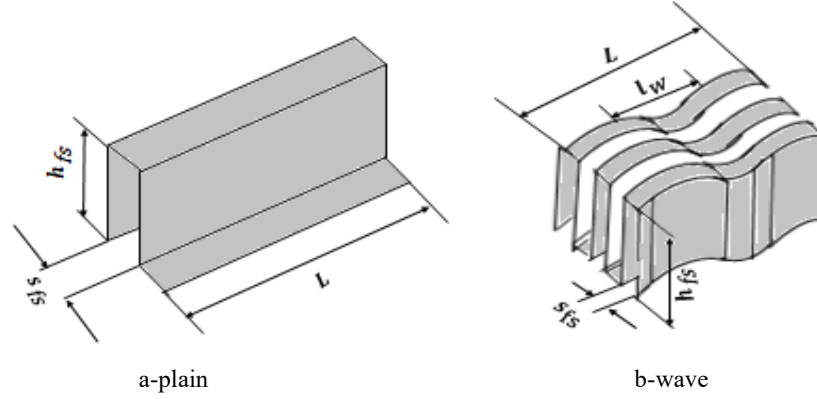


Figure 1.3: Shows the dimensions for the wavy fin type.

However, to reduce the computational model, the physical properties for each flow stream in the single pair channel have been assumed as constant properties, and air is used as the working fluid. Following are some of the assumptions made in the CFD simulation in a single pair channel of wavy fins:

- 1- All fin types are conducted in three-dimensional domains.
- 2- Steady-state operation.
- 3- Single-phase heat transfer.
- 4- Constant fluid physical properties.
- 5- Incompressible laminar flow considered.
- 6- Identical geometrical parameters for all fins employed.

The study is deliberately limited to laminar flow, as our applications call for a low pressure drop. Thus even through a turbulent flow situation and for example, serrated fins are known to have better heat transfer performance, we will focus on laminar flow.

## 1.2. FLOW ARRANGEMENT

The streams in PHEFs may be more than two streams, flowing in parallel or perpendicular directions. Therefore, there are three types of flow arrangements, namely cross-flow, counter-

flow, and cross-counter flow. Counter-flow is considered to be the most efficient of the three, as it supports the greatest range of temperature difference between the hottest cold-fluid temperature and the coldest-hot fluid temperature. The parallel flow geometry gives the lowest thermodynamic performance and the cross-flow arrangement gives an intermediate performance, through offering superior heat transfer properties and an easier mechanical layout [63].

### 1.2.1. CROSS FLOW

In a cross-flow arrangement, fluid one flows perpendicular to the second fluid, thermal energy travels from one air stream to another, one fluid flows through tubes and the second fluid passes around it. It is used for two phase flow, e.g. in a steam condenser where the steam exits the turbine and enters the condenser shell side, see figure 1.4. This heat exchanger is used in cooling and ventilation systems that require heat to be transferred from one air stream to another. A cross-flow heat exchanger is made up of thin metal panels, normally constructed out of aluminum. The thermal energy is exchanged via the panels. A traditional cross-flow heat exchanger has a square cross-section and a thermal efficiency of 40–65%. A counter-flow or dual cross-flow heat exchanger is used if greater thermal efficiencies are required – typically up to 75–85 %. In some types of exchange, humid air may cool down to the freezing point, forming ice. Cross-flow is typically less expensive than other types of heat exchangers. It is normally used when hygienic standards require that both air streams are kept completely separate from one another. It is often used in heat recovery installations in large canteens; these flow types are often used in hospitals and the food industry. Unlike a rotary heat exchanger, a cross-flow heat exchanger does not exchange humidity.

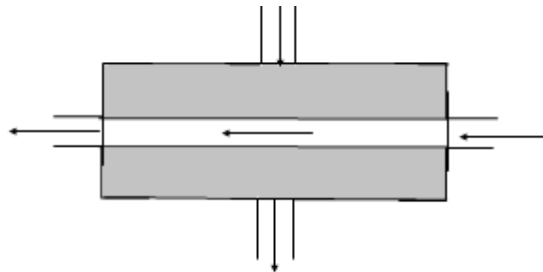


Figure 1.4: Cross-Flow Arrangement.

### 1.2.2. COUNTER-FLOW

The two fluids flow parallel to each other but in opposite directions. The cooler fluid approaches the inlet temperature of the hot fluid, as illustrated in figure 1.5. This type is the most efficient of the three types, because it can have the hottest cold-fluid temperature greater than the coldest hot-fluid temperature when compared to other two-fluid arrangements for overall thermal conductance ( $UA$ ), fluid flow rates, and fluid inlet temperatures. Cryogenic refrigeration and liquefaction equipment uses this geometry almost exclusively.



Figure 1.5: Counter-Flow Arrangement.

### 1.2.3. CROSS-COUNTER FLOW

A hybrid type, supporting a combination of both counter- and cross-flow arrangements, one of the streams flows in a straight path, whereas the second stream follows a zigzag path across the first stream, see figure 1.6. Moving along the zigzag path, the second fluid stream covers the length of the heat exchanger in an opposing direction to that of the direct stream. It can be assumed to be globally counter-flow while remaining locally cross-flow. This type of flow arrangement is used in the same applications as cross-flow exchangers, but they allow more flexibility in design and fabrication. They are particularly suited to applications where the two streams have considerably different volumetric flow-rate or permit significantly different pressure-drops.

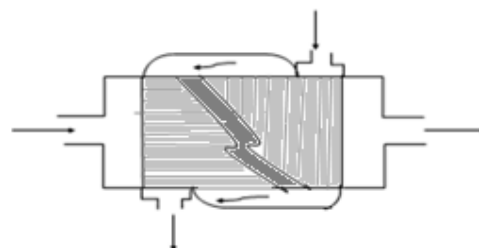


Figure 1.6: Cross-Counter Arrangement.

The fluid with the larger volumetric flow-rate or with the smallest value of allowable pressure-drop is made to flow through the straight channel while the other stream follows the zigzag path i.e., with a liquid-to-gas heat exchanger. The gas stream with a large volume flow-rate and low allowable pressure-drop is assigned to the straight path, while the liquid stream with a high allowable pressure-drop flows across it, over a zigzag path.

### 1.3. FIN FEATURES

Plate-fins are a type of compact heat exchanger that use plates and finned chambers to transfer heat between fluids. The structure of the plate-fin heat exchanger includes a nozzle-stub pipe, distributor, and the plate-fin. The typical materials are brazed aluminum, stainless steel, and titanium. The objective of fins can be summarized as follows:

- 1- Fins are a secondary surface used to increase the heat transfer surface area between cold gas and hot gas and to achieve heat transfer between the fluid streams through parting sheets.
- 2- Heat transfer is more efficient due to the higher thermal conductivity.
- 3- Fins produce the turbulence flow and enhance the heat transfer coefficient. There are different categories of fins; namely, the plain rectangular fins, plain triangular fins, offset strip fins, wavy fins, perforated fins, and louvered fins.

#### 1.3.1. HEAT TRANSFER SURFACES ENHANCEMENT

As a compact heat exchanger, the plate-fin heat exchanger is applied in many industries and occupies a unique role due to its flexible arrangement, simple shape, and good thermal effectiveness. There are a variety of plate-fin types, all of which enhance the heat transfer coefficient in PFHEs. Engineers are constantly working to create new and more effective enhanced surfaces. The number of the duct geometries have been studied, in order to examine each in detail.

In this work, the most common fin geometry type to be considered is the wavy fin at different fin amplitudes. As mentioned, based on the different applications, various kinds of fins are used in plate-fin heat exchangers. [28] conducted an experimental analysis of about 40 kinds of fins and offered their corresponding correlation curves of heat transfer and resistance. Figure 1.7 illustrates the common classifications of fin geometries in plate-fin heat exchanger strips.

Singly connected ducts that have received the most attention are offset, rectangular, and the wavy fin (this type is divided into sine ducts and arc ducts). Currently, arc ducts have not been adequately considered within the available research.

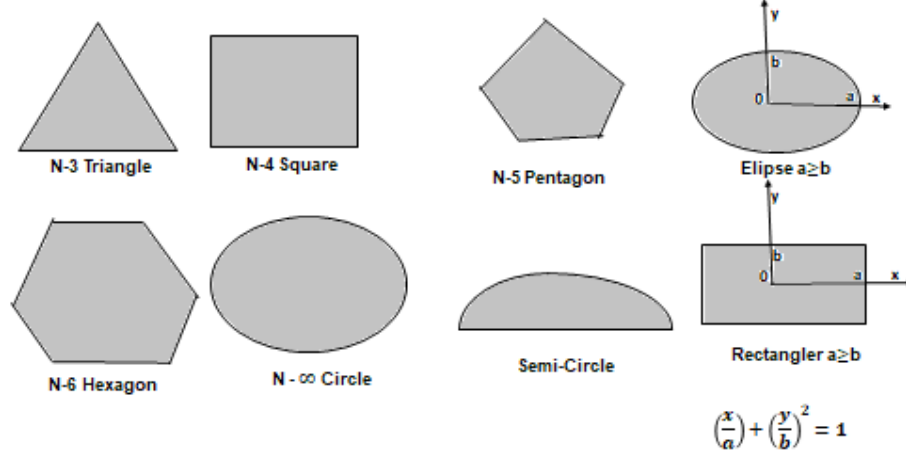


Figure 1.7: Common Duct Geometries.

## 1.4. OBJECTIVES

Our objective is to develop a new correlation of wavy fin for a plate-fin heat exchanger, using the OpenFOAM program. A numerical simulation is performed for a single pair of wavy channels in a plate-fin heat exchanger to predict the heat transfer performance in terms of Colburn  $j$  factor and Fanning friction factor  $f$ . Many researchers have carried out investigations relating to the design of a plate-fin heat exchanger. Nevertheless, there is still a lack of understanding of the fluid flow and heat transfer at different flow regimes, especially when used with tabulator fin strips such as the wavy fin. Currently, there are a few correlations which enable the prediction of heat transfer and fluid flow characteristics for each kind of enhancement surface, from both Kays and London [28] and Shah and London [1].

In this thesis, a new correlation will be developed to predict the heat transfer in terms of Colburn  $j$  factor. The models in this work could be defined as simple or traditional models, analytical models and numerical models. The geometrical parameters of wavy fin type are fixed in all

cases and adopted to achieve our objectives. Many parameters relating to the wavy fin design will rely heavily on the numerical simulation to calculate the developed models, however, we have proposed a new correlation based on the most accurate of the developed models. We have simulated single pair channel of wavy type in plate fin at various fin amplitudes ranging between (0, 1.5, 2, 2.5 mm). For zero fin amplitude, the surface of the fin is straight as the rectangular or plain fin, and at fin amplitudes ranging between (1.5, 2, and 2.5 mm) the surface of the fin is corrugated, as with wavy fin type. We have performed the numerical simulation by taking into account the variations of geometrical parameters such as the fin amplitude  $a_f$ , fin waviness length  $l_w$ , fin thickness  $\delta_f$ , plate thickness  $\delta_p$ , fin length  $L$ , fin height  $h_{fs}$ , and fin space  $s_{fs}$ , as written in chapter 4. The validity of the modeling technique is verified through comparing results of the developed models at different geometrical parameters with the available literature. The approach we take in this thesis is as follows. First, we calculate local heat transfer coefficients with extensive numerical CFD studies. Then we introduce these heat transfer coefficients into an analytical model for the heat exchanger. It is of advantage to have analytical models available as these models allow a better and faster study of sensitivities as for example, longitudinal heat conduction.

In the experiments we only measure inlet and outlet temperatures, overall pressure drops and flow rates, so additional information from the numerical and analytical model is needed to understand the heat transfer mechanisms inside the heat exchanger.

In the following, we summarize our objectives:

- 1- Numerical simulations applied by using the OpenFOAM software for a single pair channel in the plate-fin heat exchanger.
- 2- New models developed to calculate the heat transfer performance in terms of Colburn  $j$  factor.
- 3- Improve the heat conduction equation by adding plate resistance. Additionally, the thickness of the plates and fins are combined to develop the analytical model, which predicts the heat transfer performance through the ODE method.
- 4- Develop a numerical model by taking into account each cell inside the wall within its calculation, which will predict the heat transfer performance through the FDM method.
- 5- Investigate the effects of longitudinal heat conduction LHC on the heat transfer coefficient.
- 6- Develop a new correlation to predict the heat transfer performance of the wavy fin, to be valid for a range of geometrical parameters.

In the present work, the proposed methodology includes:

- A thermal-hydraulic design model of the plate-fin heat exchanger at different geometrical parameters.
- Numerical simulation performed at the operation condition of along the exchanger length and lateral heat condition through the fins constant heat flux  $\dot{q}$ .
- OpenFOAM software package used to achieve our purpose, applied for three-dimensional structures.

### 1.4.1. OUTLINE OF THE THESIS

This thesis presents a numerical simulation analysis. Each chapter has an independent subject, organized as follows: Chapter 2 will summarize the OpenFOAM program with important information and details related to this thesis. Chapter 3 reviews the currently available topics and correlations. Chapter 4 introduces the models in detail and analyzes of the effects of longitudinal heat conduction on the heat transfer (the simple or traditional model, and the analytical and numerical developed models will be included here). A new correlation will be proposed to predict the heat transfer and pressure drop in terms of Colburn  $j$  factor and frictional fanning factor  $f$  of the wavy fin in plate-fin heat exchangers. The fin amplitude parameters have a significant influence when selecting the fin type. Chapter 5 provides the design procedures for the plate-fin heat exchanger that is used in the experimental work. Chapter 6 delivers the experimental work for the test rig for the constructed heat exchanger (test section). Chapter 7 summarizes the discussion findings and suggests research areas in need of further examination.



## 2 OPENFOAM SOFTWARE

---

In this chapter, we present a brief explanation of OpenFOAM, which is a free and open-source software. The computational fluid dynamics (CFD) is distributed by Open CFD and Foundation, under public license. The multi-physics modeling platform is written in the C++ programming language. OpenFOAM was created in 1989 as a commercial product named FOAM, which is an abbreviation of (Field Operation and Manipulation), and the program was released as open-source in 2004, where it has continued receiving updates. Currently, OpenFOAM competes with other commercial software such as ANSYS Fluent, and is used in most areas of engineering science applications, as well as for a wide range of industrial sectors like heating, ventilation, air-conditioning, heat exchangers, ovens, solar panels, and cooling systems. OpenFOAM has many advantages when solving any complex fluid flows that involve chemical reactions, turbulence and heat transfer. This program consists of modifiable libraries which contain different numerical models and tools using the finite volume method (FVM), whereby separated matrix equations are created for each one of the equations and solved using iterative solvers. The OpenFOAM program is created with different numerical features, infinite volume method, and the finite element method.

In this thesis, the numerical simulation is carried out using OpenFOAM to achieve our objective and the solver used is chtMultiRegionFoam. The solver is based on a combination of heat conduction foam to conjugate heat transfer between a solid region and a fluid region. All data of numerical simulation is stored within a user-defined directory in OpenFOAM. The file structure in OpenFOAM is shown below, the diagram includes all the files necessary to initiate the preprocessing case, although there are other files that will be generated during the process. Figure 2.1 illustrates the basic steps of the overall structure of modeling supplies within pre-processing and post-processing environments. Directory 0 stores initial conditions and boundaries when the simulation runs the iterations of solution and time steps appear on the program window. These initial files are used to introduce the parameters of the simulation. The constant directory contains files specifying the physical properties of the region, and a polymesh folder where a full description of the mesh will be stored. The system directory contains files for setting parameters associated with the solution procedure [127].

The polymesh file used to be the default location required in older versions of OpenFOAM. The interface of the pre-processing and post-processing are themselves made up of the OpenFOAM utilities. Additionally, different modeling can be achieved, such as incompressible

and compressible flows in laminar and turbulent flow regimes. The basic pre-processing steps for this step of the modeling could be done with mesh generation, and by converting meshes to other formats such as Ansys, Fluent, Gambit. The initial conditions are modified through the files found directly in the program, and the post-processing is achieved directly within ParaView screen.

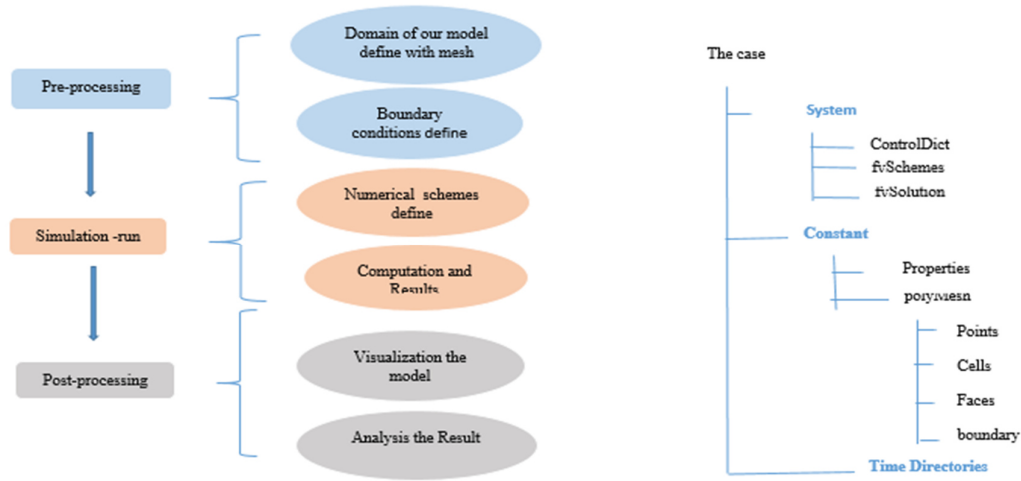


Figure 2.1: Shows the OPENFOAM framework, basic steps of a modeling task.

## 2.1. PARAVIEW

Open-source has multiple platform applications for interactive and scientific visualization, which is used to facilitate remote visualizations of data sets, generating a level of detail in models. ParaView is designed for data parallelism on shared-memory or distributed-memory multi computers and clusters. Additionally, it can be run as a single computer application and offers the possibility to extend its functionality in several directions.

### 2.1.1. MESH GENERATION

The principle behind block mesh is to decompose the domain geometry in 3D. OpenFOAM always uses 3D meshes and solves by default. In order to mesh a two-dimensional geometry, a 3D mesh is created whereby two dimensions match the geometry and the third is arbitrary. OpenFOAM includes a mesh generation utility, named blockmesh, which generates meshes

from a description specified in the blockmeshdict file in the software of OpenFOAM [9]. Creating a blockmesh in this program may be slightly more difficult to learn. The following are the steps used by blockmesh to create mesh:

- 1- The vertices of the mesh are defined; in this case the 8 vertices of a hexahedron block, where the first vector on the list represents the vertex 0, the second vector represents vertex 1, etc.
- 2- The blocks have several entries defining the mesh block and its divisions. The array after the hex keyword gives the order of the vertices, using their indexes to identify them. This order is defined by the local right-handed coordinate system of the block and follows these rules: x1 direction is described moving from the first to the second vertex, x2 direction is described moving from the first to the fourth. The 5th, 6th, 7th and 8th vertices are found by moving in the x3 direction from the 1st, 2nd, 3rd and 4th vertices, respectively. The order vector is (0 1 2 3 4 5 6 7). Figure 2.2 shows an example block with each vertex numbered. OpenFOAM is designed as a code for three-dimensional space and defines all meshes [9].

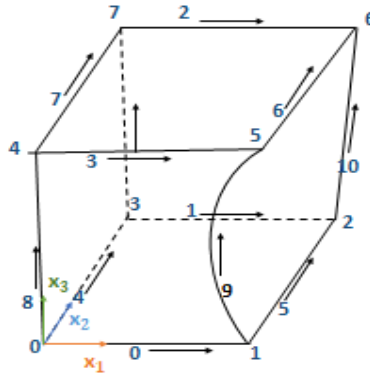


Figure 2.2: A single block.

- 3- In the second entry of blocks, the number of divisions (cells) in each of the directions is specified. The third entry defines the cell expansion ratios along a direction or an edge (this is the ratio between the length of the last cell and the length of the first one). The keyword ‘simple grading’ is used to specify the expansion ratios in the directions x1, x2, x3, which are defined by the local coordinate system. The expansion ratio enables the mesh to be graded or refined enough in the specified directions. The expansion ratio is defined as the width of the end cell  $\delta_e$  in one edge of the block to the width of the start cell  $\delta_s$  in the other side edge of the block, as shown in figure 2.3.

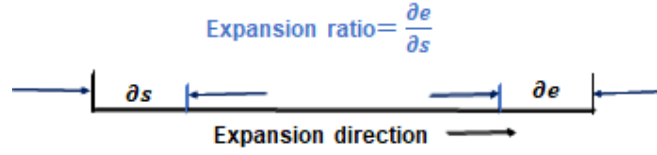


Figure 2.3: Mesh grading along a block edge.

4- The edges. This is used to describe the edges of the two vertex points joining like a line, an arc, or a curve. If there is no specification, straight lines are assumed by default.

## 2.2. SIMULATION CONTROLS

The under-relaxation factors and the number of non-orthogonal correctors are changed depending on the selection of incompressible or compressible calculation. Our simulation offers the modification of the following factors: pressure P-rgh, velocity  $u$  and turbulence  $K, \epsilon$  as listed in Table 2.1. The minimum entry pressure sets the lowest bound for the pressure. If there is a cell with a lower pressure after a solver iteration it is adjusted to the value of the minimum pressure. The minimum and maximum pressure bounds are given in numerical units.

Tabel 2.1: The relaxation factors for our simulation set-up.

Factors	Relaxation factor
Velocity, $u$	0.3
Pressure, P-rgh	0.7
Epsilon and omega, $K, \epsilon$	0.7

The finer meshes of the domain (near the wall boundaries) are generated to resolve the high velocity and temperature gradients, and to ensure that the accurate outlet data results are obtained. A structured mesh stretched in the fluid direction could be used to significantly reduce the number of meshes and thus the solution time. The mesh is viewed in ParaView through the post-processing tool, as illustrated in Figure 2.4. In the present thesis, the mesh for the single pair channels of the wavy fin in three dimensions was generated using both the blockmeshdict and topsetdict files. The model is set in three coordinates, namely  $x$ ,  $y$ , and  $z$ , which are specified by the grid size. The geometrical parameters are used to generate the mesh of the

model, these include the plate thickness  $\delta_p$ , fin height  $h_{f-s}$ , fin space  $s_{f-s}$ , and the fin thickness  $\delta_f$ . Thus we determine the minimum grid size near the wall of the wavy fin in three dimensions by setting the values of fin thickness, fin height, and fin spacing at 0.0001, 0.0001, and 0.0001 respectively, thereby creating the mesh of the wavy fin.

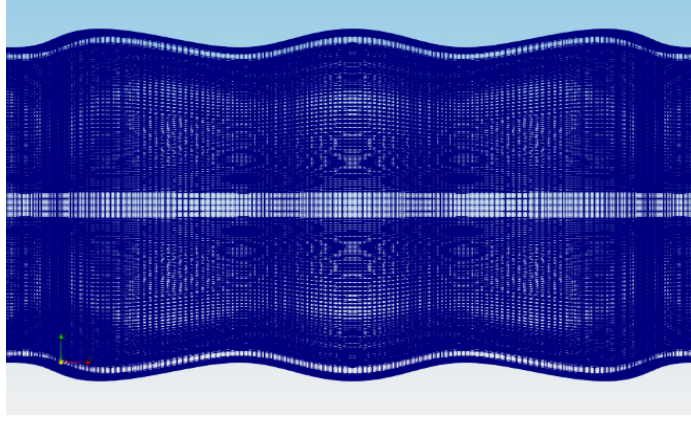


Figure 2.4: Shows Block for fin channel.

### 2.2.1. BOUNDARIES

The boundary of the mesh is broken into patches and regions. Take a 2D-simulation of the fluid flow in a cavity as an example. The four patches are left, right, top-bottom, and front-back. The patch contains the planes of the z-dimension (front-back) and is otherwise empty, which instructs OpenFOAM to solve in other two dimensions. The face's entry consists of one or several vectors containing the vertices of the faces assigned to the corresponding patch. The faces are assigned to a default patch of type empty. The files generate, which describes the mesh in the poly mesh file and sets up the boundary conditions for each patch, which is defined in the mesh generation as follows:

- Left patch: A fixedGradient uses fixed thermal flux condition,  $-\frac{\partial T}{\partial x} = \frac{\dot{q}}{k}$ .
- Right patch: A fixedValue is directly specified as the fixed temperature condition.
- Top-Bottom patch: ZeroGradient sets the normal gradient, establishing the adiabatic condition,  $\pm \frac{\partial T}{\partial y}$  to 0.
- Front-Back patch: BlockMeshDict is specified as the empty type here.

### 2.2.2. INITIAL CONDITIONS SETUP IN OPENFOAM

The initial boundary conditions are set independently for each line and specified in the field files. These files mainly deal with data requirements and the fundamental properties to get outstanding results. Doing this manually requires specifying a uniform initial value for the individual fields. The dictionary named (0) in OpenFOAM is used to set up the initial conditions. The files included in dictionary (0) to set boundary conditions are described as follows:

- 1- The entry temperature (T) sets a constant value of initial temperature throughout the computational domain.
- 2- The entry pressure (P) sets a constant value of initial pressure throughout the computational domain.
- 3- The entry velocity (U) sets a constant value of initial velocity throughout the computational domain.
- 4- The entry turbulent energy sets a constant value of initial turbulent energy (k) throughout the computational domain. This is only needed when using the (K- $\omega$  or K- $\epsilon$ ) turbulence model.
- 5- The entry turbulent dissipation sets a constant value of the initial turbulent dissipation rate ( $\epsilon$ ) or ( $\omega$ ) throughout the computational domain. This is only needed when using the (K- $\epsilon$ ) or (K- $\omega$ ) turbulence model.

In the present work, the initial conditions are set for the two fluids, the hot and cold gases, and the solid walls. Every patch includes a type of entry, which specifies the types of boundary conditions. The boundary conditions in the OpenFOAM program are defined as the inlet and outlet conditions. As the fluid flows out of the domain, a patch face switches to the condition of zero Gradient; as the fluid flows into the domain a patch face switches to the condition of fixed Value. At inflow, the inlet value is specified by a fixed value or uniform. The subject of boundaries is quite complex because their role in modeling not simply a geometric entity but an integral part of the solution.

A discussion of boundaries sits uncomfortably between a discussion of meshes, fields, discretization, and computational processing.

### 2.2.3. THERMOPHYSICAL PROPERTIES

Thermophysical models are concerned with heat and physical properties. The thermophysical

properties are located in the constant directory in the OpenFOAM program. The user can set up these directories depending on the purpose i.e., pressure, temperature and other properties that are then computed. The main thermos model's type, (psiThermo) model, is applied at a fixed composition case or compressibility case, (rhoThermo) model is applied at the composition case, which is dependent on the density, (psiuReactionThermo) model is applied at the combustion case based on compressibility, (rhoReactionThermo) model at reacting mixture and (multiphaseMixtureThermo) model can be applied at multiple phases. The composition of each constituent is easily specified by the (n Moles), which means the number moles of the component. The equation of state includes the (rhoConst) and (perfectGas) states, and is used at constant density, as shown below. An example entry for thermos type:

```
Type          heRhoThermo; // includes heat transfer
Mixture        pureMixture;
Transport       polynomial; // const, polynomial
Thermo          polynomial; // hConst, hPolynomial
equationOfState icoPolynomial; // perfectGas, icoPolynomial
Specie          specie;
Energy          sensibleEnthalpy; // form of energy
```

In our case, we have adopted the physical settings in constant directory in OpenFOAM, which are dependent on the hot and cold fluids. The properties should be defined as the dynamic viscosity specifies( $\mu$ ) of the fluid and for incompressible case, the viscosity definition is  $\mu = \rho\nu$ , where  $\nu$  is the kinematic viscosity, and the value of density ( $\rho$ ) is used for post-processing at the case of incompressible. The Transport Model is used to select the preferred transport (viscosity) model. The molar weight is the standard chemical property of a substance, which is identified in the file of thermophysical properties of the fluid.

#### 2.2.4. CONTROL TIME SETUP

The parameters related to the control of the time for simulation, and to the input/output of the data, which are introduced in the controlDict dictionary. In the case of steady-state simulations, the time controls relate to the number of iterations. The calculation mode is chosen in input data within the OpenFOAM program, depending on the time management through the control time file. The read and write data in the controlDict file is found in the system directory.

We can also choose between a simple steady-state calculation or its combination with the transient extensions. In the current work, the simulation is running with the entry solver at steady state. For finer mesh sizes, the courant number for large time intervals will choose a smaller time step automatically. The correct temperature response due to the finer mesh size is generated, and we chose the real-time step of around 0.001 value within the ControlDict file.

The following is a description of the parameters:

```
Application      chtMultiRegionFoam;
writeControl      adjustableRunTime;
writeInterval     1000;
Delta            0.001;
writePrecision    12;
timePrecision     10;
```

The writeControl term is used to control the timing of the write output file. With timestep writes every writeInterval time-steps and with run time every writeInterval simulated seconds. To reach the steady-state solution, the converge is dependent on the Reynolds number. For the counter-flow arrangement with the Reynolds number at 50, we need 70 seconds to reach the steady state. Each one-second within the program equates to two hours in real time. In contrast, at Reynolds numbers ranging between (1500-2000), we need less time to reach the steady state; around 20 seconds. In another type of heat exchanger, using a parallel flow arrangement and Reynolds number (50), only 10 seconds are needed to reach the steady state. This indicates that less time is needed when using the parallel flow arrangement.

### 2.3. TYPES OF TURBULENCE MODELS

Several turbulence models are supported by the OpenFOAM software program. The models range from Reynolds-Averaged Simulation (RAS) models to Large Eddy Simulation (LES) models. The most common turbulent model is the Large Eddy Simulation (LES); it was initially proposed by Joseph Smagorinsky in 1963 and is used to simulate atmospheric air currents. The Reynolds-Averaged Simulation K- $\epsilon$  model allows a two-equation model to account for history effects like convection and diffusion of turbulent energy [17]. The models are listed as the laminar model (no turbulence), K- $\omega$  SSTmodel, K- $\epsilon$ \_model, and RAS model.

### 2.3.1 THE PHYSICAL MODELING

The solution methodology was implemented through the OpenFOAM program method. OpenFOAM generates solutions with a variety of defined solvers. The solver codes in OpenFOAM are largely procedural since they are a close representation of the solution for the algorithms and equations. The solvers are designed to solve a specific problem in computational continuum mechanics. The OpenFOAM 4-dev version was chosen and the solver is chtMultiRegionFoam. The solver is used for the resolution of the steady state, which allows the solution of conjugate heat transfer problems (problems combining conduction and convection). The physical modeling of the fluid flow with heat transfer is based on conservation laws for mass, momentum, and energy. In present work, the laminar model was adopted to achieve our objective with the Reynolds number range (50-2000).

### 2.3.2. MATHEMATICAL LANGUAGE IN OPENFOAM

In order to analyze and understand the processes of heat transfer performance on a surface, we must first state the relevant equations of continuity, momentum, and thermal energy in the fluid domain at laminar flow. The fluid flow is required to satisfy the laws of physical conservation equations.

Continuity, momentum, and energy are the governing equations of the three-dimensional fluid flow at steady state, and are applied in the single pair of wavy passage. The mass conservation (continuity) equation is given by:

$$\frac{\partial \rho}{\partial t} = - \left( \frac{\partial}{\partial x} (\rho u_x) + \frac{\partial}{\partial y} (\rho u_y) + \frac{\partial}{\partial z} (\rho u_z) \right) \quad (2.1)$$

For incompressible cases, the density of the fluid is constant, which can simplify the mass conservation equation. We have assumed constant density, there is no expansion or compression phenomena, therefore the time derivative becomes zero. While using the Nabla-Operator  $\nabla$  and the velocity vector  $\mathbf{U}$ , the equation can be written as:

$$\boxed{\nabla \bullet \mathbf{U} = 0} \quad (2.2)$$

The conserved momentum equation is given in x, y, z components, which are written as:

$$\frac{\partial}{\partial t} \rho u_x = - \left( \frac{\partial}{\partial x} \rho u_x u_x + \frac{\partial}{\partial y} \rho u_y u_x + \frac{\partial}{\partial z} \rho u_z u_x \right) - \left( \frac{\partial}{\partial x} \tau_{xx} + \frac{\partial}{\partial y} \tau_{yx} + \frac{\partial}{\partial z} \tau_{zx} \right) - \frac{\partial \rho}{\partial x} + \rho g_x \quad (2.3)$$

$$\frac{\partial}{\partial t} \rho u_y = - \left( \frac{\partial}{\partial x} \rho u_x u_y + \frac{\partial}{\partial y} \rho u_y u_y + \frac{\partial}{\partial z} \rho u_z u_y \right) - \left( \frac{\partial}{\partial x} \tau_{xy} + \frac{\partial}{\partial y} \tau_{yy} + \frac{\partial}{\partial z} \tau_{zy} \right) - \frac{\partial \rho}{\partial y} + \rho g_y \quad (2.4)$$

$$\frac{\partial}{\partial t} \rho u_z = - \left( \frac{\partial}{\partial x} \rho u_x u_z + \frac{\partial}{\partial y} \rho u_y u_z + \frac{\partial}{\partial z} \rho u_z u_z \right) - \left( \frac{\partial}{\partial x} \tau_{xz} + \frac{\partial}{\partial y} \tau_{yz} + \frac{\partial}{\partial z} \tau_{zz} \right) - \frac{\partial \rho}{\partial z} + \rho g_z \quad (2.5)$$

The conserved momentum equation uses the Nabla-Operator  $\nabla$  and the velocity vector  $\mathbf{U}$ , the equation is written as:

$$\boxed{\rho \frac{D\mathbf{U}}{Dt} = -\nabla \cdot \boldsymbol{\tau} - \nabla p + \rho \mathbf{g}} \quad (2.6)$$

The conserved total energy equation is given in x, y, z components as:

$$\begin{aligned} \frac{\partial}{\partial t} \left( \rho e + \frac{1}{2} \rho |\mathbf{U}|^2 \right) = & - \frac{\partial}{\partial x} \left[ u_x \left( \rho e + \frac{1}{2} \rho |\mathbf{U}|^2 \right) \right] - \frac{\partial}{\partial y} \left[ u_y \left( \rho e + \frac{1}{2} \rho |\mathbf{U}|^2 \right) \right] - \frac{\partial}{\partial z} \left[ u_z \left( \rho e + \frac{1}{2} \rho |\mathbf{U}|^2 \right) \right] \\ & - \left[ \frac{\partial}{\partial x} q_x + \frac{\partial}{\partial y} q_y + \frac{\partial}{\partial z} q_z \right] + \rho (u_x g_x + u_y g_y + u_z g_z) - \left[ \frac{\partial}{\partial x} \rho u_x + \frac{\partial}{\partial y} \rho u_y + \frac{\partial}{\partial z} \rho u_z \right] \\ & - \left[ \frac{\partial}{\partial x} (\tau_{xx} u_x + \tau_{xy} u_y + \tau_{xz} u_z) + \frac{\partial}{\partial y} (\tau_{yx} u_x + \tau_{yy} u_y + \tau_{yz} u_z) + \frac{\partial}{\partial z} (\tau_{zx} u_x + \tau_{zy} u_y + \tau_{zz} u_z) \right] + \rho S \end{aligned} \quad (2.7)$$

The above derived formulation is then transformed into the vector notation, which is written as follows:

$$\boxed{\rho \frac{De}{Dt} = -(\boldsymbol{\tau} [\nabla \otimes \mathbf{U}]) - p(\nabla \cdot \mathbf{U}) - \nabla \cdot \mathbf{q} + \rho S} \quad (2.8)$$

## 2.4. RADIATION HEAT TRANSFER

The radiation heat transfer processes are important and cannot be ignored, because they are concerned with the exchange of thermal energy. The heat transfer through radiation takes place in the form of electromagnetic waves, which (in contrast to conduction or convection heat transfer) requires no medium. The intermediaries are photons, which travel at the speed of light. The radiation heat transferred into and out of an object is a function of several components like surface reflectivity, emissivity, surface area, and temperature. For many purposes, it is important to calculate or simulate the radiation heat transfer between bodies. In the following

sections of our thesis, we will explain the several radiation heat transfer models that are performed in OpenFOAM [56].

Radiation only effects the boundaries through surface-to-surface radiation exchange. The radiation models of the simulation are based on the (radiosity method). The method relies on two assumptions that allow the radiosity (radiant energy abandoning a surface, represented as  $J$ ), and the irradiation (incidental radiant energy, represented as  $G$ ) of a specific surface, to be defined as  $k$ . This is calculated as follows:

$$J_k = \varepsilon_k \sigma T^4 + (1 - \varepsilon) G_k \quad (2.9)$$

$$G_k = \sum_{i=1}^N F_{ki} J_i \quad (2.10)$$

The view factors,  $F_{ki}$  depend on the geometry, defined as:

$$F_{ki} = \frac{A_k}{A_k} \int_{A_k} \int_{A_i} \frac{\cos \theta_k \cos \theta_i}{\pi S^2} dA_k dA_i \quad (2.11)$$

OpenFOAM uses positive values for the heat flux entering the surface, written as  $\dot{q}_{\text{rad}, k} = G_k - J_k$ , by [57].

### 2.4.1. RADIATION HEAT TRANSFER SOLVER

The solvers simulate radiation heat transfer. The buoyantSimpleFoam solver (which is used at steady-state buoyant turbulent flow of compressible fluids to transfer heat) and buoyantSimpleRadiationFoam solver are almost the same solver just with the added radiation heat transfer.

### 2.4.2. RADIATION MODELS

There are several radiation models available in the OpenFOAM program. The models are widely applied and are described in the following.

#### 2.4.2.1. NO RADIATION MODEL

This model sets member functions ( $R_u$ ) and ( $R_p$ ) equal to zero. Therefore, the additional term of the enthalpy equation ( $S_h$ ) becomes 0. The original enthalpy equation will be unaffected by adiation, as it runs without the influence of radiation heat transfer. Those functions of ( $R_u$ ) and

( $R_p$ ) are defined based on the different radiation models.

Here,  $R_u$  represents the constant part of the source term component, which is added to the enthalpy equation, and the term  $R_p$  represents the source term component that goes with  $T^4$ .

#### **2.4.2.2. FINITE VOLUME DISCRETE ORDINATES MODEL**

The fvDOM model is another radiation model implemented in OpenFOAM. In this model, the radiative heat transfer equation is solved for a discrete number of finite solid angles. It is a conservative method that leads to a heat balance for a coarse discretization. The accuracy is increased by using a finer discretization that accounts for scattering, semi-transparent media, specular surfaces, and wavelength-dependent transmission, using banded-gray option. However, in this model, we need many ordinates for CPU-intensive.

#### **2.4.2.3 P1 MODEL**

The main assumption of this model is that the directional dependence in the radiative transfer equation is integrated out, which results in a diffusion equation for incident radiation. The P1 model has many merits, including that the radiative heat transfer equation is easy to solve with little CPU demand, and it works reasonably well in application. These models can be used in combustion where the optical thickness is large. Besides this, there are both advantages and limitations to using this model: It assumes all surfaces are diffuse, if the optical thickness is small it may result in a loss of accuracy (depending on the complexity of the geometry), and it tends to over predict radiative fluxes from localized heat sources or sinks.

#### **2.4.2.4 VIEW FACTOR MODEL**

In addition to the no-radiation model, finite volume discrete-ordinate method (fvDOM), and P1 model, OpenFOAM has an implementation with another model type; a view factor model to simulate the heat transfer between surfaces. The method begins with the generation of rays between discrete faces of the surfaces, then calculates by summing energy exchanges between ray endpoints. The benefit of this model approach is that energy is only exchanged between parts of the surface that are directly visible to one another.

The view factor is the geometric function that describes the radiative contribution for the ray that accounts for ray length and face size orientation.

The model takes no account of any absorption, emission, or scattering of radiation in fluids. The computational time and memory requirements of the model is largely determined by the number of faces from which the rays emanate.



### 3 LITERATURE REVIEW

---

Heat exchangers are considered to be a fundamental piece of technology, used in a wide variety of industrial applications such as automobile engineering, aerospace engineering, chemical industries, air conditioning, gas turbines, and power plants, among other industries. The World's energy resources can be protected through good legislation and safety regulations, which should become obligations for all industrial countries. It is essential to make this a top priority by focusing on energy reduction through heat transfer enhancement, to achieve additional heat recovery by reducing emissions to an acceptable limit during the manufacturing process.

The plate-fin heat exchanger is a significant and essential part of the industrial field. It improves heat recovery performance via heat transfer enhancement in order to achieve the general objectives. The major challenges of this work are the lack of generalized heat transfer and pressure drop correlations for wavy fin type, particularly with small ranges of fin amplitude and short length fins.

In this chapter, we discuss our research carried out with the OpenFOAM program, to develop a new correlation that is related to the plate-fin heat exchanger. Many works of literature have already examined the fluid mechanics and the heat transfer characteristics. Regarding the Colburn  $j$  factor and Fanning friction factors  $f$ , the work of [1] provides a comprehensive review of this problem, providing a particular focus on the PFHE type, and the work of [28] provides an excellent introduction to the analysis of plate-fin heat exchangers. There is a significant database available that includes heat transfer performance in terms of Colburn  $j$  factor and Fanning factor  $f$  for different fin geometries in PFHE type. Additionally, there are a few researchers who have been developing correlations for different fin types.

#### 3.1. PLATE-FIN HEAT EXCHANGER

A plate-fin heat exchanger (PFHE) is a type of compact heat exchanger (CHE), which uses a plate and finned chambers to transfer energy between fluids. PFHE has multiple applications as previously mentioned. In the last 50 years, the compact heat exchanger has appeared in a wide variety of engineering applications due to its beneficial features, such as low weight, an area density greater than  $700 \text{ m}^2/\text{m}^3$  when operating in gas streams, and above  $300 \text{ m}^2/\text{m}^3$  when operating in liquid or two-phase streams. In 1930, the secondary surface plate and corrugation construction was established for aero-engine radiators, using dip soldered copper as the material

of construction. In early 1940, the introduction of the aluminum dip-brazing process came about, after which aircraft heat exchangers were manufactured using aluminum, resulting in a substantial reduction in weight. Thereafter, researchers continued to reduce the weight and volume by increasing the surface area density in the plate-fin heat exchanger in different applications, which was then applied during gas-gas heat exchange for cryogenic and chemical industry applications and was later extended to include boiling and condensation applications. In 1949, Trane (US) was the first company to manufacture dip brazing commercially, with five members of the organization are Chart Heat Exchanger USA, Kobe Steel Ltd Japan, Linde AG Germany, Nordon Cryogenic France, and Sumitomo Precision Products Co Ltd Japan, [63].

### 3.2. PFHE RELATED STUDIES

Extensive research into the plate-fin heat exchanger has been undertaken over the last eight decades, in order to understand the heat-transfer phenomena. The heat transfer and pressure drop are determined through dimensionless terms of Colburn  $j$  factor and friction factor  $f$ . However, several methods have been applied to investigate the fluid flow behavior and heat transfer in plate-fin heat exchangers. In this chapter, we will review some of the prominent research related to this type of heat exchanger, which are characterized by their varying study methods.

#### 3.2.1. PROPOSED CORRELATIONS STUDIES

A comprehensive review of the heat transfer problem was compiled from the available literature. The various geometric surfaces have been analyzed using a variety of analytical and numerical techniques, which are investigated at different thermal boundary conditions for developing flows and fully developed laminar flows. The most popular fins used in CHEs are plain fins, offset strip fins, louvered fins, and wavy fins. The thermohydraulic performance of the aforementioned fins is strongly dependent upon the geometric parameters and the flow parameters. [1] proposed the correlations for fully developed laminar flow in rectangular channels, with aspect ratios at 0.25, 5, 2/3, and 1. The correlations below are applied in this thesis to validate the numerical simulation results. The correlations for a finite difference method as proposed by Shah and London 1978 [1] are presented as follows:

$$Nu_T = 7.541(1 - 2.610\alpha^* + 4.970\alpha^{*2} - 5.119\alpha^{*3} + 2.702\alpha^{*4} - 0.548\alpha^{*5}) \quad (3.1)$$

$$Nu_H = 8.235(1 - 2.0421\alpha^* + 3.0853\alpha^{*2} - 2.4765\alpha^{*3} + 1.0578\alpha^{*4} - 0.1861\alpha^{*5}) \quad (3.2)$$

$$f Re = -24[1 - 1.3553\alpha^* + 1.9467\alpha^{*2} - 1.7012\alpha^{*3} + 0.9564\alpha^{*4} - 0.2537\alpha^{*5}] \quad (3.3)$$

Very little research has investigated the heat transfer and pressure drop in the plate-fin heat exchanger (PFHE). In this thesis, to develop a new correlation that predicts the heat transfer performance, our emphasis is placed on the wavy fin at different ranges of fin amplitude, due to their characteristic curved shape that promotes heat transfer. We have proposed a new correlation for heat transfer performance prediction during fluid flow, which is discussed in detail in next chapters. The most reliable source for experimental heat transfer performance (in terms of the Colburn  $j$  and Fanning factor  $f$  of the primary and secondary surfaces for combined heat exchangers) is Shah and London [1].

Wieting [35] developed the empirical relationships by correlating experimental heat transfer and flow friction data from 22 rectangular offset fin-plate heat exchanger configurations, over two Reynolds number ranges:  $Re < 1000$  (which is primarily laminar) and  $Re > 2000$  (which is primarily turbulent). The effects of fin length, height, thickness, spacing and hydraulic diameter are assessed through the performance. These relationships indicate that the flow passages aspect ratio is significant only in the laminar flow, and the fin thickness parameter to the hydraulic diameter ratio ( $\delta_f/D_h$ ) is significant only in the turbulent flow. The correlations may only be applicable when air or gas is the heat transfer fluid and when it is used only for limited extrapolation, as serious error may occur if the correlations are employed outside of the specific parameter range used in their development. New correlations have been developed by an empirical correlation of experimental heat transfer and flow friction data on 22 offset strip fin surfaces.

$$Re < 1000, \quad j = 0.483 \left( \frac{x}{D_h} \right)^{-0.162} \left( \frac{s_{fs}}{h_{fs}} \right)^{-0.184} (Re)^{-0.536} \quad (3.4)$$

$$f = 7.661 \left( \frac{x}{D_h} \right)^{-0.384} \left( \frac{s_{fs}}{h_{fs}} \right)^{-0.092} (Re)^{-0.712} \quad (3.5)$$

$$Re > 2000, \quad j = 0.242 \left( \frac{x}{D_h} \right)^{-0.322} \left( \frac{\delta_f}{D_h} \right)^{0.08} (Re)^{-0.368} \quad (3.6)$$

$$f = 7.661 \left( \frac{x}{D_h} \right)^{-0.384} \left( \frac{s_{fs}}{h_{fs}} \right)^{-0.092} (\text{Re})^{-0.712} \quad (3.7)$$

Alur [63] proposed other correlations for offset fin type at different flow regimes.

For laminar flow:

$$j = 0.36 \text{Re}^{-0.51} \left( \frac{h_{fs}}{s_{fs}} \right)^{0.275} \left( \frac{x}{s_{fs}} \right)^{-0.27} \left( \frac{\delta_f}{s_{fs}} \right)^{-0.0632} \quad (3.8)$$

$$f = 4.67 \text{Re}^{-0.70} \left( \frac{h_{fs}}{s_{fs}} \right)^{0.196} \left( \frac{x}{s_{fs}} \right)^{-0.181} \left( \frac{\delta_f}{s_{fs}} \right)^{-0.104} \quad (3.9)$$

For turbulent flow:

$$j = 0.18 \text{Re}^{-0.42} \left( \frac{h_{fs}}{s_{fs}} \right)^{0.288} \left( \frac{x}{s_{fs}} \right)^{-0.184} \left( \frac{\delta_f}{s_{fs}} \right)^{-0.05} \quad (3.10)$$

$$f = 0.32 \text{Re}^{-0.286} \left( \frac{h_{fs}}{s_{fs}} \right)^{0.221} \left( \frac{x}{s_{fs}} \right)^{-0.185} \left( \frac{\delta_f}{s_{fs}} \right)^{-0.023} \quad (3.11)$$

Manglik et al. [10] examined the heat transfer and friction data for 18 offset strip fin surfaces, which are presented in [28]. He also analyzed the effect of the various geometrical attributes of offset strip fins. The equations have been devolved to the asymptotic behavior of the data in deeper laminar and fully turbulent zones. These asymptotics are combined to give the single predictive equation for  $j$  and  $f$  factors, which are valid for laminar, turbulent, and transition zones;

$$j = 0.6522 \text{Re}^{-0.5403} \sigma^{-0.1541} \delta^{0.1499} \gamma^{-0.0678} \left[ 1 + 5.269 \text{Re}^{1.34} \sigma^{0.504} \delta^{0.456} \gamma^{-1.055} \right]^{0.1} \quad (3.12)$$

$$f = 9.6243 \text{Re}^{-0.7422} \sigma^{-0.1856} \delta^{0.3053} \gamma^{-0.2659} \left[ 1 + 7.66910^{-8} \text{Re}^{4.429} \sigma^{0.920} \delta^{3.767} \gamma^{0.236} \right]^{0.1} \quad (3.13)$$

$$\sigma = \left( \frac{s_{fs} - \delta_f}{h_{fs}} \right), \quad \delta = \left( \frac{\delta_f}{L} \right), \quad \gamma = \left( \frac{\delta_f}{s_{fs}} \right) \quad (3.14)$$

The above correlations (3.12) and (3.13) are valid at Reynolds number ranges between  $120 < \text{Re} < 10^4$ ,  $0.134 < \sigma < 0.997$ ,  $0.012 < \delta < 0.048$ , and  $0.041 < \gamma < 0.121$ .

Tinaut et al. [36] provided the relations to heat transfer and flow friction coefficients for plane parallel plates and offset strip-fin plates over the range that is used in compact heat exchangers. The proposed correlations allow one to adequately predict experimental data available for the heat exchanged and pressure losses in plate-type heat exchangers.

The proposed correlations continuously cover the full range of laminar and turbulent flow at both short and long pipes. The mathematical expressions proposed for the heat transfer coefficients over three Reynolds number ranges are: laminar ( $Re < 2000$ ), transitional ( $2000 < Re < 10000$ ) and turbulent ( $Re < 10000$ ). The heat transfer coefficient allows the computation of Nusselt number for short ducts, and for Reynolds numbers at several flow regions. The application of these heat transfer and friction factor expressions in a plate-type heat exchanger (with both parallel plates and offset strip fin plates) are in very good agreement with other referenced experimental data.

$$j = 0.0944Re^{-0.353} \quad (3.15)$$

$$f = 8Re^{-0.3} \quad (3.16)$$

Chennu [11] proposed the correlations for plain fin type.

$$100 \leq Re \leq 1000, \quad j = 0.454Re^{-0.977} \left( \frac{h_{fs}}{s_{fs}} \right)^{0.435} \left( \frac{\delta_f}{s_{fs}} \right)^{-0.227} \quad (3.17)$$

$$f = 12.892Re^{-1.229} \left( \frac{h_{fs}}{s_{fs}} \right)^{0.452} \left( \frac{\delta_f}{s_{fs}} \right)^{-0.198} \quad (3.18)$$

$$1000 \leq Re \leq 7500, \quad j = 0.166Re^{-1.011} \left( \frac{h_{fs}}{s_{fs}} \right)^{0.228} \left( \frac{\delta_f}{s_{fs}} \right)^{-0.366} \quad (3.19)$$

$$f = 3.133Re^{-1.236} \left( \frac{h_{fs}}{s_{fs}} \right)^{0.247} \left( \frac{\delta_f}{s_{fs}} \right)^{-0.181} \quad (3.20)$$

The heat transfer and friction factor correlations were presented for plain triangular fin surfaces of plate fins within a plate-fin heat exchanger by Rao et al. [41]. It would be prohibitively expensive and time-consuming to fabricate the heat exchanger cores and conduct experiments over reasonable ranges of the geometric variables. In contrast, it is relatively easy and cost effective to carry out a parametric study through numerical simulation to derive acceptable correlations. A numerical model has been developed for the triangular plain fin of a plate-fin heat exchanger. The CFD analysis is carried out using FLUENT 12.1. The Colburn  $j$  factor and fanning Friction factor  $f$  are calculated for different Reynolds number ranges, including in the laminar and turbulent regions. These values are compared with the data in the available literature to validate the results of the heat transfer performance.

The correlations have been expressed in terms of two separate equations  $j$  and  $f$  over the low and high Reynolds numbers with geometric parameters. The correlations for the Fanning friction factor  $f$  and Colburn  $j$  factor are in good agreement with other referenced sources.

$$300 \leq \text{Re} \leq 1000, \quad j = 0.718 \text{Re}^{-0.625} \left( \frac{h_{fs}}{s_{fs}} \right)^{0.765} \left( \frac{\delta_f}{s_{fs}} \right)^{-0.765} \quad (3.21)$$

$$f = 3.12 \text{Re}^{-0.852} \left( \frac{h_{fs}}{s_{fs}} \right)^{0.156} \left( \frac{\delta_f}{s_{fs}} \right)^{-0.184} \quad (3.22)$$

$$1000 \leq \text{Re} \leq 10000, \quad j = 0.789 \text{Re}^{-1.1218} \left( \frac{h_{fs}}{s_{fs}} \right)^{1.235} \left( \frac{\delta_f}{s_{fs}} \right)^{-0.764} \quad (3.23)$$

$$f = 2.69 \text{Re}^{-0.918} \left( \frac{h_{fs}}{s_{fs}} \right)^{0.355} \left( \frac{\delta_f}{s_{fs}} \right)^{-0.175} \quad (3.24)$$

Taler [34] developed the new correlations for the heat transfer coefficients on the air and coolant sides. The proposed methods for identification of heat transfer for both fluid and air sides are effective mathematical tools in determining new heat exchanger characteristics. A numerical method has been determined for the heat transfer coefficients in cross-flow heat exchangers with extended heat exchanger surfaces. The coefficients in the correlations defying heat transfer on the liquid and air side were determined using a nonlinear regression method and from the sum of the squared fluid temperature difference at the heat exchanger outlet, which are measured and calculated. The minimum of the squared sum was found using the Levenberg-Marquardt method. The correlation for the average heat transfer coefficient on the air side based on the experimental data was compared with the correlation obtained from CFD numerical simulation of the fluid and heat flow. The results revealed that the numerical predictions are in good agreement with the experimental data. The new correlations for the friction factors and the air side heat transfer coefficient for inline oval tube geometries with plain fins can be used in the design of air-cooled heat exchangers.

$$100 \leq \text{Re} \leq 1500,$$

$$\text{Nu} = 0.06963 \text{Re}^{0.6037} \text{Pr}^{1/3} \quad (3.25)$$

$$j = 0.08207 \text{Re}^{-0.4132} \quad (3.26)$$

Rao et al. [41] proposed the heat transfer correlations for triangular perforated fins. The perforations are made on plain triangular fins to study the effects of the heat transfer coefficient.

A numerical model has been developed for the perforated fin of a triangular plate-fin heat exchanger. Perforated fin performance has been analyzed with the help of computational fluid dynamics (CFD), by changing the various parameters of the fin type. The Colburn  $j$  factor and the Fanning friction factor  $f$  are calculated for different Reynolds number ranges. The correlations have been developed between Reynolds number, Colburn  $j$  factor, and fanning Friction factor  $f$  by taking into account the effects of various geometrical parameters, such as fin height  $h_{fs}$ , fin thickness, and fin spacing  $s_{fs}$ . The present numerical analysis is carried out for air media. For validation, a plain triangular fin with the same dimensions as those of the perforated fin has been analyzed using FLUENT 12.1. Afterwards, the characteristic curves were compared with the data from Kays and London. It was observed that both the curves have good agreement within  $\pm 7\%$  in  $j$  and about  $\pm 8\%$  in  $f$  values. These expressions are well formed in the laminar and fully turbulent regions, so they were considered the standard expressions, which are modified by correction factors. The values obtained from these expressions are in good agreement with the existing data. The correlations have been developed for Fanning friction factor  $f$  and Colburn  $j$  factor as a function of  $Re$ ,  $h_{fs}/s_{fs}$ , and  $\delta/s_{fs}$ .

$300 \leq Re \leq 1000$ ,

$$j = 0.544 Re^{-1.673} \left( \frac{h_{fs}}{s_{fs}} \right)^{2.278} \left( \frac{\delta_f}{s_{fs}} \right)^{-1.589} \quad (3.27)$$

$$f = 10.127 Re^{-1.588} \left( \frac{h_{fs}}{s_{fs}} \right)^{0.778} \left( \frac{\delta_f}{s_{fs}} \right)^{-0.868} \quad (3.28)$$

$1000 \leq Re \leq 10000$ ,

$$j = 7.579 Re^{-1.626} \left( \frac{h_{fs}}{s_{fs}} \right)^{1.185} \left( \frac{\delta_f}{s_{fs}} \right)^{-1.689} \quad (3.29)$$

$$f = 1.685 Re^{-0.798} \left( \frac{h_{fs}}{s_{fs}} \right)^{0.447} \left( \frac{\delta_f}{s_{fs}} \right)^{-0.276} \quad (3.30)$$

Shinde and Lin [33] developed correlations for Colburn  $j$  factor and Fanning friction factor  $f$ , using eight non dimensional parameters based on the experimental data for compact heat exchangers. Within the investigated parameters, it seems that both the  $j$  and  $f$  factors were better represented by two correlations in two flow regimes, and Reynolds number ranging between  $20 < Re < 80$ , and  $80 < Re < 200$ . The results support the conclusion that airflow and heat transfer at very low Reynolds numbers behaves differently from those at higher Reynolds numbers.

An experimental investigation has been undertaken into the heat transfer and pressure drop of compact heat exchangers with 26 samples of the corrugated louvered fin type. The test matrix was covered a fairly wide range of geometrical parameters such as the fin pitch, fin height, fin thickness, louver pitch, louver angle, louver length, tube height, and tube depth. All parameters used in the correlations were non dimensional and based on the louver pitch.

$20 \leq \text{Re} \leq 80$ ,

$$j = \text{Re}^{-0.324} \left( \frac{F_p}{L_p} \right)^{-0.2} \left( \frac{H}{L_p} \right)^{-2.3} \left( \frac{\delta}{L_p} \right)^{-0.001} \left( \frac{\theta}{90} \right)^{1.1} \left( \frac{L_d}{L_p} \right)^{1.72} \left( \frac{D_m}{L_p} \right)^{1.88} \left( \frac{F_d}{L_p} \right)^{-0.195} \quad (3.31)$$

$80 \leq \text{Re} \leq 200$ ,

$$f = \text{Re}^{-0.4} \left( \frac{F_p}{L_p} \right)^{-0.07} \left( \frac{H}{L_p} \right)^{-2.48} \left( \frac{\delta}{L_p} \right)^{-0.006} \left( \frac{\theta}{90} \right)^{0.09} \left( \frac{L_d}{L_p} \right)^{1.83} \left( \frac{D_m}{L_p} \right)^{1.65} \left( \frac{F_d}{L_p} \right)^{-0.012} \quad (3.32)$$

Chennu [11] proposed empirical correlations to estimate the characteristics of heat transfer and pressure drop in terms of Colburn  $j$  and Fanning  $f$  factors, and to describe the complex behavior of fluid flow in the wavy fin. The empirical correlations for heat transfer were performed by multiple linear regressions for wavy fin geometrical parameters. The investigation was carried out in different cases with air and water as the working fluids. The corresponding correlations are given as the following formulations, depending on the author:

$100 \leq \text{Re} \leq 800$ ,

$$f = 9.827 \text{Re}^{-0.705} \left( \frac{h_{fs}}{s_{fs}} \right)^{0.322} \left( \frac{2a_f}{s_{fs}} \right)^{-0.394} \left( \frac{l_w}{2a_f} \right)^{-0.603} \quad (3.33)$$

$$j = 2.348 \text{Re}^{-0.786} \left( \frac{h_{fs}}{s_{fs}} \right)^{0.312} \left( \frac{2a_f}{s_{fs}} \right)^{-0.192} \left( \frac{l_w}{2a_f} \right)^{-0.432} \quad (3.34)$$

$1000 \leq \text{Re} \leq 15000$ ,

$$f = 10.628 \text{Re}^{-0.359} \left( \frac{h_{fs}}{s_{fs}} \right)^{0.264} \left( \frac{2a_f}{s_{fs}} \right)^{-0.848} \left( \frac{l_w}{2a_f} \right)^{-1.931} \quad (3.35)$$

$$j = 0.242 \text{Re}^{-0.375} \left( \frac{h_{fs}}{s_{fs}} \right)^{0.235} \left( \frac{2a_f}{s_{fs}} \right)^{-0.288} \left( \frac{l_w}{2a_f} \right)^{-0.553} \quad (3.36)$$

Junqi et al. [68] proposed the correlations for wavy fin type:

$$f = 1.16\text{Re}^{-0.309} \left( \frac{\delta_f}{h_{fs}} \right)^{0.3703} \left( \frac{2a_f}{s_{fs}} \right)^{0.25} \left( \frac{l_w}{L} \right)^{0.326} \quad (3.37)$$

$$j = 0.0836\text{Re}^{-0.2309} \left( \frac{\delta_f}{h_{fs}} \right)^{0.1284} \left( \frac{2a_f}{s_{fs}} \right)^{0.153} \left( \frac{l_w}{L} \right)^{0.326} \quad (3.38)$$

Guo [31] proposed new correlations to estimate the values of heat transfer and pressure drop in terms of  $j$  and  $f$  factors. A three-dimensional computational fluid dynamics simulation and a neural network model are presented to investigate the behaviors of heat transfer and pressure drop for wavy-fin and flat-tube (WF/FT) heat exchangers. The accuracy of the calculations of the  $j$  and  $f$  factors is evaluated by the values of the Absolute Average Relative Deviation (AARD). These were 3.8% and 8.2% for the CFD simulation, and 1.3% and 1% for the neural network model. The correlations predicted the heat transfer performance for WFFT heat exchangers with good accuracy using Reynolds number, fin pitch, fin height, fin length, and wave length.

$$j = 0.0482\text{Re}^{-0.23725} \left( \frac{F_p}{F_h} \right)^{-0.1230} \left( \frac{L_d}{L} \right)^{-0.21835} \quad (3.39)$$

$$f = 0.4006\text{Re}^{-0.28666} \left( \frac{F_p}{F_h} \right)^{-0.09879} \left( \frac{L_d}{L} \right)^{-0.072543} \quad (3.40)$$

Here,  $F_p$ ,  $F_h$ ,  $L_d$ , and  $L$  define the fin pitch, fin height, wavy fin length, and wave length, respectively. Muppala [53] proposed a single  $f$  correlation and separate  $j$  correlation of wavy fin for both water and liquid refrigerant R134a as the working medium. The effect of the fin geometry such as fin spacing, fin height, wave height and wave length are investigated to enhance the heat transfer and pressure drop. The Colburn  $j$  factor and Fanning friction factor  $f$  correlations are proposed in terms of  $\text{Re}$  and geometry parameters ( $h_{f-s}/s_{f-s}$ ,  $a_f/s_{f-s}$ ,  $l_w/a_f$ ) for water and liquid refrigerant R134a. This type of wavy fin is widely used in the aerospace and automobile industries. The expressions provided for the heat transfer coefficient allow the computations for all values of the Reynolds number including in laminar and turbulent regions. The results conclude that the variation of  $f$  is less than 5%, whereas  $j$  varies up to 15%. The data for wavy fin surfaces shows significant non-linearity over the range of Reynolds numbers.

$$100 \leq \text{Re} \leq 1000,$$

$$\text{For R134 a} \quad j = 2.989 \text{Re}^{-0.54241} \left( \frac{h_{fs}}{s_{fs}} \right)^{-0.72276} \left( \frac{a_f}{s_{fs}} \right)^{-0.83914} \left( \frac{l_w}{a_f} \right)^{-0.7588} \quad (3.41)$$

$$\text{For Water} \quad j = 1.154 \text{Re}^{-0.65938} \left( \frac{h_{fs}}{s_{fs}} \right)^{-0.96698} \left( \frac{a_f}{s_{fs}} \right)^{0.176702} \left( \frac{l_w}{a_f} \right)^{0.28878} \quad (3.42)$$

$$f = 18.607 \text{Re}^{-0.59381} \left( \frac{h_{fs}}{s_{fs}} \right)^{-0.088954} \left( \frac{a_f}{s_{fs}} \right)^{-0.46976} \left( \frac{l_w}{a_f} \right)^{-0.9262} \quad (3.43)$$

1000 ≤ Re ≤ 15000 ,

$$\text{For R134 a} \quad j = 3.245 \text{Re}^{-0.66388} \left( \frac{h_{fs}}{s_{fs}} \right)^{-0.53614} \left( \frac{a_f}{s_{fs}} \right)^{-0.80626} \left( \frac{l_w}{a_f} \right)^{-0.6346} \quad (3.44)$$

$$\text{For Water} \quad j = 0.323 \text{Re}^{-0.69341} \left( \frac{h_{fs}}{s_{fs}} \right)^{-0.9602} \left( \frac{a_f}{s_{fs}} \right)^{0.633246} \left( \frac{l_w}{a_f} \right)^{0.889252} \quad (3.45)$$

$$f = 24.413 \text{Re}^{-0.46532} \left( \frac{h_{fs}}{s_{fs}} \right)^{-0.226497} \left( \frac{a_f}{s_{fs}} \right)^{-0.94256} \left( \frac{l_w}{a_f} \right)^{-1.70937} \quad (3.46)$$

### 3.2.2 NUMERICAL AND ANALYTICAL STUDIES

Numerical methods play a major role in the analysis of heat transfer performance in plate-fin heat exchangers, which are cost-effective and fast. [15] suggested that the wavy fin could be a suitable choice as an optimization methodology for the design of compact heat exchangers, which is formulated with consideration of heat transfer area reservation. Gewande et al. [61] presented a two-dimensional numerical study of fully developed flow and heat transfer through a horizontal wavy surface. The flow and heat transfer characteristics do not show any dependence on the length of the periodic domain, which shows that the geometric and flow periodicity are the same. The flow in the channels was observed to be steady up to a critical Reynolds number, which is dependent the geometric configuration. The results concluded that the heat transfer rate is increased, and the effect of the surface waviness is present on flow separation, pressure drop and heat transfer. Stone and Vanka [45] analyzed flow and heat transfer in a wavy passage, using an accurate numerical scheme that solves the two-dimensional unsteady flow and energy equations, by developing flow that are presented for two different wavy channels, each consisting of 14 waves.

The results reveal the effects of individually varying in the height, amplitude, and wave length of a selected wavy passage. Sui et al. [43] studied fully developed flow and heat transfer in periodic wavy channels with rectangular cross sections by using direct numerical simulation, which found that the steady flow is characterized by the formation of symmetric secondary flow, or Dean vortices when liquid flows, leading to chaotic advection. Mohamed et al. [64] numerically investigated the fluid flow and heat transfer in the entrance region in a converging-diverging channel with sinusoidal wall corrugations. In the channel entrance zone, the viscous constraint tangential and the local Nusselt number are characterized by a very fast decrease, and their amplitudes increase with the increasing of the wall corrugations and the Reynolds number. Ismail and Ranganayakulu [12] performed the computational fluid dynamics CFD analysis for compact wavy plate-fin heat exchangers using Fluent software. Additionally, they generated design data for eighteen different fin geometries such as plain fins, offset strip fins, louvered fins and wavy fins. The general heat transfers and pressure drop correlations have been developed using power law expressions. Further, the effect of the dimensionless geometrical parameters of the wavy fins has been studied in regard to thermos hydraulic performance, which was noted for higher Reynolds numbers. The value of both  $f$  and  $j$  decreased due to the diminishing of recirculation zones. Zhu, and Li [14] modeled and simulated, depending on the various types of enhancement surfaces of the plate-fin heat exchanger, such as the rectangular plain fin, strip offset fin, perforated fin and wavy fin. They took into account the fin thickness, thermal entry effect and end effect. The simulation was carried out at Laminar flow regime for Reynolds number ranges between 132.3-1323. The results reveal good agreement between the results of computations and correlations. Correlations of the thermal entry length for four PFHE fins are obtained by analyzing the variation of the local Nusselt number along the flow direction.

### 3.2.3. OPENFOAM STUDIES

The optimal design of a 3D-printed, high-temperature wavy fin for a plate-fin heat exchanger is based on the numerical simulation in the OpenFOAM program. Luo et al. [15] performed the radiation heat transfer in a plate-fin heat exchanger, which might have a negative effect on the thermal efficiency of heat exchangers due to longitudinal heat transfer from the hot-temperature end to the low-temperature end. The radiation heat transfer supplies an additional path from the fins to the plates, parallel to the thermal conduction through the fins.

The heat transfer mechanism benefits the heat exchanger by using the radiation model in a numerical simulation example, during which more than 2% enhancement in the heat duty is observed.

Ma et al. [65] performed the numerical simulation with the help of a frosting model for the wavy fin-and-tube heat exchanger surfaces, which was performed in OpenFOAM. The frost distribution on the wavy fin is obtained and no frost appears on the fin surfaces in the tube wake region due to the low water vapor concentration there. The simulated frost distribution agrees with the experimental observed frost distribution. The results concluded that the frost layer on the heat exchanger surface restricts the air flow and the pressure drop increases about 140% after 45 min frosting. The air flow pressure drop is larger for the wavy fin-and-tube heat exchanger than it is for the plain fin-and-tube heat exchanger.

#### **3.2.4. EXPERIMENTAL STUDIES**

One of the earliest and most comprehensive works carried out on compact heat exchangers is from Kays and London [28]. This authoritative and reliable source first predicted the heat transfer performance through the terms of Colburn  $j$  and Fanning friction  $f$  factors, via methods that are still used today for the geometries tested. PFHEs are widely used for their merits as described in chapter one. In the 1930s, the secondary surface in the tabulated step shape was established for aero-engine radiators, using dip soldered copper as the material of construction. In the 1940s, the aluminum dip-brazing process was introduced for the manufacture of aircraft heat exchangers using aluminum, and to reduce the weight and volume of heat the exchanger. Experiments involving the heat transfer over plate-fin surfaces are an expensive and difficult process. Further, it became necessary for us to develop the design methodology and manufacture the plate-fin heat exchangers.

Rush et al. [66] developed the design of the wavy passages, which obtained a better understanding of flow instabilities and heat transfer. Flow visualization experiments on twelve different geometries have revealed the flow patterns and behaviors in laminar flow, in wavy-channel passages at low Reynolds numbers. Heat transfer experiments confirmed that the instabilities observed in the flow visualization experiments could enhance the heat transfer in wavy channels. Tolentino et al. [67] performed an experimental investigation of the entrance section of the channels, formed with sinusoidal corrugations plates. A water tunnel and laser-

illuminated particle tracking was used as a technique of flow visualization. The phase angle that best promotes unsteady flow depends on the average distance between plates. A channel with eight waves is sufficiently long and the flow features presented in the first eight waves of a longer channel were similar.

Junqi et al. [68] studied an experimental plate-fin heat exchanger with wavy fins. The number of experimental samples was 16 wavy fin samples with different geometry parameters, including different fin heights, fin pitches, fin lengths, wavy amplitudes, and wavy lengths. Air and hot water were used as the working fluids. The main components of the systems were the heat exchangers, water flow loop, air supply, instrumentation, and data acquisition system. The wind tunnel system was designed to suck room air over the finned side of the heat exchanger with a 15-kW centrifugal fan. The speed of the fan was adjusted by a frequency inverter. The results revealed that the ratio of geometrical parameters that were evaluated (such as the ratio of the wavy amplitude, wavy length, fin height, fin pitch, and fin length) have great influence on the heat transfer and pressure drop.

### 3.3. HYDRAULIC DIAMETER

The hydraulic diameter is calculated as 4 times of the flow area divided by the perimeter of the conduit. The hydraulic diameter (hydraulic mean diameter) is used in a fluid that flows in a pipe, duct or any other shape. The general equation for hydraulic diameter  $D_h$  for all duct shapes is defined as the following:

$$D_h = \frac{4 \times \text{Free flow area}}{\text{Wetted perimeter}} = \frac{4A_c}{P} \quad (3.47)$$

The wavy fin surfaces are high-performance surfaces with performance quite similar to the louvered fin surfaces, and strip fin surfaces. The difference in the flow direction of the fin construction induced the turbulent flow and caused boundary layer separation with an effect similar to complete fin interruption [Manglik and Bergles 1995].

$$D_h = \frac{4s_{fs}h_{fs}l_w}{2(s_{fs}l_w + h_{fs}l_w + \delta_f h_{fs}) + \delta_f s_{fs}} \quad (3.48)$$

Sidramappa Alur [63] proposed the hydraulic diameter as the following formula:

$$D_h = \frac{2(s_{fs} - \delta_f)h_{fs}}{(s_{fs}l_w + h_{fs}l_w + \delta_f h_{fs})} \quad (3.49)$$

Kays and London [28] proposed the following formula:

$$D_h = \frac{4s_{fs}h_{fs}}{2(s_{fs} + h_{fs})} = \frac{2s_{fs}h_{fs}}{(s_{fs} + h_{fs})} \quad (3.50)$$



## 4 ANALYTICAL MODELING ANALYSIS

---

The importance of compact heat exchangers (CHEs) has been recognized in different specialized applications, as mentioned in previous chapters. Compact heat exchangers are a class of heat exchanger that incorporate a large amount of heat transfer surface area per unit volume. CHEs are popular due to their lightweight volume, high compactness and high performance. This high demand for CHEs has led to their cost-effective design and manufacturing techniques. The design of the heat exchanger determines the dimensions for the heat exchanger during each specific heat transfer and pressure drop application, through the use of the appropriate correlations. Nevertheless, there are no correlations available that could cover all the geometrical parameters of the design, which is required for designing a heat exchanger and predicting its heat transfer performance. Therefore, to reduce this problem to a classification problem, it's essential to propose a new correlation, covering the dimensions required for the design plate-fin heat exchanger (PFHEs). Our objective is to develop a new correlation to predict the heat transfer performance that is valid for the wavy fin in PFHE design and with various fin amplitudes (0, 1.5, 2, and 2.5 mm).

In the present chapter, we will develop three models that concentrate on the numerical and analytical methods. The mathematical model is based on the CFD simulation of the fluid flow and heat transfer using OpenFOAM to predict the heat transfer performance in terms of Colburn  $j$  factor. The physical constant is considered, as listed in the table 4.1 below. To develop new models, the value of the mean heat transfer coefficient ( $\alpha$ ) is required, which is an unknown value. We use the traditional model or simple model as described by other authors to calculate the mean heat transfer coefficient ( $\alpha$ ) and we utilize the Logarithm Mean Temperature Difference method (LMTD). The simple model calculation depends on the outlet temperatures and pressure, which are obtained from a simulation using OpenFOAM. Colburn  $j$  factor will be calculated through the MATLAB program. The numerical and analytical models' analyses for the counter-flow heat exchanger arrangement consider the effect of longitudinal wall conduction within their calculations. For validation of the developed models, they are compared with the available correlations developed by [1] and [28].

### 4.1. DATA REDUCTION

The governing equations calculated for the fluid side heat transfer for a single-pair wavy fin in PFHE are described in the following. The general equation for the hydraulic diameter  $D_h$  for

different wavy fin amplitude  $a_f$ , as seen in figures 4.1, is written as follows:

$$a_f \text{ ranges (1.5, 2, and 2.5 mm),} \quad D_h = \frac{2h_f s_{fs}}{h_{fs} \psi + s_{fs}} \quad (4.1)$$

$$a_f \text{ ranges (0),} \quad D_h = \frac{2s_{fs} h_{fs}}{h_{fs} + s_{fs}} \quad (4.2)$$

The basic heat exchanger design equation describes the heat transfer capacity of the fin, which is defined as  $Q = KA\Delta T_{LM}$ . It is used to calculate the required overall heat transfer coefficient, which is based on the temperature's potential  $(T_h - T_c)$ , and a unit's total area of fluid flow. The overall heat transfer coefficient  $K$  is a known value of the other three parameters such as  $Q$ ,  $A$  and  $\Delta T_{LM}$  which is an abbreviation of the Logarithmic Mean Temperature Difference. The rate of heat transfer is represented through the heat duty  $Q$  between the hot and cold fluid flow of the stream, and  $A$  denotes the heat transfer area.

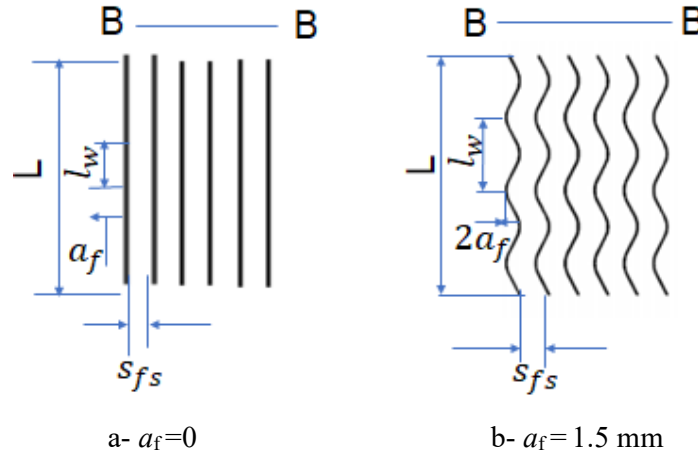


Figure 4.1: Shows the wavy fin at different fin amplitudes.

In the case that there are no fouling layers, the equation of the heat transfer capacity will be simplified.

$$\frac{1}{KA} = \frac{1}{R_h} + \frac{1}{R_w} + \frac{1}{R_c} \quad (4.3)$$

$$\frac{1}{KA} = \frac{\Delta T_{LM}}{Q} = \frac{1}{\alpha_h \eta_{0-h} A_h} + \frac{\delta_p}{\lambda_p / A_p} + \frac{1}{\alpha_c \eta_{0-c} A_c} \quad (4.4)$$

The constant physical properties have been assumed for both hot-fluid flow and cold-fluid flow. Furthermore, to reduce the possible creep deformation of the plates that separate the two fluids,

we use the same fin geometries for these passages. The geometry parameter of the wavy fin flow is shown in figure 4.2. Since the flow rates, fluid properties and fin geometries in both flow passages are the same, the heat transfer coefficient for hot fluid is equal to the heat transfer coefficient for the cold fluid as  $\alpha_h = \alpha_c = \alpha$ . The overall efficiency of the fin for both fluid flows are also the same as  $\eta_{0-h} = \eta_{0-c} = \eta$ , where the average wall area (the plate between hot and cold gas channels) is denoted as  $A_w = (s_{fs} + \delta_f)L$ . Additionally, the heat transfer area for the cold-flow side is equal to the hot-flow side as  $A_h = A_c = A$ , which is calculated depending on the formula  $A = 2(h_{fs}\psi_f + s_{fs})L$ .

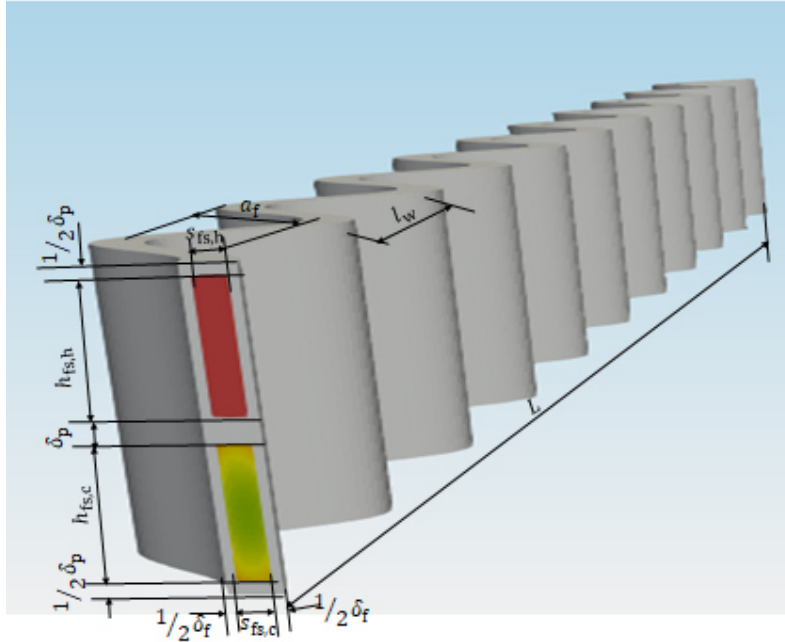


Figure 4.2: Shows the perspective view of the computational domain with geometrical parameter of the single pair wavy channel.

The ratio of the waviness length to the fin length is defined as the fin surface enlargement factor, which is denoted as  $\psi_f = l_w/L$ .

The sine function of the wavy fin is formed as  $y = a_f \sin(2\pi x/l_w)$ . The surface enlargement for the sine wavy fin is calculated according to the following equation from Luo et al. [15]:

$$\psi_f = \frac{2}{\pi} \int_0^{\pi/2} \sqrt{1 + (2\pi a_f / l_w)^2 \cos^2 \theta} d\theta \quad (4.5)$$

#### 4.1.1. HEAT TRANSFER PERFORMANCE

The flow regime is important to set up the numerical simulation. Therefore, the Reynolds number is the mandatory parameter for the solution. The characteristic of the hydraulic diameter is calculated for the rectangular and wavy fin types. The Reynolds number is calculated as the following expression:

$$Re = \rho u D_h / \mu \quad (4.6)$$

Here,  $u$  is the average velocity in the channel, based on the cross-sectional area and the properties of the fluid flow. The heat transfer coefficient is calculated depending on the outlet temperatures, which are found within the numerical simulation using the OpenFOAM program.

#### 4.1.2. STANTON NUMBER AND COLBURN $j$ FACTOR

The common terminology expression that has been applied to predict the thermal performance criteria is Colburn  $j$  factor. Further, to indicate the thermal performance of each fin type in the plate-fin heat exchanger, common thermal performance criteria are used, such as Stanton number  $St$  and Colburn  $j$  factor, which are given as the following:

$$j = \frac{Nu}{Re Pr^{2/3}} = St Pr^{1/3} \quad (4.7)$$

The Stanton number  $St$  is directly related to the heat transfer coefficient on one fluid-side of the exchanger, as follows:

$$St = \frac{\alpha}{Gc_p} \quad (4.8)$$

The heat transfer performance is defined in terms of the convective heat transfer coefficient as:

$$\alpha = \frac{\dot{q}}{|T_w - T_{fd,m}|} \quad (4.9)$$

#### 4.1.3. FANNING FRICTION FACTOR ( $f$ )

The pressure drop, used to calculate Fanning friction factor  $f$ , is based on an equivalent shear force in the flow per unit surface area, and it is given in the following expression:

$$f = \frac{\Delta p_f \rho D_h}{2L_d G^2} \quad (4.10)$$

## 4.2. CFD SIMULATION METHODOLOGY

The methodology of the plate-fin heat exchanger's design is based on the numerical simulation of fluid flow and heat transfer using OpenFOAM software. The additive manufacturing technique '3D-print of plate-fin heat exchangers' is used, with suitable thickness of fin and plate to produce an integrated compact heat exchanger unit. The numerical simulation depends on the finite volume method (FVM), to compute the outlet conditions of the flow such as the temperature of both fluids, pressure drop, and velocity. The fluid flow is required to satisfy the governing equations such as the mass conservation equation, the momentum conservation equation, and the energy conservation equation, which are described in Chapter 2.

One way to enhance the heat transfer on the air-side of the heat exchanger is to modify the fin geometry. Extended or finned surfaces are widely used in the compact heat exchanger to enhance the heat transfer and to reduce the size of exchanger. The wavy fin is one of the most popular fin types for PFHEs, particularly because of its superior heat transfer performance, particularly under the restrictions of a tight pressure drop allowance. The wavy-fin type has an uninterrupted surface in a cross-section shape, similar to that of plain fins except for the undulations in the flow direction. The proposed heat transfer enhancement techniques for the wavy fin are selected for their advantages over the other traditional fin types, such as (1) A surface enhancement located in passive methods that leads to high heat transfer coefficients (2) Its simple construction (3) Its economic benefits for industrial applications (4) The wavy fin has uninterrupted walls in each channel that are less likely than other types of fins (like the offset fin type) to catch particles that block the gas flow. For these reasons, in the current thesis we focus on the wavy fin.

Furthermore, currently this type of wavy fin is still not as widely used in applications as other types of fins, but in the near future, the wavy fin's application possibilities are set to expand [3]. For our purpose, we have studied two different types of fin geometry at fin amplitude zero, meaning the fin is a plain or rectangular duct, and at the fin amplitude ranges between (1.5, 2, and 2.5 mm), denoting that the fin is corrugated like the wavy fin.

#### 4.2.1. SETUP OF FIN TEST IN OPENFOAM

Extensive computations have been carried out using numerical simulations for various geometric parameters of the wavy fin, such as the fin amplitude  $a_f$ , fin space  $s_{fs}$ , and fin length  $L$ . The solver (chtMultiRegionFoam) is applied for solving the differential equations which describe the convective heat transfer in both the hot and cold fluid, and in parallel, the heat conduction within the wall. This conjugate heat transfer is studied neither under constant wall temperature nor constant heat flux boundary conditions as these conditions may only be applied to check existing correlations. In this simulation, we have neglected the influence of the heat radiation. This should be done in future work, as the possibility for high temperature applications may become increasingly important. The preprocessing sets up the mesh generation of the domain, and the post-processing takes care of the mean outlet gas temperatures and pressure drops. Version 3.0 is used for the post-processing. We have modeled and simulated the wavy fin geometry of the plate-fin heat exchanger with different geometrical parameters, considering fin amplitude  $a_f$ , fin thickness  $\delta_f$ , wave length  $l_w$ , fin height  $h_{fs}$ , and fin space  $s_{fs}$ . We have created a block mesh of the domain heat exchanger by using the OpenFOAM program version 2.2.1. The simulation terminated when the deviation between the last two files had reached a lower limit. The polynomial model in OpenFOAM is used to determine the properties of the fluids i.e., the density, isobaric specific thermal capacity, thermal conductivity and dynamic viscosity. The numerical simulation is carried out under three specified typical operating conditions on behalf of the inlet temperatures, pressures, and flow rates. We have adopted a variety of cases to develop models to accomplish our objectives, all cases are described in table 4.1.

Table 4.1: Geometrical parameters cases that are adopted in the present thesis.

Cases No.	$a_f$ (mm)	$s_{fs}$ (mm)	$l_w$ (mm)	$L$ (mm)
1	0	1	10	100
2	0	1.1	13	130
3	0	1.1	13	65
4	0	1.1	13	195
5	1.5	1.1	13	130
6	2.0	1.1	13	130
7	2.5	1.1	13	130
8	0	1.2	13	130

Table 4.2 includes all data for the flow property's conditions and some fixed geometrical parameters. The geometrical parameters on a single channel are illustrated in Fig. 3.

Table 4.2: Thermodynamic properties of the working fluid and wall materials with fixed geometrical parameters of wavy fin

Parameter	Variable	Unit	Value
Fin height	$h_{fs}$	Mm	8
Fin thickness	$\delta_f$	Mm	0.7
Plate thickness	$\delta_p$	Mm	1.5
Wave length	$l_w$	Mm	10-13
<b><u>Air, working fluid</u></b>			
Density	$\rho$	kg/m <sup>3</sup>	1.2
Specific Heat capacity	$c_p$	J/mK	1005
Thermal conductivity	$\lambda$	W/mK	0.026
Viscosity	$M$	Pa.s	$18 \times 10^{-6}$
Prandtl number	$Pr$	-	0.7
Inlet pressure	$P_{in}$	Bar	1.0
Inlet temperature- hot fluid	$T_{hot-in}$	K	303.15
Inlet temperature- cold fluid	$T_{cold-in}$	K	283.15
<b><u>Stainless steel (wall)</u></b>			
Density	$\rho_s$	kg/m <sup>3</sup>	7825
Specific Heat capacity	$c_{p-s}$	J/kg.K	460
Thermal conductivity	$\lambda_s$	W/mK	15

The computational domain of the three-dimensional wavy fin is simulated using OpenFOAM. The effectiveness and the heat transfer characteristics are determined by using the numerical simulation. The heat transfer area or frontal area is calculated depending on the fin geometry shape, as illustrated in figure 4.3. For the counter-flow heat exchanger, the results revealed that at Reynolds number 50, the outlet temperature for the hot gas reduced gradually until it reached the steady state at 16.36 °C, and at Reynolds number 2000, the outlet temperature for the hot gas reached the steady state at 19.09 °C.

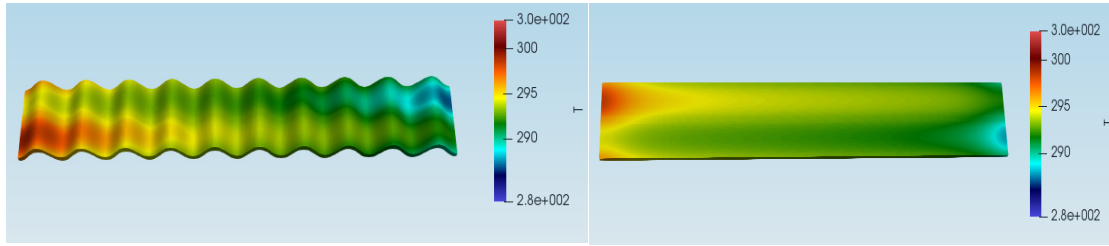
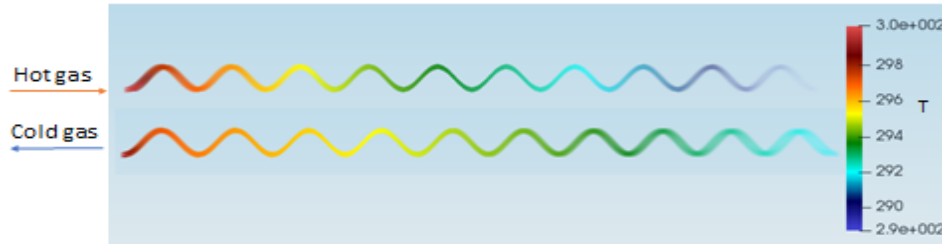
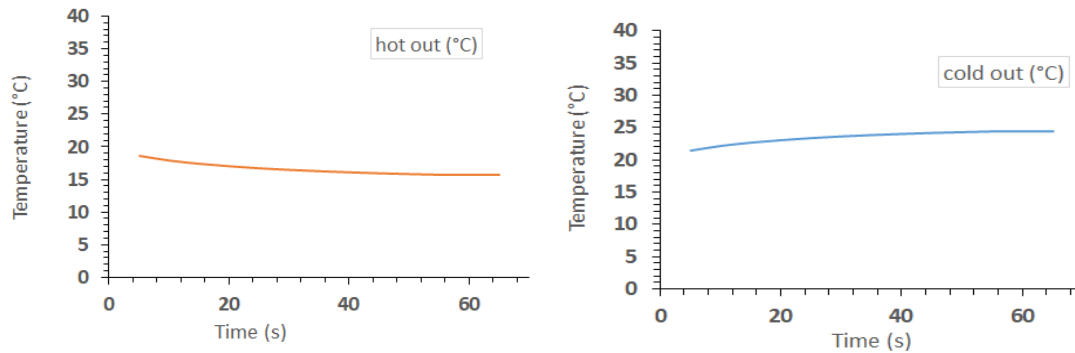
a- Wavy fin,  $a_f = (1.5, 2, \text{ and } 2.5 \text{ mm})$ b- Rectangular fin,  $a_f = 0$ 

Figure 4.3: Wall temperature distribution.

The outlet temperatures of a parallel-flow heat exchanger indicated two major disadvantages for this arrangement: The first is the large temperature differences at the ends of the heat exchanger which can cause high thermal stress, whereby the expansion and contraction of the construction materials due to the difference in temperature could eventually lead to material failure. The second is that the temperature of the cold fluid exiting the heat exchanger doesn't exceed the lowest temperature of the hot fluid, see in figure (4.4).



-a-



-b-

Figure 4.4: Temperature distributions for two fluids in a single channel.

The inlet temperatures of the hot and cold fluid flow are fixed in all cases at 30°C and 10°C, respectively. The results of the numerical simulation are reported accordingly for each case investigated in this work. A simulation example for a wavy fin at a different range of fin amplitude in the plate-fin heat exchanger is shown in the figures above.

Table 4.3 includes the outlet simulation results for air as the working fluid. The solid wall of the plate and fin is constructed from stainless steel. The negative signs in the cold-gas outlet velocity values are indicated to the opposite direction.

Table 4.3: Simulation results for counter flow heat exchanger of fluids, at geometrical parameters case  $a_f=0$ ,  $s_{fs}=1,1$  mm,  $l_w=13$  mm.

Re	HotGas			ColdGas		
	$u_{out}$ , m/s	$\Delta P$ , Pa	$T_{out}$ , K	$u_{out}$ , m/s	$\Delta P$ , Pa	$T_{out}$ , K
50	0.39	9.77	288.76	-0.39	9.77	297.53
70	0.54	13.7	288.24	-0.54	13.7	298.05
100	0.78	19.7	287.83	-0.78	19.7	298.46
150	1.16	29.7	287.66	-1.16	29.7	298.63
200	1.55	40	287.80	-1.55	40	298.49
300	2.33	61	288.39	-2.33	61	297.90
500	3.88	105	289.79	-3.88	105	296.49
700	5.43	151	291.03	-5.43	151	295.24
1000	7.76	225	292.51	-7.76	225	293.75
1500	11.63	362	294.23	-11.63	362	291.98
2000	15.51	513	295.38	-15.51	513	290.77

Several simulations were performed with different geometrical parameters for wavy fins using the OpenFOAM program. Around (176) calculations were accomplished for the counter-current-flow heat exchangers, the laminar model was applied in OpenFOAM with Reynolds numbers ranging between (50-2000).

### 4.3. NUMERICAL SIMULATION ANALYSIS

A numerical simulation approach is presented for the heat transfer performance of fluid flow. The same constant properties as well as the mass flow rates are set for the hot and cold fluid flow the fin geometrical parameters are assumed the same for a single pair of wavy channels as  $(a_f, h_{fs}, s_{fs})$ .

The major work of this research relies heavily on the numerical simulation to predict the behavior of the heat transfer of fluid flow in terms of Colburn  $j$  factor and Fanning friction factor  $f$  at developing flow region and fully developed flow region.

#### 4.3.1. DEVELOPING FLOW AND FULLY DEVELOPED REGIONS

The CFD numerical results validated through comparison with the experimental data from the current literature. Shah and London [1] obtained the combined hydrodynamic and thermal entry length solutions for rectangular ducts.

Table 4.4 includes the data of the boundary condition based on constant axial wall heat flux  $H1$ . The mean Nusselt number is defined as  $Nu_{m, H1}$ , and the Local Nusselt number is defined as  $Nu_{x, H1}$ . In the present thesis, validation is considered for the aspect ratio  $a^*=0.1375$ . The dimensionless axial distance in the flow direction for the hydrodynamic entrance region is given in the table below.

The term  $x^+$  represents the duct length required to reach a duct section maximum velocity at the fully developed magnitude when the entering flow is uniform. To validate our CFD results the variation range of aspect ratio  $a^*=s_{f-s}/h_{f-s}$  is written in table 4.4, in order to calculate the heat transfer with respect to Colburn factor  $j$  at different boundary conditions, which are presented as constant heat flux  $j_{H1}$ , and at a constant wall temperature  $j_T$ . The results have been validated in the case of the fully developed region and developing region at  $a^*=0.25$  in the literature.

The CFD numerical results validated through comparison with the experimental data from the current literature. Shah and London [1] obtained the combined hydrodynamic and thermal entry length solutions for rectangular ducts.

Table 4.4: Data from developing Laminar is used for our analysis results, the data is presented at fin amplitude  $a_f=0$  as rectangular duct shape, and at a different aspect ratio by Shah and London 1978[1].

1 / x+	$Nu_{m,H1}$				$Nu_{x,H1}$			
	$a^* = 1$	$a^* = 0.5$	$a^* = 1/3$	$a^* = 0.25$	$a^* = 1$	$a^* = 0.5$	$a^* = 1/3$	$a^* = 0.25$
5	4.60	5	5.57	6.06				
10	5.43	5.77	6.27	6.65	4.18	4.6	5.18	5.66
20	6.60	6.94	7.31	7.58	4.66	5.01	5.5	5.92
30	7.52	7.83	8.13	8.37	5.07	5.4	5.82	6.17
40	8.25	8.54	8.85	9.07	5.47	5.75	6.13	6.43
50	8.90	9.17	9.48	9.7	5.83	6.09	6.44	6.7
60	9.49	9.77	10.07	10.32	6.14	6.42	6.74	7
80	10.53	10.83	11.13	11.35	6.8	7.02	7.32	7.55
100	11.43	11.7	12	12.23	7.38	7.59	7.86	8.08
120	12.19	12.48	12.78	13.03	7.9	8.11	8.37	8.58
140	12.87	13.15	13.47	13.73	8.38	8.61	8.84	9.05
160	13.50	13.79	14.1	14.48	8.84	9.05	9.38	9.59
180	14.05	14.35	14.7	14.95	9.28	9.47	9.7	9.87
200	14.55	14.88	15.21	15.49	9.69	9.88	10.06	10.24
220	15.03	15.36	15.83	16.02				

The following correlations are used in the case of fully developed flow in laminar flow forced convection for rectangular ducts at fin amplitude zero. The correlations are developed by [1].

$$Nu_T = 7.541(1 - 2.610\alpha + 4.970\alpha^{*2} - 5.119\alpha^{*3} + 2.702\alpha^{*4} - 0.548\alpha^{*5}) \quad (4.11)$$

$$Nu_H = 8.235(1 - 2.0421\alpha + 3.0853\alpha^{*2} - 2.4765\alpha^{*3} + 1.0578\alpha^{*4} - 0.1861\alpha^{*5}) \quad (4.12)$$

The correlations are available according to the different boundary conditions at a constant wall temperature  $Nu_T$  and constant heat flux  $Nu_H$ . We have calculated the heat transfer in terms of Colburn  $j$  factor at developing region, which occurs at the entrance length of channel according to the following formula:

$$j = NuRePr^{1/3} \quad (4.13)$$

Figure 4.5 shows the validation of the numerical results with the literature in a different aspect ratio  $a^*$ , which demonstrates a good agreement between our case and the data from Shah and London and is written in table 4.4.

The figure below demonstrates that the trend line of  $j$  for our case at aspect ratio  $a^* = 0.1375$  is better than at the aspect ratio for the literature  $a^* = 0.25$ , which is presented in the fully developed region and dependent on the experimental data, as listed in Table 4.4. The aspect ratio parameter had a significant influence on the heat transfer performance. The passage of the fin is narrow enough that it can enhance and induce the turbulent flow in the channel and subsequently increase the heat transfer.

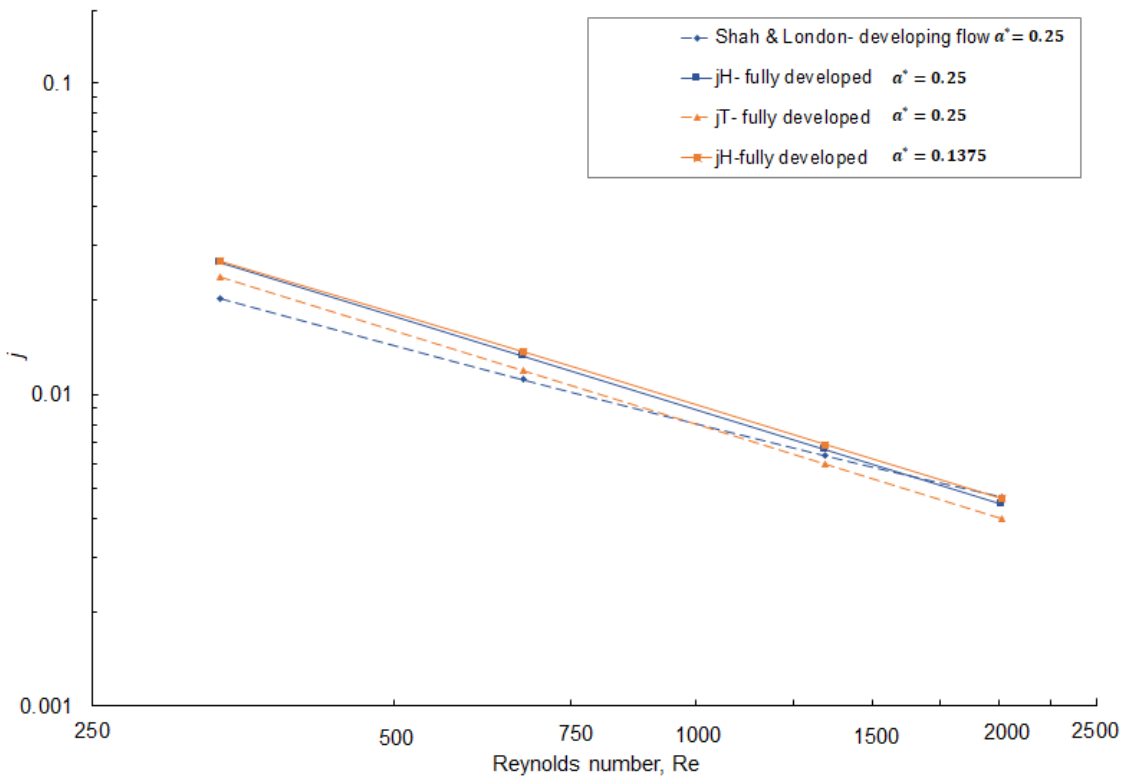


Figure 4.5: The experimental data from the current literature is written in Table 4.4. The comparison aspect ratio is at 0.25, and for our case at 0.1375.

To examine the trend of Fanning factor  $f$ , the Equation 4.15 uses fully developed flow with laminar flow forced convection at fin amplitude written as  $a_f=0$  for rectangular duct shape. The friction factor equation is not only dependent on the Reynolds number, but also on the shape of the cross-section duct, which is represented by [1].

$$f Re = -24 \left[ 1 - 1.3553a^* + 1.9467a^{*2} - 1.7012a^{*3} + 0.9564a^{*4} - 0.2537a^{*5} \right] \quad (4.14)$$

The experimental data from the available literature was used in present work to analyze the hydrodynamic problem for Fanning factor  $f$ . Table 4.5 shows the experimental data used for our simulation results analysis at fin amplitude  $a_f=0$  for rectangular fin type, to represent the relationship between  $fRe$  with  $1/x^+$  at aspect ratio  $a^*=0.2$ .

Table 4.5: The data at developing laminar flow for the rectangular duct when fin amplitude is zero [1].

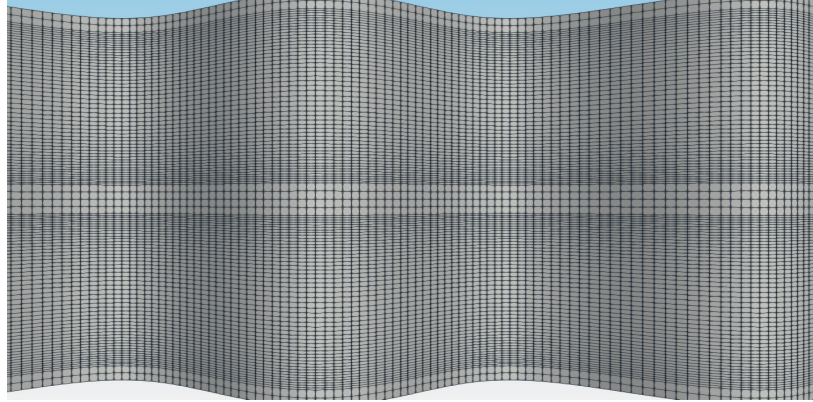
$fRe$				
$x^+=z/D_h Re$	$a^*=1$	$a^*=0.5$	$a^*=0.2$	$1/x^+$
0.001	111	111	111	1000
0.002	80.2	80.2	80.2	500
0.003	66	66	66.1	333.33
0.004	57.6	57.6	57.9	250
0.005	51.8	51.8	52.5	200
0.006	47.6	47.6	48.4	166.66
0.007	44.6	44.6	45.3	142.8
0.008	41.8	41.8	42.7	125
0.009	39.9	40	40.6	111.11
0.01	38	38.2	38.9	100
0.015	32.1	32.5	33.3	66.66
0.02	28.6	29.1	30.2	50
0.03	24.6	25.3	26.7	33.33
0.04	22.4	23.2	24.9	25
0.05	21	21.8	23.7	20
0.06	20	20.8	22.9	16.66
0.07	19.3	20.1	22.4	14.29
0.08	18.7	19.6	22	12.5
0.09	18.2	19.1	21.7	11.11
0.1	17.8	18.8	21.4	10

To validate the numerical simulation results of the Fanning friction factor  $f$  with the experimental data, the ratio of friction factor  $f$  from a developing flow region to a fully developed region is defined as  $f(x^+)/f_{s-L}$ . The term  $f(x^+)$  represents the simulation results of the fluid flow in the entrance of the channel, and  $f_{s-L}$  represents the results of the literature [Shah and London 1978] at a fully developed. The results conclude that at Reynolds number 50, the ratio of  $f(x^+)/f_{s-L}$  is approximately equal to 0.99, in contrast to Reynolds number 2000, where

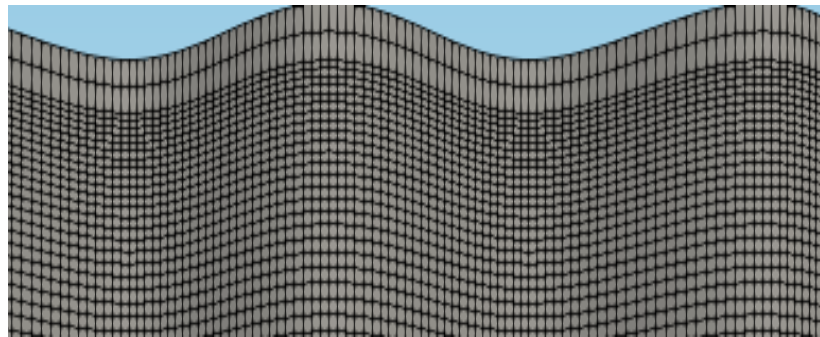
the ratio of  $f(x^+)/f_{s-L}$  increases to 2.46. The friction factor is more significantly affected at the developing entry region of the fluid flow than at the fully developed region.

#### 4.3.2. GRID SENSITIVITY

The grid structure is fine enough to resolve the heat transfer flow problem. In the present work, we have two mesh sizes to check the grid independence of the CFD numerical simulation. The first grid size was (number of points = 928353, number of cells = 864000, number of faces = 2655728, and number of internal faces = 2528272). The second mesh of the grid size was (number of points = 1628109, number of cells = 1536000, number of faces = 4699360, and number of internal faces = 4516640). The second mesh required around 120 seconds more time to reach a steady state than the first mesh. Each second in OpenFOAM is equivalent to two hours of real time. Figure 4.6 shows the two computational domains.



-a-



-b-

Figure 4.6: shows the mesh close to the wall.

Figure 4.7 shows the conditions of the output temperature, which were computed through OpenFOAM for both grid sizes as a result of a change in the number of divisions. The several geometrical parameters denoted above were adopted for the fin, the difference between the outlet temperatures for the two meshes were then generated.

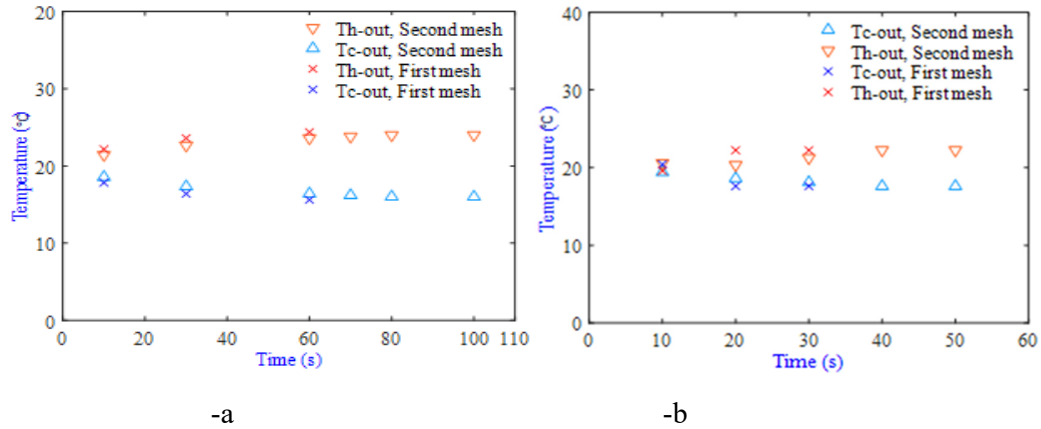


Figure 4.7: Shows the comparison of the two mesh generations by their outlet temperature results, which were obtained from numerical simulations for hot and cold fluids, (a) Re=50, (b) Re=2000.

The results revealed that the first mesh required less time (around 60 seconds) to reach the steady state than the second mesh, which reached the steady state at 100 seconds. The results were taken at Reynolds number 50 and at Reynolds number 2000. At the same Reynolds number, the first mesh reached the steady state 30 seconds faster than the second mesh, which required around 50 seconds. In fact, to achieve the steady state in the second mesh took more than 120 seconds, meaning around one week of real time is required in order to obtain the results. In our calculation, the results were obtained in 100 seconds instead of 120 seconds. As previously mentioned, each second in OpenFOAM is the equivalent of two hours.

The results for case 5 regarding the Colburn  $j$  factor for the two mesh are illustrated in Figure 4.8. We can identify good agreement between the two meshes generated by the simulation, especially at high Reynolds numbers (there's deviation of about  $\pm 9\%$  at the lower Reynolds numbers (between 50-200)).

The results reveal heat transfer for the first grid size is better resolved than when using the second grid mesh, therefore we have used the first mesh in all numerical simulations to achieve our objectives.

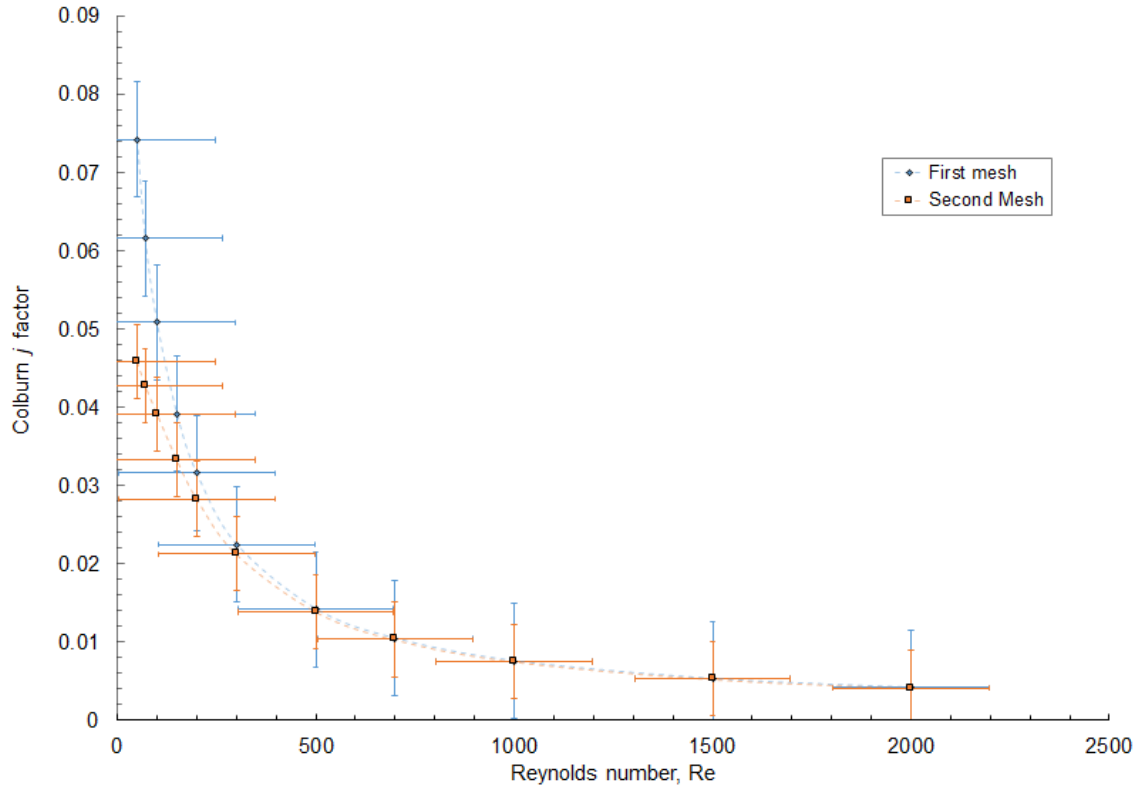


Figure 4.8: The heat transfer performance in terms of Colburn  $j$  factor comparison between two mesh generations.

#### 4.4. MODELS FORMULATION APPROACH

During this thesis, models will be developed to calculate the heat transfer coefficient in terms of Colburn  $j$  factor, taking into account the effect of longitudinal heat conduction for both plate and fin cross-section areas within the calculations. The MATLAB program prepared each model with the essential equations to calculate the heat transfer in term of Colburn  $j$  factor. Our motivation is to develop new correlations for wavy fin type in a plate-fin heat exchanger with various fin amplitudes ranging (0, 1.5, 2, and 2.5 mm), through modifying the heat transfer conduction equation.

New correlations are proposed according to the developed models; a detailed explanation will be provided later within this section. Models will be calculated according to the heat transfer coefficient ( $\alpha$ ), which is calculated through model (1). The three models will be compared with the available data from Shah and London [1] and Chennu [11]. The literature was chosen for their respective fin type configurations. The Fanning friction factor  $f$  has been directly calculated from the CFD simulation results, no model has been developed for it.

#### 4.4.1. MODEL (1)

Model (1) is defined as a simple model or traditional model. The simple model has been discussed by various authors within the literature. The heat transfer performance in terms of Colburn  $j$  factor will be calculated separately for each model in our program. In this work, we use the simple model to calculate the mean heat transfer coefficient ( $\alpha$ ) through the simulation results. In the simple model, the longitudinal heat conduction effects of the plate and fin thickness are neglected. However, the heat transfer in terms of Colburn  $j$  factor is calculated one-dimensionally and takes into account the heat transfer conduction around the fin, which is also considered as the fin efficiency in its calculation. The steady state energy balance of the hot-fluid side and cold-fluid side is given as:

$$\frac{dE}{dt} = 0 = \dot{m}_h (h_{h,in} - h_{h,out}) + \dot{m}_c (h_{c,in} - h_{c,out}) = \dot{Q}_h - \dot{Q}_c \quad (4.15)$$

The heat transfer rate of the hot-fluid side and cold-fluid side is given as:

$$Q_h = (\dot{m}c_p)_h (T_{h,in} - T_{h,out}), Q_c = (\dot{m}c_p)_c (T_{c,out} - T_{c,in}) \quad (4.16)$$

If the heat exchanger is well insulated,  $Q_h$  and  $Q_c$  should be equal. Then, the heat lost by the hot fluid is gained by the cold fluid.

The numerical energy balance error is calculated according to the following expression:

$\varepsilon = |Q_h + Q_c| / Q$ , the error rate for calculations is approximately 0.15 %. Because of the same Reynolds number and geometry, we have  $\alpha_h = \alpha_c = \alpha$  and  $\eta_{0-h} = \eta_{0-c}$ . The equation (4.4) is therefore written as:

$$\frac{2}{\alpha \eta_0 A} = \frac{\Delta T_{LM}}{\dot{Q}} - \frac{\delta_p}{\lambda_w A_w} \quad (4.17)$$

In this model, we used the simulation results and the outlet temperatures are known. Therefore, the method of the log mean temperature difference is adopted for a counter flow exchanger (LMTD or  $\Delta T_{LM}$ ). The calculation of the first model is based on the logarithm mean difference temperature method, it is applied for the counter-flow heat exchanger arrangement, as shown in Figure 4.9. It is defined as following expression:

$$\Delta T_{LM} = \frac{\Delta T_1 - \Delta T_2}{\ln[\Delta T_1 / \Delta T_2]} \quad (4.18)$$

According to our assumptions, to solve the simple model, the mean heat transfer coefficients and the geometrical parameters of the fin in both flow paths are the same, and by substituting the heat load of the hot and cold gases as  $Q = (Q_h + Q_c)/2$  in eq. (4.17), it becomes:

$$\alpha = \frac{2}{\left[ \frac{\Delta T_{LM}}{Q} - \frac{\delta p}{\lambda_w A_w} \right] \eta_0 A} \quad (4.19)$$

The average heat transfer surface efficiency, or overall fin efficiency of the fin is denoted by the term  $\eta_0$ . It is related to the fin efficiency; the fin efficiency of the hot fluid is assumed to be the same as the cold fluid  $\eta_{0-h} = \eta_{0-c} = \eta_0$ .

$$\eta_0 = 1 - (1 - \eta_f) \frac{A_f}{A_t} \quad (4.20)$$

Here,  $A_f$  and  $A_t$  are defined as the heat transfer area per fin, and the total heat transfer area respectively. They are calculated depending on the following geometric configuration:

$$A_f = 2\psi h_{fs} L \quad (4.21)$$

$$A_t = 2(s_{fs} + \psi h_{fs}) \quad (4.22)$$

For the exchanger fins,  $a_f = 0$ ,  $\psi = 1$ .

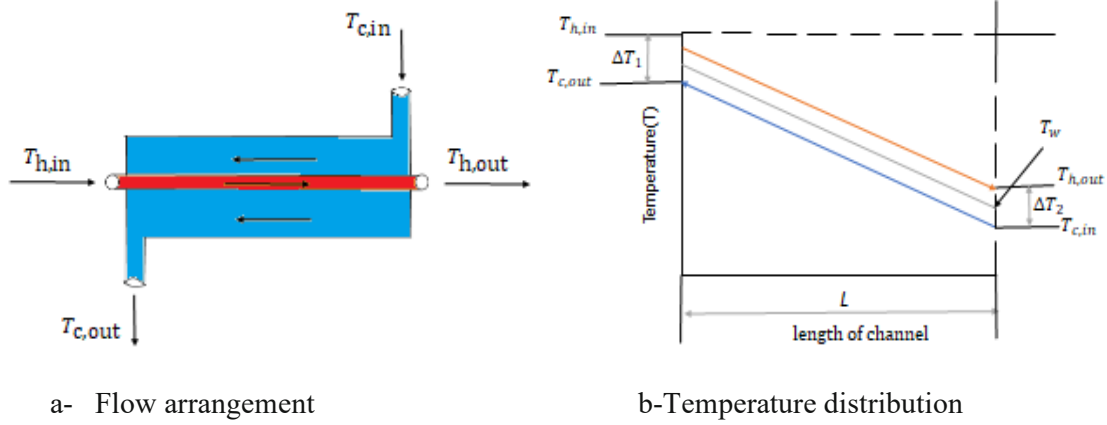


Figure 4.9: The counter flow arrangement.  $\Delta T_1 = (t_{h,in} - t_{c,out})$  and  $\Delta T_2 = (t_{h,out} - t_{c,in})$ .

The fin efficiency  $\eta_f$  is determined by using the available definition. The theoretical fin effectiveness  $\eta_f$  is derived from the assumption of thermal equilibrium at the fin  $\eta_f = Q_{actual}/Q_{ideal}$ . It is the actual heat transfer per maximum heat transfer for our case, it becomes the following formula [15]:

$$m = \sqrt{\frac{2\alpha}{\lambda_p \delta_f}} \quad (4.23)$$

$$\eta_0 = \frac{\tanh\left[\frac{h_{fs}\sqrt{\frac{2\alpha}{\lambda_f \delta_f}}}{2}\right]}{\frac{h_{fs}}{2}\sqrt{\frac{2\alpha}{\lambda_f \delta_f}}} = \frac{\tanh\left(\frac{h_{fs}m}{2}\right)}{\frac{h_{fs}}{2}m} \quad (4.24)$$

Here,  $m$  is the average fin effectiveness parameter, it is calculated depending on the fin type. Equation 4.24 represents the plain and wavy fin types.

#### 4.4.2. MODEL (2)

The analytical solution is applied to develop a new model. This method is adopted in our calculation because the fluid flow in a single pair of wavy channels will be at lower ranges of Reynolds numbers, particularly in laminar flow regimes. We utilize the manufacturing technique of 3D-printing for metallic plate-fin heat exchangers. In addition, the thickness of the

plate and fin is larger than usual, in the hope that the longitudinal heat conduction will have a significant influence on the heat transfer. The longitudinal heat conduction is considered in our calculation using MATLAB program. Model (2) is a more detailed model that still solves analytically and was achieved by applying the ordinary differential equation method (ODE). The analytical solution applied to develop the mathematical model through evaluating the simulation results was performed in OpenFOAM. The analytical solution is solved to obtain a new model through the ODE method by setting the energy balance equations, and modifying the heat transfer conduction equation.

Overall balance heat exchanger at stationary state,

$$\frac{dE}{dt} = \frac{du}{dt} = 0 \quad (4.25)$$

$$0 = \dot{m}h_{in} - \dot{m}h_{out} + \dot{Q} \quad (4.26)$$

$$0 = \dot{Q}_{loss} + \dot{m}_c (h_{c,in} - h_{c,out}) + \dot{m}_h (h_{h,in} - h_{h,out}) \quad (4.27)$$

Energy balance equation for each fluid separately:

- For cold fluid,

$$0 = \dot{Q}_{fluid} + \dot{m}_c (h_{c,in} - h_{c,out}) \quad (4.28)$$

- for hot fluid,

$$0 = \dot{Q}_{fluid} + \dot{m}_h (h_{h,in} - h_{h,out}) \quad (4.29)$$

The following assumptions have been made in the analytical solution; (1) Steady-state heat transfer of conduction has been assumed in one-dimension instead of the real temperature distribution in three-dimensions (2) The effect of the plate's thermal heat resistance will be added to the heat convection resistance form by dividing the plate thickness into two parts, one part close to the hot-fluid channel and the other part close to the cold-fluid channel (3) Cross-section area of the plate and fin thickness are combined, to verify the effect of the heat conduction significance on the total heat transfer. The energy balance equations were applied in the control volume on the entrance side and exit side of the fluid flow in the hot and cold single pair channels, as illustrated in figure 4.10.

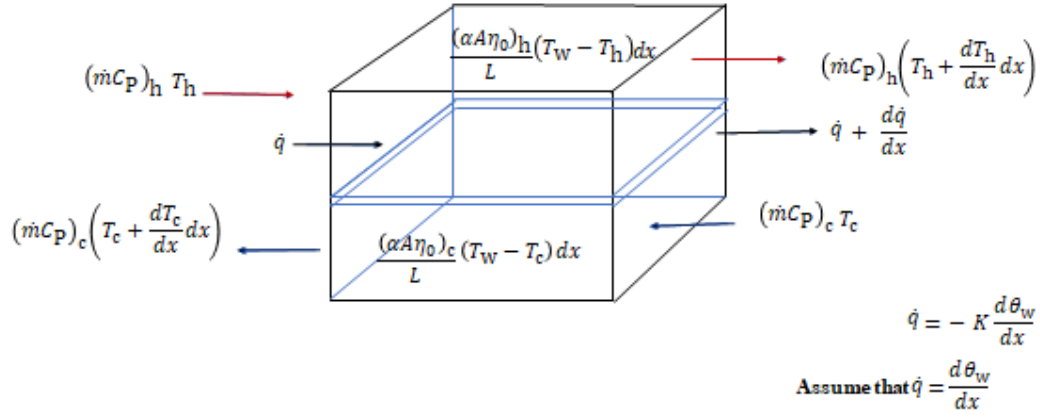


Figure 4.10: A differential control volume element represents the heat conduction, and the heat convection analysis in the counter-flow heat exchanger.

#### 4.4.2.1. ENERGY BALANCE (HOT GAS)

The model describes the steady-state convection in hot fluid for single channel. The heat transfer takes place between the temperature of the wall and the temperature of the hot fluid. The heat convection in the hot fluid is assumed in one-dimension, and takes into account the heat transfer coefficient, which is calculated depending on the CFD results because the outlet temperatures are known. Now that the heat transfer coefficient ( $\alpha$ ) is known, the Colburn  $j$  factor is calculated within the MATLAB program. The energy balance of the hot fluid channel is represented as follows:

$$(\dot{m}c_p)_h \frac{dT_h}{dx} + \frac{(\alpha A \eta_0)_h}{L} (T_h - T_w) = 0 \quad (4.30)$$

#### 4.4.2.2. ENERGY BALANCE (COLD GAS)

The heat transfer convection in the cold fluid is assumed in one-dimension. The heat transfer takes place between the temperature of the wall and the temperature of the cold fluid. As the same procedures have been adopted in the hot fluid to calculate the heat transfer coefficient and Colburn factor  $j$ , the energy balance of the cold fluid channel is represented as follows:

$$(\dot{m}c_p)_c \frac{dT_c}{dx} - \frac{(\alpha A \eta_0)_c}{L} (T_c - T_w) = 0 \quad (4.31)$$

#### 4.4.2.3. ENERGY BALANCE METALLIC (PLATE AND FIN)

The model describes the steady-state heat conduction with different assumptions as mentioned: the cross-section area of the plate and the fin thickness have been combined to verify the heat conduction significance and the plate heat resistance effect, added by dividing the plate thickness into two parts. The heat transfer of conduction will take place in both sides of the fluid (hot and cold); between the temperature of the wall and the hot fluid on one side, and between the wall temperature and cold fluid on the other side. The heat will transfer from the higher temperature to the lower temperature by the mode of conduction, for each metal wall interacts with the adjacent hotter and colder streams, as shown in figure 4.11. The governing differential equation for the matrix wall temperature during the hot gas and the cold gas flow is presented as follows:

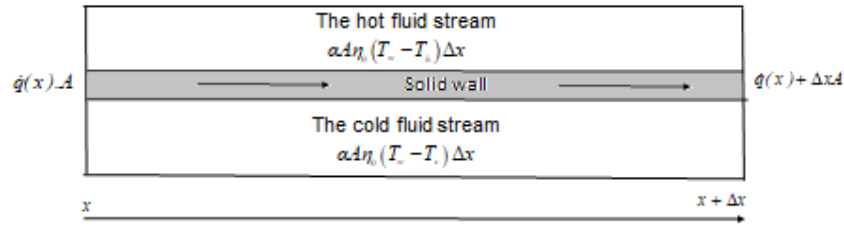


Figure 4.11: The schematic of the metal wall in two channels.

$$\frac{\lambda_m A_m}{(\dot{m} c_p)_h} \frac{d^2 T_m}{dx^2} - \frac{(\alpha A \eta_h)_h}{L (\dot{m} c_p)_h} (T_w - T_h) - \frac{1}{R_h} \frac{(\alpha A \eta_c)_c}{L (\dot{m} c_p)_c} (T_w - T_c) = 0 \quad (4.32)$$

In which  $A_m$  is the wall cross-section area of the plate and the fins.

#### 4.4.2.4. BOUNDARY CONDITIONS

To solve the new model analytically, we need to define the boundary conditions for hot and cold fluids and the wall as follows:

$$T_{h(x=0)} = T_{h-in}, \quad T_{c(x=L)} = T_{c-in} \quad (4.33)$$

The metal at the hot and cold ends of the heat exchanger may be adiabatic or staked to particular temperatures ( $T_w$  and  $T_{w-cold}$ ). The adiabatic condition assumes no heat lost or gained to the surroundings. However, the wall temperature  $T_w$  boundary condition is unknown and the heat flux  $\dot{q}$  is assumed to be zero,

$$\dot{q}_{x=0} = \dot{q}_{x=L} = 0, \quad (4.34)$$

$$\text{or} \quad \left( \frac{dT_w}{dx} \right)_{(x=0)} = 0, \quad \left( \frac{dT_w}{dx} \right)_{(x=L)} = 0 \quad (4.35)$$

#### 4.4.2.5. ANALYTICAL MODEL APPROACH

The heat-transfer coefficients change due to the alterations in the fluid-flow rates and the inlet fluid temperatures. Those may either be calculated experimentally or theoretically through LMTD and NTU methods. LMTD method is very useful for determining the size of the heat exchanger, LMTD method is used when the inlet and outlet temperatures of the fluids are known. For variable heat-transfer coefficients NTU varies and determined from the following:

$$NTU = \frac{1}{C_{\min}} \frac{1}{\frac{1}{(\eta_0 \alpha A)_h} + R_w + \frac{1}{(\eta_0 \alpha A)_c}} \quad (4.36)$$

The heat exchanger effectiveness is a property of number of transfer units (NTU), which is used to calculate the theoretical overall heat-transfer coefficient. In addition to the effectiveness, the ratio of  $C_{\min}/C_{\max}$  is needed; the smaller of the two heat capacity rates are

$C_c$  or  $C_h$ , and  $C_{\max}$  is the higher one. This method is used in the case that the outlet temperatures for the hot and cold gases are unknown. In this thesis, NTU is used to evaluate the simulation data results and to develop model (2). The  $\varepsilon$ -NTU method proposed by [28] uses three-dimensionless parameters to solve the heat exchange analysis, namely the heat capacity rate ratio  $R$ , effectiveness  $\varepsilon$ , and the number of transfer units NTU. The effectiveness of the heat exchanger is a function of the number of transfer units and the capacity ratio. The relationship between these three parameters depends on the type of heat exchanger and the internal flow pattern. The heat capacity rate ratio ( $R$ ) is defined as the ratio of the mass-flow rate for each

fluid multiplied by its heat capacity. The heat exchanger effectiveness is an important compact parameter used for characterizing the heat exchanger's performance, and it is a function for capacity ratio  $R$ ,  $NTU$ , and flow arrangement.

$$\varepsilon = \varphi (NTU, C^* = C_{\min}/C_{\max}, \text{ and flow - arrangement})$$

$$C_{\min}/C_{\max} = (\dot{m}c_p)_{\min}/(\dot{m}c_p)_{\max} = \begin{cases} (T_{c,o} - T_{c,i})/(T_{h,i} - T_{h,o}) & \text{for } (\dot{m}c_p)_h \leq (\dot{m}c_p)_c \\ (T_{h,i} - T_{h,o})/(T_{c,o} - T_{c,i}) & \text{for } (\dot{m}c_p)_c \leq (\dot{m}c_p)_h \end{cases} \quad (4.37)$$

Here,  $C^*$  is the heat exchanger operating parameter. It is dependent on the mass-flow rates or the temperatures of the fluid flow [18]. The  $NTU$  is defined as the ratio of overall thermal conductance of the minimum heat capacity rate; it is a non-dimensional size of heat transfer. Further, the theoretical heat transfer coefficient value ( $K$ ) is calculated by the following equation:

$$\left. \begin{aligned} NTU &= \frac{KA}{C_{\min}} \\ K &= \frac{((NTU)C_{\min})}{A} \end{aligned} \right] \quad (4.38)$$

To reduce the number of model parameters and simplify the above equations, the more common terminology of dimensionless quantities used in engineering analysis are defined as:

$$k = \frac{\lambda_w A_w}{(\dot{m}c_p)_h L}, \quad \theta = \frac{T - T_{c,i}}{T_{h,i} - T_{c,i}}, \quad NTU_h = \frac{(\alpha A \eta_0)_h}{(\dot{m}c_p)_h}, \quad NTU_c = \frac{(\alpha A \eta_0)_c}{(\dot{m}c_p)_c}, \quad R = \frac{(\dot{m}c_p)_h}{(\dot{m}c_p)_c} \quad (4.39)$$

As mentioned earlier, we have assumed the same mass flow rate and properties for both hot and cold fluids, therefore, we have  $R=1$ , and number of heat transfer units  $NTU_h=NTU_c=NTU$ .

To calculate the heat transfer in terms of Colburn  $j$  factor, we need the heat-transfer coefficient ( $\alpha$ ). So, it is assumed or calculated depending on the simple model, and then the Colburn  $j$  factor for analytical models can be calculated by preparing and implementing the MATLAB program and by substituting the equations (4.39) with the major heat equations (4.30, 4.31 and 4.32). The final forms of the governing equations are arranged as:

$$\frac{d\theta_h}{dx} + NTU_h (\theta_h - \theta_w) = 0 \quad (4.40)$$

$$\frac{d\theta_c}{dx} - NTU_c (\theta_c - \theta_w) = 0 \quad (4.41)$$

$$k \frac{d^2\theta_w}{dx^2} - NTU_c (\theta_w - \theta_h) - \frac{NTU_c}{R} (\theta_w - \theta_c) = 0 \quad (4.42)$$

The ordinary differential equations (ODE) method is used to solve the above differential equations, by integrating the above equations and substituting and arranging the dimensionless quantities, as written in formula (4.39). In equation (4.42), we have a second-order differential equation with respect to x dimension. It should be solved and separated into two equations instead of one. After it is solved, we have the wall temperature equation (4.43), and the heat flux equation (4.44), they are expressed below:

$$\frac{d\theta_w}{dx} + \frac{1}{k} \dot{q} = 0 \quad (4.43)$$

$$\frac{d\dot{q}}{dx} + NTU_c (\theta_w - \theta_h) + \frac{NTU_c}{R} (\theta_w - \theta_c) = 0 \quad (4.44)$$

One of the major purposes of this research is to modify the conduction equation by combining the cross-section area of the plate  $\delta_p$ , and fin  $\delta_f$  thickness by incorporating the presence of longitudinal heat conduction at the wall into the thermal effectiveness formula and the longitudinal conduction parameter  $k$ .

It combines the cross-section area of the plate and the fin thickness, as shown in figure 4.12.

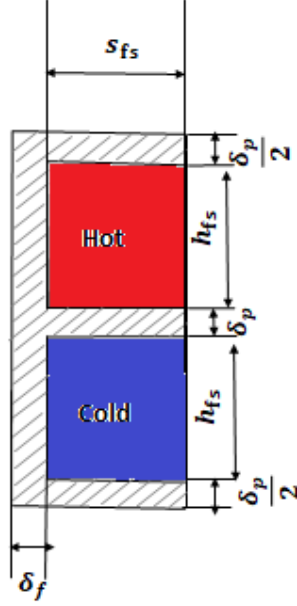


Figure 4.12: Cross-section area for plate and fin thickness.

Both the fin and plate thickness are greater than usual, they were 0.7 mm and 1.5 mm, respectively. These two geometrical parameter values were adopted for all cases to conduct the analytical solution. The longitudinal heat conduction cross-sectional area then becomes:

$$A_{c-p} = 2\delta_p(s_{fs} + \delta_f) \quad (4.45)$$

$$A_{c-f} = 2h_{fs}\delta_f \quad (4.46)$$

$$A_w = A_{c-p} + A_{c-f}/\psi \quad (4.47)$$

Here,  $A_{c-p}$  and  $A_{c-f}$  denote the cross-section area for plate and fin respectively. For the calculation of NTU, because of the assumption we have,  $NTU_h = NTU_c = NTU$ , in which the plate thickness resistance is added to the heat convection term by dividing it into two parts  $\delta_p/2$ , as illustrated in Figure 4.13.

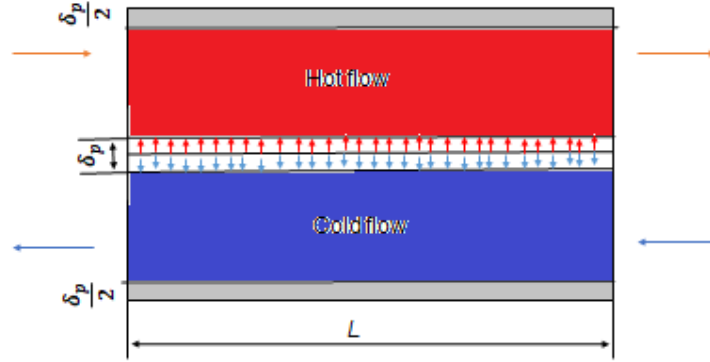


Figure 4.13: The split of the plate thickness.

$$NTU = \frac{\left[ \frac{1}{\alpha \eta_0 A} + \frac{\delta_p/2}{\lambda_w A_w} \right]^{-1}}{(\dot{m} c_p)} \quad (4.48)$$

Now all four equations (4.40), (4.41), (4.43) and (4.44) are included and arranged. These are converted into the matrix form  $\frac{d\theta}{dx} = [A\theta]$ , and prepared for the MATLAB program to solve.

$$\begin{bmatrix} \frac{d\theta_h}{dx} \\ \frac{d\theta_c}{dx} \\ \frac{d\theta_w}{dx} \\ \frac{d\dot{q}}{dx} \end{bmatrix} = \begin{bmatrix} -NTU_h & 0 & NTU_h & 0 \\ 0 & NTU_c & -NTU_c & 0 \\ 0 & 0 & 0 & -\frac{1}{k} \\ NTU_h & \frac{NTU_c}{R} & -\left(NTU_h + \frac{NTU_c}{R}\right) & 0 \end{bmatrix} \begin{bmatrix} \theta_h \\ \theta_c \\ \theta_w \\ \dot{q} \end{bmatrix}$$

We have applied our MATLAB program to solve the above system of equations and to obtain the value of the outlet temperatures of the fluids, the heat flux, and the wall temperature via evaluating the numerical data that was obtained from the simulation.

The analytical solution depends on the boundary conditions. Once the MATLAB program obtains the value of Eigenvector, we can then calculate the heat transfer coefficient in terms of Colburn factor  $j$  for the analytical model. As previously stated, the analytical solution depends on the boundary condition, identified in the MATLAB program.

By solving the above equation system together with the boundary condition, the outlet fluid temperatures can be obtained. The outlet temperature difference between the analytical solution and the numerical results from OpenFoam-simulation can then be used to determine the heat transfer coefficient used in the analytical solution.

#### 4.4.3. MODEL (3)

The numerical model is defined as model (3). It has been developed to find the effects of longitudinal thermal conductivity in 3D within the finite difference method (FDM). The MATLAB program is applied to calculate the heat transfer performance in terms of Colburn  $j$  factor through the model (3), which takes into account some assumptions that have already been adopted to solve the analytical solution. The effects of longitudinal thermal conductivity on heat transfer is studied in 3D instead of 1D for solid materials in the single-pair wavy channel. The comparison between the simple model, analytical model, and the present numerical model will be provided in more detail later, in order to show which model has a good agreement with the available literature. Model (3) is developed by combining the cross-section area of the plate and fin together. FDM method is used to develop the numerical model in each cell within the wall. The problem of longitudinal thermal conductivity can be investigated by knowing the distribution of the temperature within the solid wall, by applying the energy balance equation in each cell direction. A differential control volume is applied to find the solution of the differential equations. In the numerical model, the finite-difference method is used and it calculates the energy balance equation. The total heat transfer in each direction can be expressed as:

$$\left. \begin{aligned} Q_x &= \Delta y \Delta z \dot{q}_x = -\lambda_x \Delta y \Delta z \frac{\partial T}{\partial x} \\ Q_y &= \Delta x \Delta z \dot{q}_y = -\lambda_y \Delta x \Delta z \frac{\partial T}{\partial y} \\ Q_z &= \Delta x \Delta y \dot{q}_z = -\lambda_z \Delta x \Delta y \frac{\partial T}{\partial z} \end{aligned} \right\} \quad (4.49)$$

It is achieved by calculating the expressions in Equation 4.62 in the volume of  $\Delta x \Delta y \Delta z$ . The heat conduction equation for a steady-state system, expressed in cartesian coordinates, is as follows:

$$\frac{\partial}{\partial x} \left[ \lambda_x \frac{\partial T}{\partial x} \right] + \frac{\partial}{\partial y} \left[ \lambda_y \frac{\partial T}{\partial y} \right] + \frac{\partial}{\partial z} \left[ \lambda_z \frac{\partial T}{\partial z} \right] = 0 \quad (4.50)$$

In Eq. 4.50, the heat conduction problem in the solid material is solved with a directional variation of the thermal conductivity. The thermal conductivity is taken as a non-directional property: it is isotropic. For such materials in the present model, we write the heat conduction equation as the thermal conductivity constant at steady state. The governing equation for the present model is then represented as follows:

$$\left( \frac{\partial^2 T}{\partial x^2} + \frac{\partial^2 T}{\partial y^2} + \frac{\partial^2 T}{\partial z^2} \right) = 0 \quad (4.51)$$

The energy balance equations are applied in the control volume on the entrance side and exit side for each channel in 3D, as illustrated in Figure 4.14. The Finite difference method is used to analyze the effect of longitudinal heat conduction inside each cell within the solid wall material.

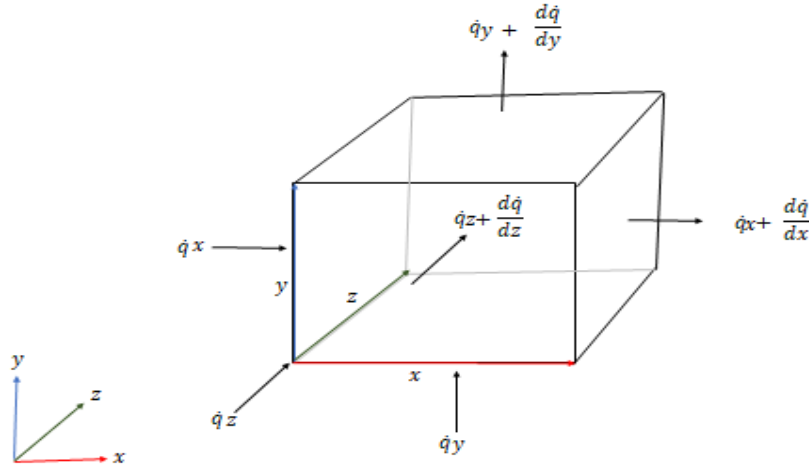


Figure 4.14: A differential control volume of solid material in 3D.

Through the MATLAB program, the heat transfer in terms of Colburn  $j$  factor for Model (3) is calculated and is determined by comparing with the CFD-simulation. Figure 4.15 shows the control size around the central point P through dashed lines in each cell inside the solid wall.

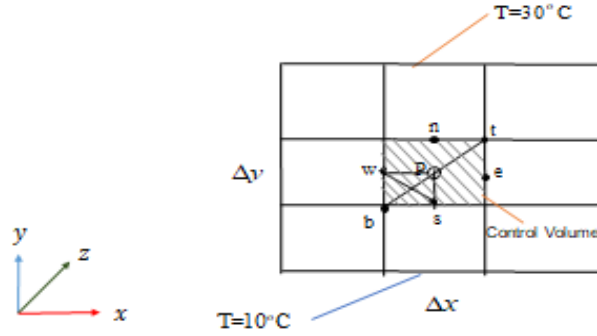


Figure 4.15: A differential control volume of wall material in 3D.

The temperature distribution in the solid material is calculated for each cell inside the wall; it is calculated in 3D. The given domain is divided into  $n$  numbers;  $n$  represents the number of finite elements in the control volume in the cells inside the solid wall. The energy equation is applied for the heat conduction at steady state with negligible viscous dissipation, and the control difference scheme is used.

$$0 = \frac{(T_E - 2T_P + T_W)}{\Delta x^2} + \frac{(T_N - 2T_P + T_S)}{\Delta y^2} + \frac{(T_T - 2T_P + T_B)}{\Delta z^2} \quad (4.52)$$

The discretization equation can be easily expressed in 3D grid points as follows:

$$0 = a_E T_E^0 + a_W T_W^0 + a_N T_N^0 + a_S T_S^0 + a_T T_T^0 + a_B T_B^0 - a_P T_P^0 + S_C \quad (4.53)$$

Equation (4.66) represents the point coefficients and the internal energy contained in the control volume, which indicates the sum of all the coefficients in the neighboring points, surrounding the central point  $P$ .

To calculate the temperature distribution in the single pair channels, we divide the fin space  $s_{f-s}$  in the x-direction, fin height  $h_{f-s}$  in the y-direction, and the fin length  $L$  in the z-direction. The calculations are made in a single pair of wavy channels, one channel for the hot-gas flow and other for the cold-gas flow. The divisions have been specified as  $x=9$  divisions,  $y=64$  divisions, and  $z=200$  divisions. The coordinate system  $(i, j, k)$  represents the exact location for the divisions in  $(x, y, z)$  in the MATLAB program. The numerical solution of the temperature discretization will be coupled with the energy equations of the hot and cold fluids as,

$$\dot{m}_h c_{p,h} \frac{dt_h}{dz} = \lambda_h A_{c,h} \frac{d^2 t_h}{dz^2} + 2\alpha_h \left[ \psi_{f-h} \int_0^{h_{f-h}} (t_w - t_h) dy + \int_0^{s_{f-h}} (t_w - t_h) dx \right] \quad (4.54)$$

$$\dot{m}_c c_{p,c} \frac{dt_c}{dz} = \lambda_{c,c} A_{c,c} \frac{d^2 t_c}{dz^2} + 2\alpha_c \left[ \Psi_{f,c} \int_0^{h_{f,c}} (t_w - t_c) dy + \int_0^{s_{fs}} (t_w - t_c) dx \right] \quad (4.55)$$

#### 4.4.3.1. CELL COEFFICIENTS CALCULATIONS

The MATLAB program is prepared with the computational procedures to calculate the numerical model, which is defined as model (3). The divisions in each direction in a single pair of wavy channels are dependent on some geometrical parameters, as mentioned above. The expressions below describe our procedures to achieve the temperature distribution in a solid wall in 3D. These have been arranged in our program. We then calculate the heat transfer in terms of Colburn  $j$  factor for the numerical model (3). The following calculations represent the coefficients for each cell inside the solid material, point coefficient P denotes the center point for each cell in 3D yields:

- 1- Point  $a_w$ , to find the temperature distribution for the solid wall in the fin thickness through x-direction of the channel, the formula below is calculated depending on the thermal conductivity of the solid wall, the fin spacing  $s_{fs}$  is divided by the number of divisions in the fin thickness  $n_f$ .

$$\begin{aligned} i > n_f + 1, a_{w(i,j,k)} &= \frac{\lambda_w}{(s_{fs}/2/n_f)/(s_{fs}/2/n_f)} \\ i = n_f + 1, a_{w(i,j,k)} &= \frac{\lambda_w}{(s_{fs}/2/n_f)/(\delta_f/2/n_f + s_{fs}/2/n_f) \times 2} \\ 1 < i < n_f + 1, a_{w(i,j,k)} &= \frac{\lambda_w}{(\delta_f/2/n_f)^2} \end{aligned}$$

- 2- Point  $a_e$ , to find the temperature distribution for the solid wall in the fin thickness through the x-direction of the channel, the formula below is calculated depending on the thermal conductivity of the solid wall, the fin space  $s_{fs}$  is divided by the number of divisions in the fin thickness  $n_f$ .

$$\begin{aligned} i < n_f, a_{e(i,j,k)} &= \frac{\lambda_e}{(\delta_f/2/n_f)^2} \\ j > n_{h-c} + n_p, a_{e(i,j,k)} &= \frac{\lambda_e}{(\delta_f/2/n_f) + ((\delta_f/2/n_f)^2/2/\lambda_w)} \end{aligned}$$

$$a_{E(i,j,k)} = \frac{\lambda_e}{\left( (\delta_f/2/n_{ft})^2 + (s_{fs}/2/n_{fs}) \times \delta_f/2/n_f \right) \times 2}$$

3- Point  $a_S$ , to find the temperature distribution for the solid wall in the fin thickness through the y-direction of the channel, the formula below is calculated depending on the thermal conductivity of the solid wall, the fin height  $h_{fs}$  is divided by the number of fin divisions  $n_f$ , and the number of plate divisions  $n_p$ . The plate thickness will be taken into account in the present point coefficient.

$$\begin{aligned} j > n_{fh-c} + n_{pt} + 1, a_{S(i,j,k)} &= \frac{\lambda_s}{(h_{fs-h}/2/n_f)/(h_{fs-h}/2/n_f)} \\ j = n_{fh-c} + n_{pt} + 1, a_{S(i,j,k)} &= \frac{\lambda_s}{(h_{fs-h}/2/n_{fh-h})/((\delta_p/n_p) + (h_{fs-h}/2/n_f) \times 2)} \\ j > n_{fh-c} + 1, a_{S(i,j,k)} &= \frac{\lambda_s}{(\delta_p/n_p)/(\delta_p/n_p)} \\ j = n_{fh-c} + 1 \text{ and } i \leq n_f, a_{S(i,j,k)} &= \frac{\lambda_s}{(\delta_p/n_p)/((h_{fs-c}/2/n_{fh-c}) + (\delta_p/n_p)) \times 2} \\ a_{S(i,j,k)} &= \frac{\lambda_s}{(h_{fs-c}/2/n_{fh-c})/(h_{fs-c}/2/n_{fh-c})} \end{aligned}$$

4- Point  $a_N$ , to calculate the temperature distribution for the solid wall in the fin thickness through the y-direction of the channel, the formula below is calculated depending on the thermal conductivity of the solid wall, the fin height  $h_{fs}$  is divided by the number of the fin divisions  $n_f$ , and the number of plate divisions  $n_p$ . The plate thickness will be taken into account in the present point coefficient.

$$\begin{aligned} i \leq n_f, a_{N(i,j,k)} &= \frac{\lambda_n}{(h_{fs-c}/2/n_{fh-c})/(h_{fs-c}/2/n_{fh-c})} \\ i = n_f, a_{N(i,j,k)} &= \frac{\lambda_n}{(h_{fs-c}/2/n_{fh-c})/((h_{fs-c}/2/n_{fh-c}) + (\delta_p/n_p) \times 2)} \\ j < n_{fh-c} + n_{pt}, a_{N(i,j,k)} &= \frac{\lambda_n}{(\delta_p/n_p)/(\delta_p/n_p)} \end{aligned}$$

$$j=n_{th-c}+n_{pt} \text{ and } i \leq n_f, a_{N(i,j,k)} = \frac{\lambda_n}{\left(\delta_p/n_p\right)/\left(\left(\delta_p/n_p\right)+\left(h_{fs-h}/2/n_{th-h}\right)\times 2\right)}$$

$$a_{N(i,j,k)} = \frac{\lambda_n}{\left(\delta_p/n_p\right)/\left(\delta_p/n_p\right)}$$

5- Point  $a_B$ , to calculate the temperature distribution for the solid wall in the fin thickness through the z-direction of the channel, the formula below is dependent on the thermal conductivity of the solid wall, the fin length  $L$  and is divided by the number of divisions in the fin length  $n_z$ .

$$k > 1, a_{B(i,j,k)} = \frac{\lambda_b}{L/n_z}$$

6- Point  $a_T$ , to calculate the temperature distribution for the solid wall in the fin thickness through the z-direction of the channel, the formula below is dependent on the thermal conductivity of the solid wall, the fin length  $L$  and divided by the number of divisions in the fin length  $n_z$ .

$$k < 1, a_{T(i,j,k)} = \frac{\lambda_t}{L/n_z}$$

Here, the terms  $n_p$  and  $n_f$  denote the number of divisions in the plate and fin thickness, as  $n_p=10$  and  $n_f=5$  respectively.

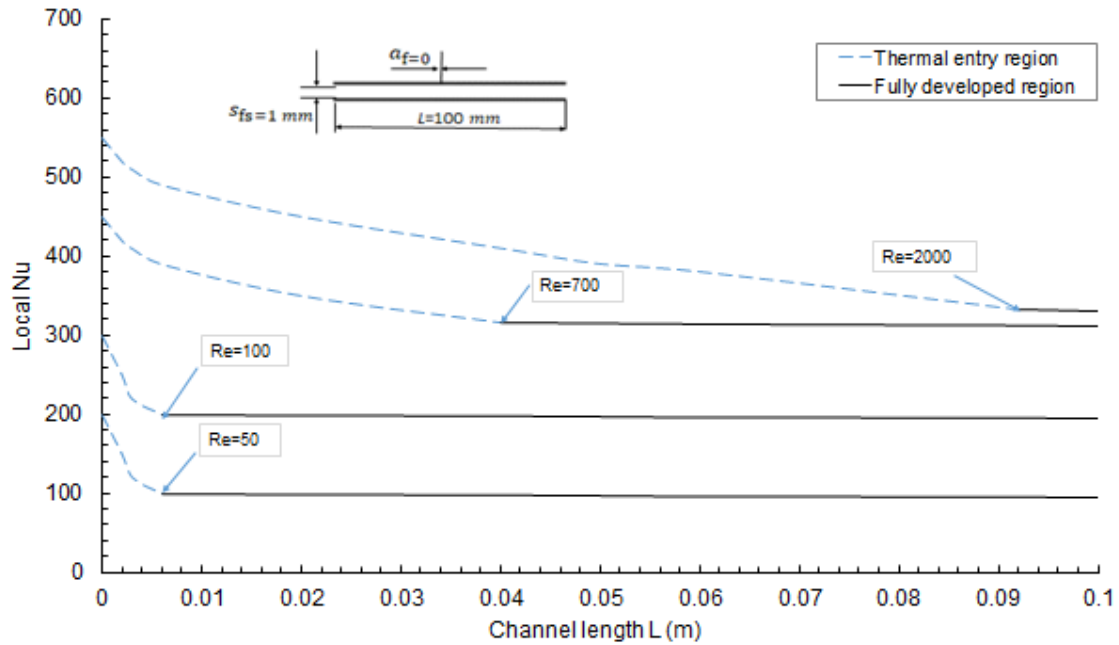
## 4.5. RESULTS

### 4.5.1. THERMAL ENTERANCE LENGTH

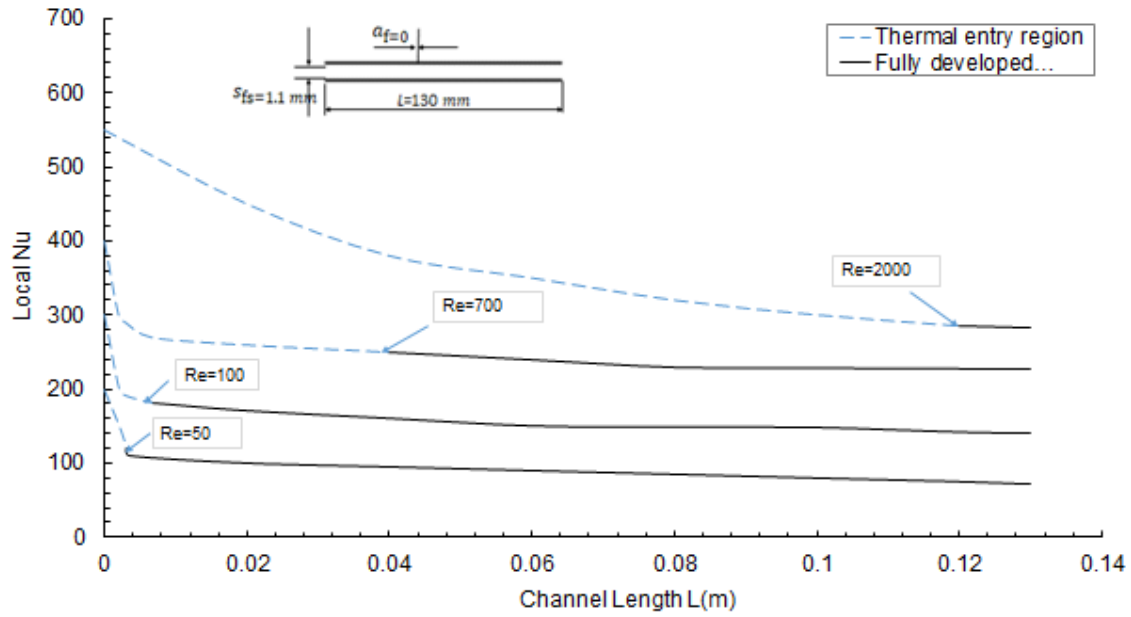
In the entrance region of the duct, regardless of the fin geometry, the results are identical, and the heat transfer is usually high. The thermal entry length, the boundary layer thickness at the entrance of the fin length  $L$  is zero, and the heat transfer performance has significant influence at the entrance region for the fin length. Figure 4.16 illustrates the thermal entry region. The fully developed region is given separately. In the fully developed region, the velocity profile is invariant across any flow cross-section. The dashed line represents the thermal entry length, and the solid line represents the fully developed region, at Reynolds numbers ranging between (50, 100, 700, and 2000) with varying geometrical parameters, as written above in Table 4.1. The results show that at low Reynolds numbers (50), the fluid flow reaches the fully developed

region for short-length wavy channel ranges between (0.0026-0.0031 m) for all cases that have been adopted in this thesis. This is shown in the figure below. In contrast, at high Reynolds numbers (2000), the access to the fully developed region requires a longer wavy channel, approximately at the end of the channel length ranges between (0.1-0.126 m). High Reynolds numbers require enough channel length to reach the fully developed region, due to the high velocity that induces the turbulent flow.

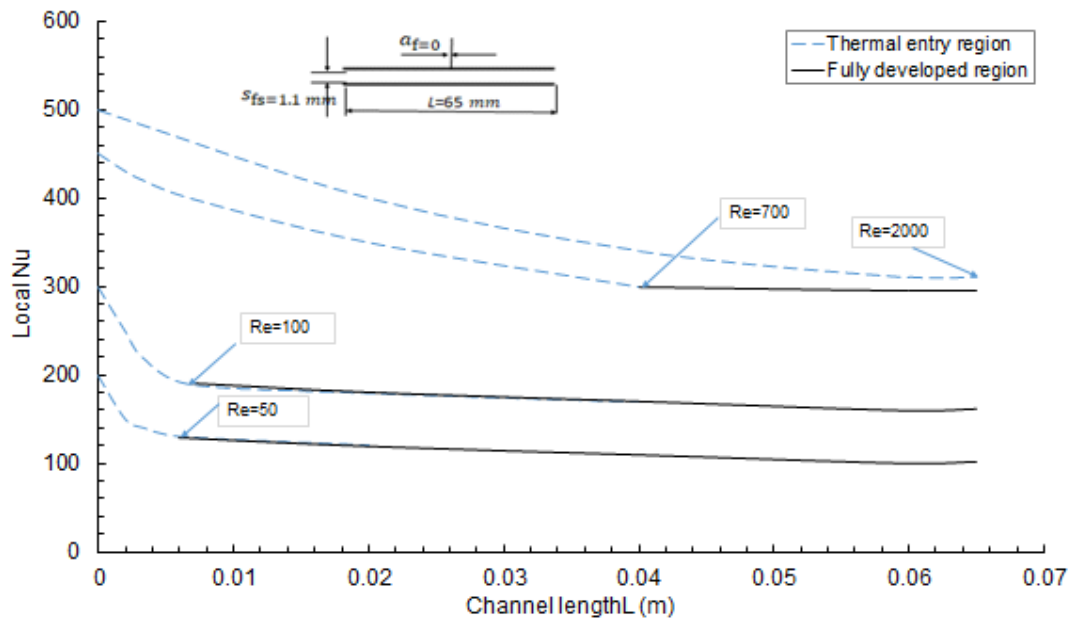
For the rectangular plain fin, at fin amplitude zero, if the local heat transfer coefficient along the flow direction increases, the heat transfer has been fully developed. Also, for wavy fin, at fin amplitude ranges between (1.5, 2, and 2.5 mm), the fully developed heat transfer coefficient and entrance length should be determined according to the mean heat transfer coefficient in a waviness length.



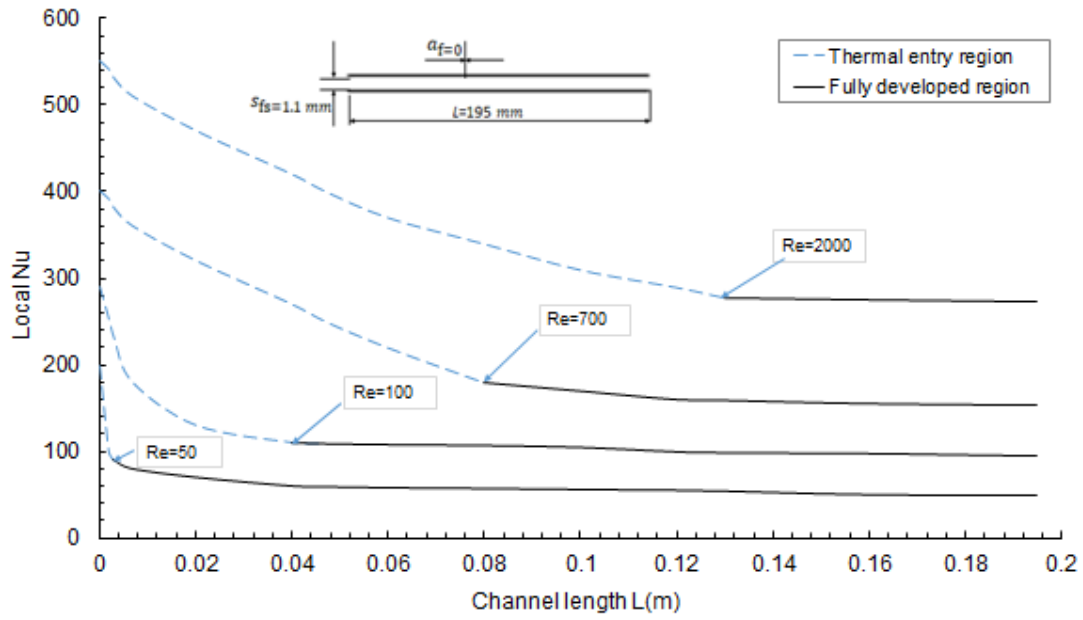
Case -1-



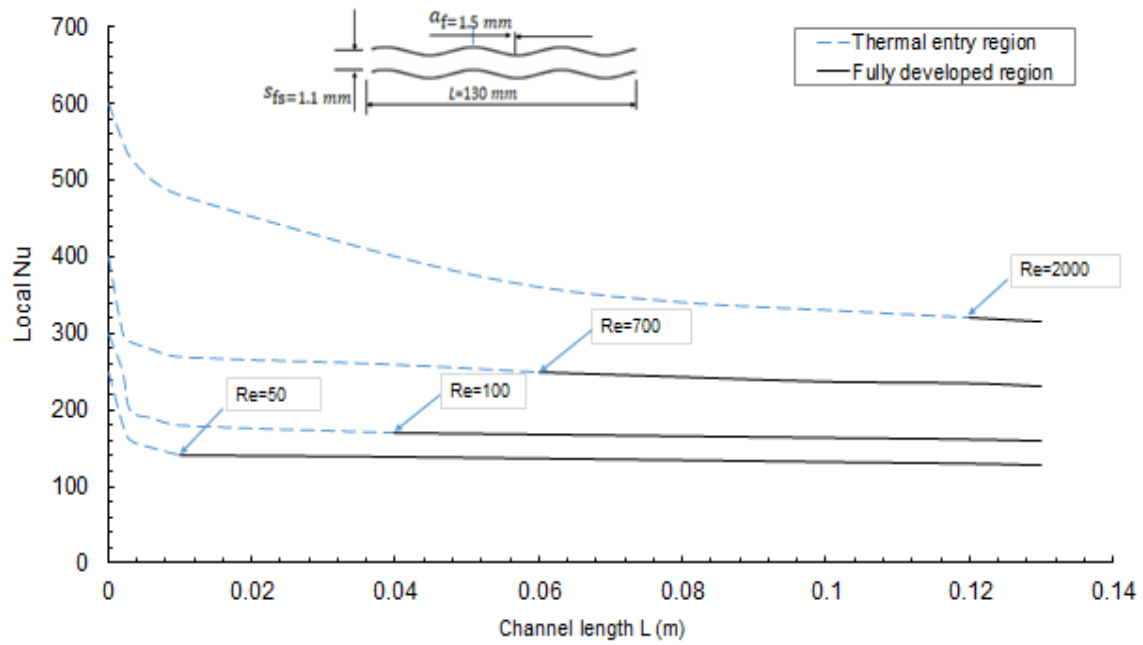
Case -2-



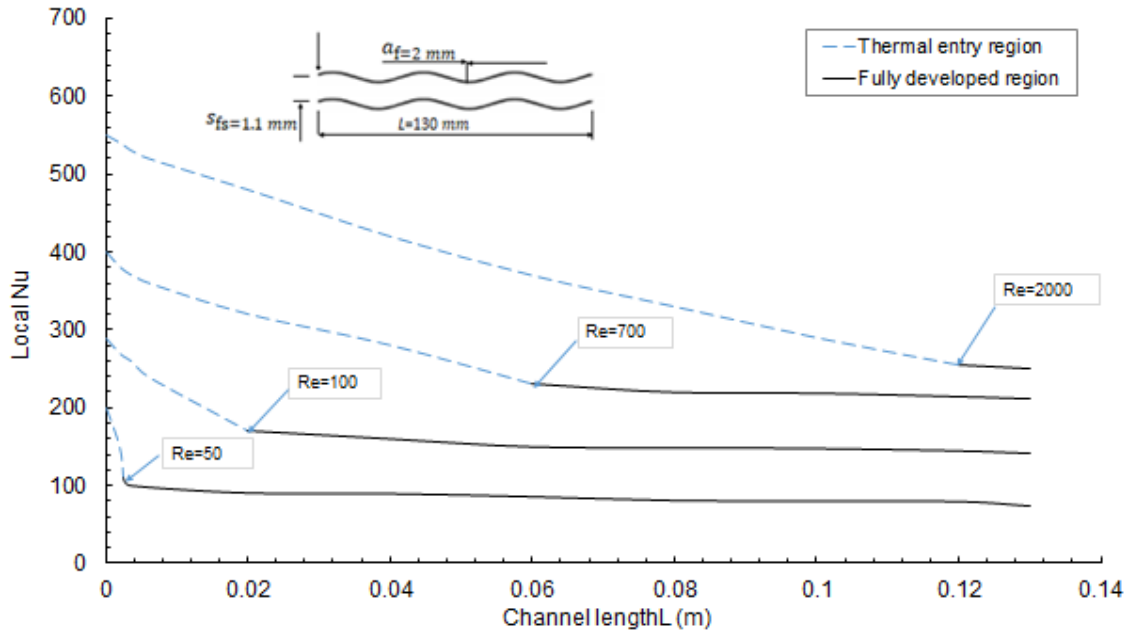
Case-3-



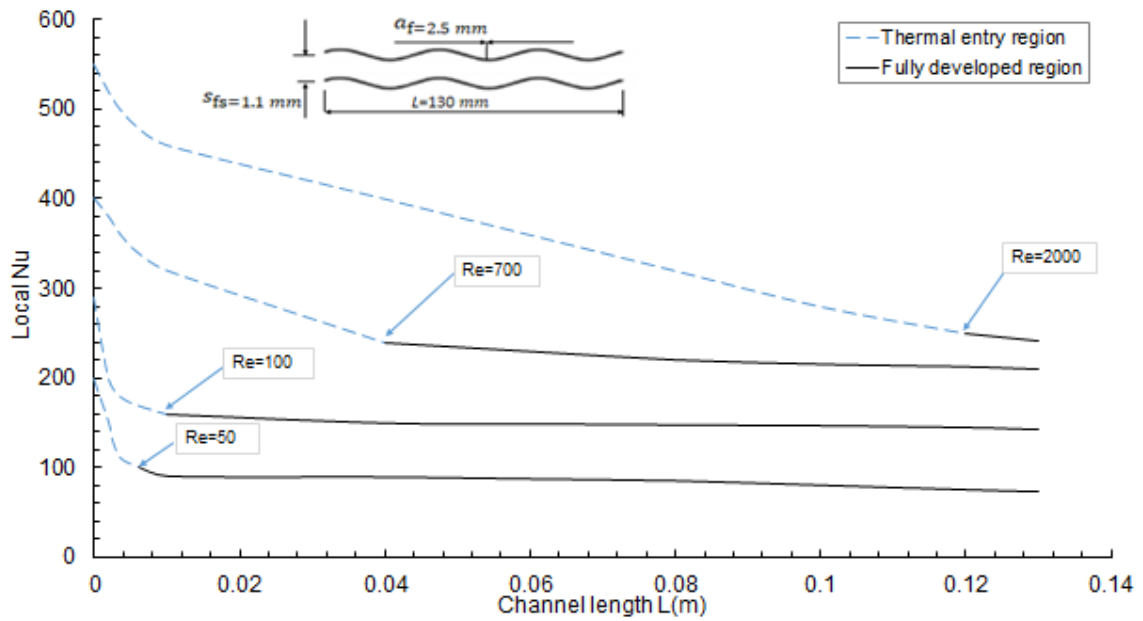
Case -4-



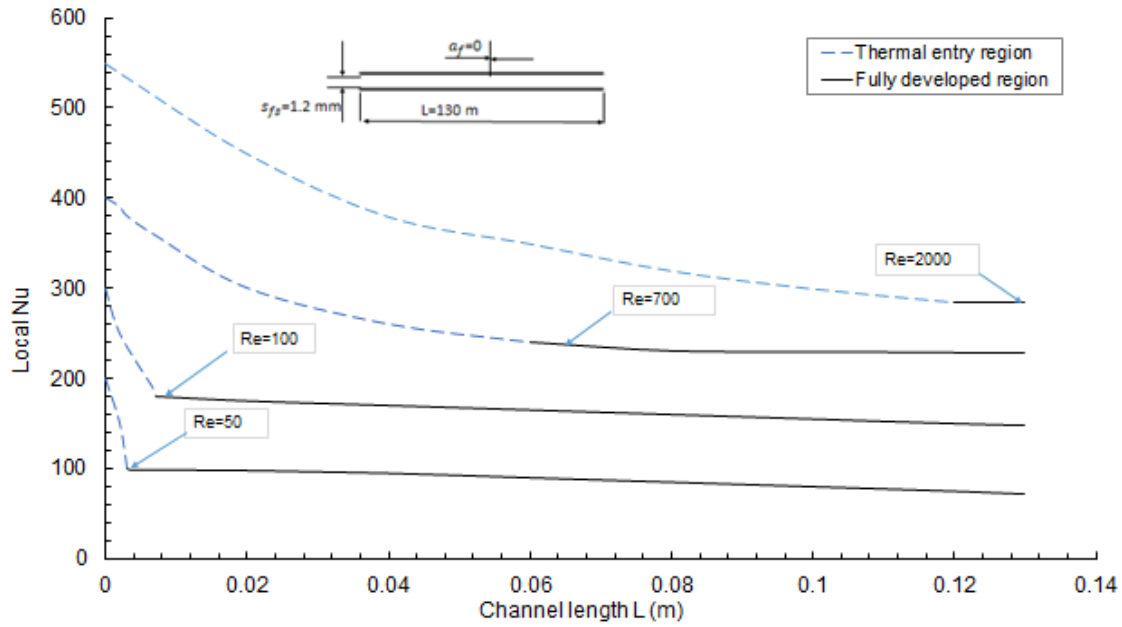
Case-5-



Case-6-



Case-7-



Case-8-

Figure 4.16: Shows the local Nusselt number distributions along the flow direction of the channel, depending on our cases as written in Table 4.1, and Model (1).

The local heat transfer was calculated for each location in the fin length flow with the integration method and was dependent on the mean Nusselt number. The local heat transfer coefficient was calculated based on the simple model, which is defined in model (1). The thermal entry length has been calculated based on the proposed correlations for fin types, such as the plain and wavy fins correlations from Zhu and Li [14]. The equations to calculate the thermal entrance region are: for plain fin  $L_e = 0.05 \text{ Re Pr } d_h$ , and for wavy fin  $L_e = 0.25 \text{ Re}^{0.52} d_h$ .

#### 4.5.2. LONGITUDINAL HEAT CONDUCTION EFFECT

The longitudinal heat conduction is considered in the present work, in order to investigate the effects of longitudinal heat conduction on heat-transfer performance. One end of the counter flow in a plate-fin heat exchanger is hotter than the other end. The longitudinal heat conduction in the matrix wall occurs in the same direction for both fluid-flow channels. The effect of axial heat conduction in two-stream heat exchangers has been discussed in detail in [1]. The temperature distribution and the heat exchanger effectiveness are affected by axial conduction

along the separating walls. The counter-flow exchanger problem with finite longitudinal wall conduction was analyzed by Shah and Sekulic [18], who identified that the influence of the longitudinal wall conduction can be taken into account by one parameter, which is defined as the wall conduction parameter ( $k$ ), besides  $NTU, C^*$  and  $\varepsilon = \varphi(NTU, C^*, k, (\eta_0 hA))$ .

The penalty on exchanger effectiveness due to the longitudinal wall conduction increases with the increasing values of  $NTU, C^*$  and  $k$ , and is at its largest when the term  $C^* = 1$ . The effectiveness of a heat exchanger neglects the longitudinal heat conduction. The equation to calculate the effectiveness is found in Alur [63]. When taking the effects of longitudinal heat conduction into account, which are given by the relation from Shah and Sekulic [18], the longitudinal heat conduction reduces the effectiveness of the heat exchanger along the separating surfaces of the two streams, which causes serious performance deterioration in heat exchangers, see Figure 4.17. This is due to the short conduction lengths and higher number of transfer units.

a- without LHC

$$\varepsilon = \frac{1 - e^{-NTU(1-C_r)}}{1 - C_r e^{-NTU(1-C_r)}} \quad (4.56)$$

b- with LHC

$$\varepsilon = 1 - \frac{1}{1 + NTU \times (1 + k\varphi) / (1 + k \times NTU)} \quad (4.57)$$

where for  $NTU \geq 3$ ,

$$\varphi = \left( \frac{k \cdot NTU}{1 + k \cdot NTU} \right)^{1/2} \quad (4.58)$$

Here, the term ( $k$ ) denotes the wall conduction parameter, which is calculated depended on the following formula:  $k = \lambda_w A_w / LC_{min}$ .

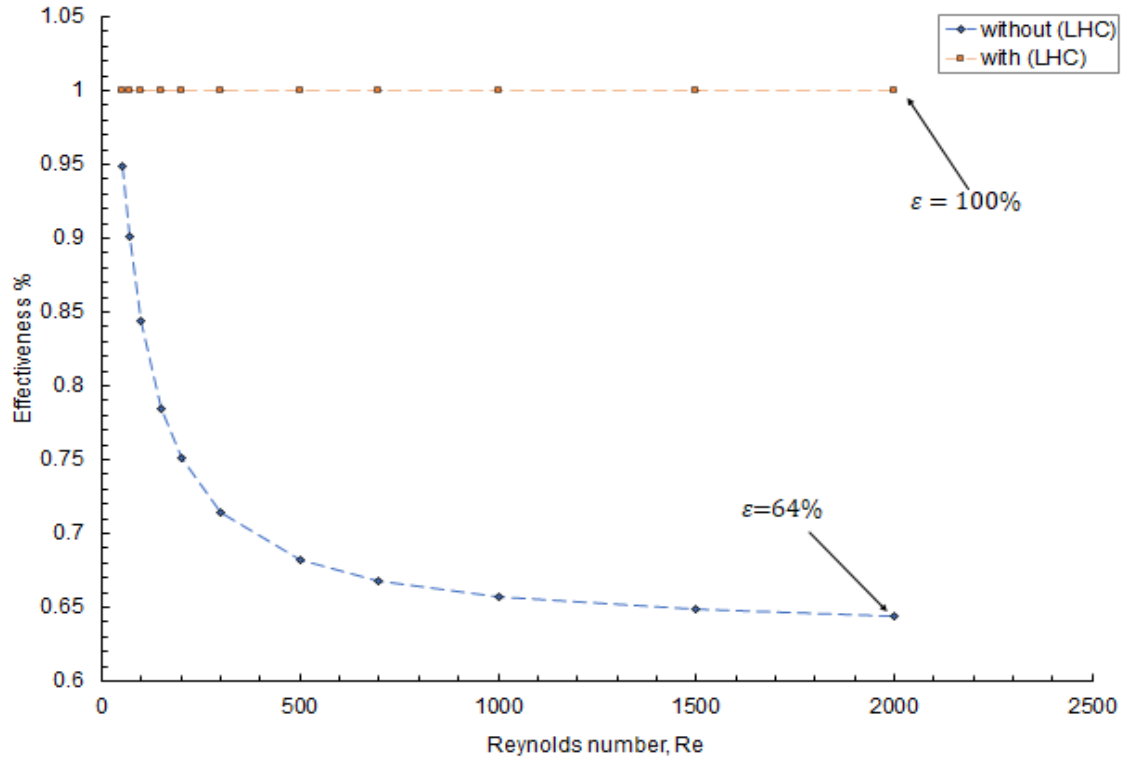


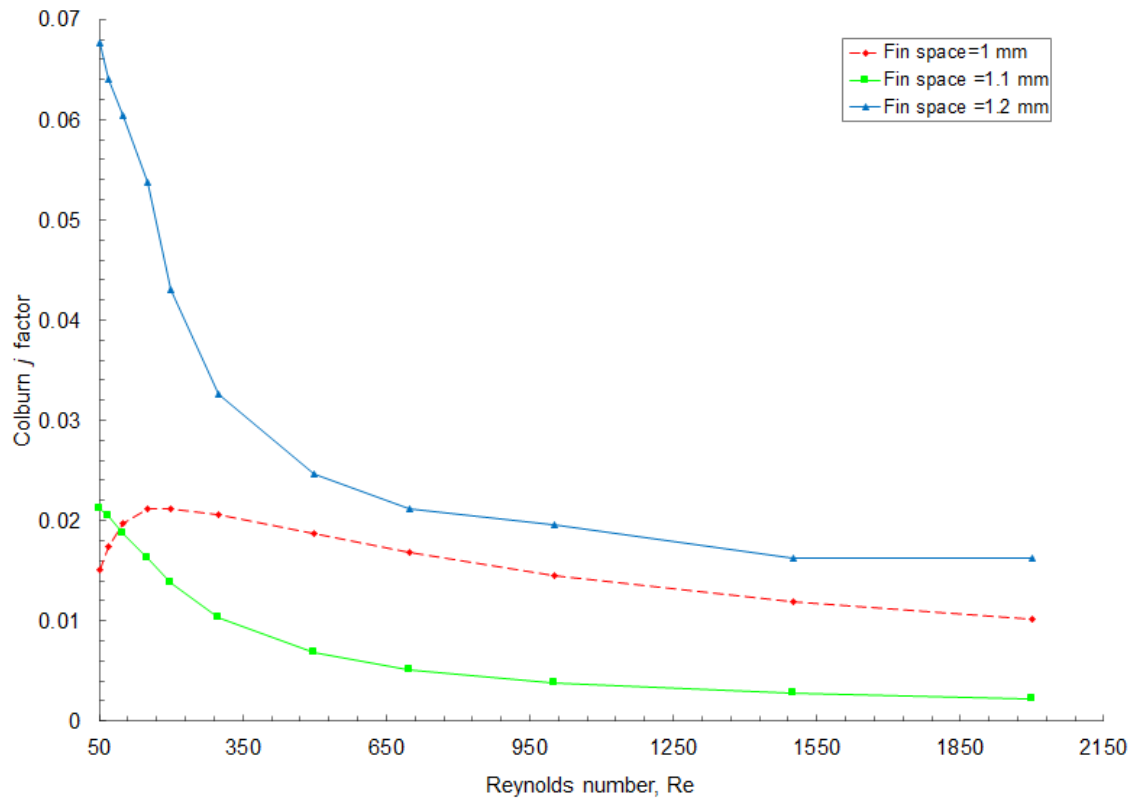
Figure 4.17 Shows the effectiveness with LHC and without LHC.

According to our results, the effectiveness when neglecting the LHC reduced between (94-65 %), and is increased between the range of (99-100 %) when the LHC is taken into account. The larger the factor of the longitudinal heat conduction, the greater the deterioration of the exchanger effectiveness [2].

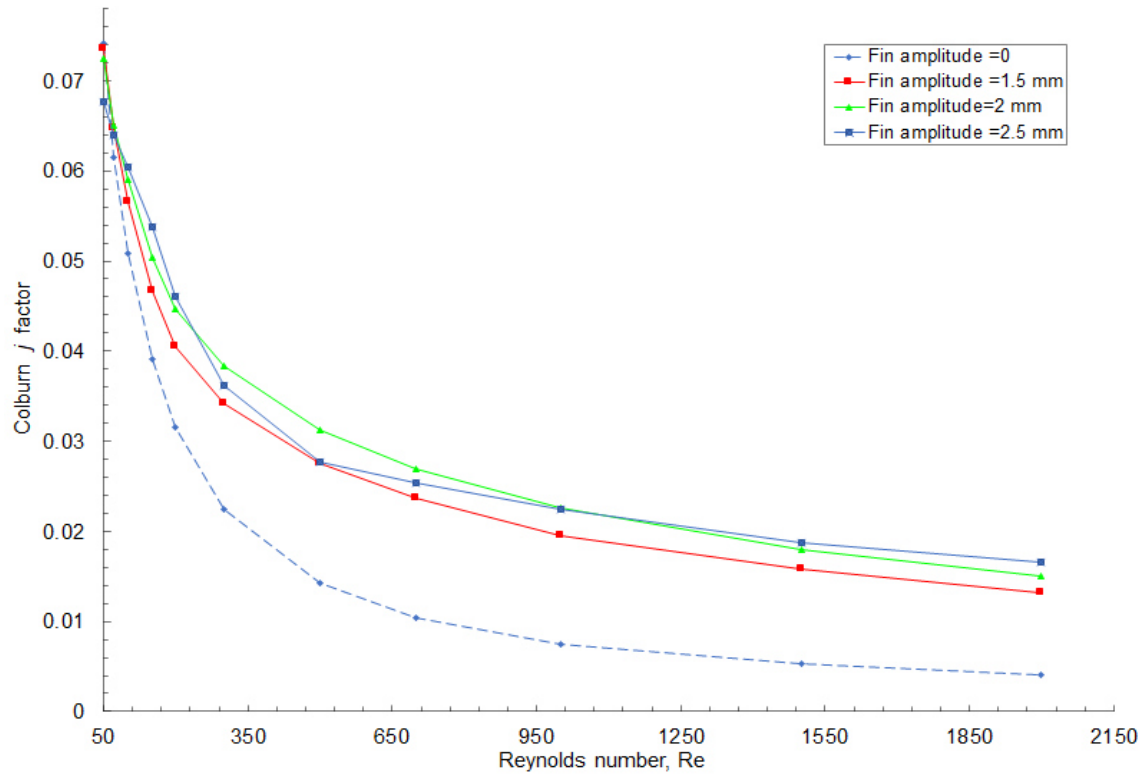
### 4.5.3. GEOMETRICAL PARAMETERS EFFECT

The heat-transfer performance in terms of Colburn  $j$  factor has been analyzed with different geometrical parameters for 8 cases, as listed in table 4.1. Heat transfer is affected by fin geometrical parameters with multiple ranges of Reynolds numbers. The influence of the fin geometry on the heat performance is identified with model (3), which was the best and most accurate of the models. The geometrical parameters of the wavy fin were investigated as the fin space  $s_{fs}$ , fin length  $L$ , and fin amplitude  $a_f$ . Each case has a different influence of the heat transfer performance, as demonstrated in Figure 4.18. It is clearly shown that generally, with

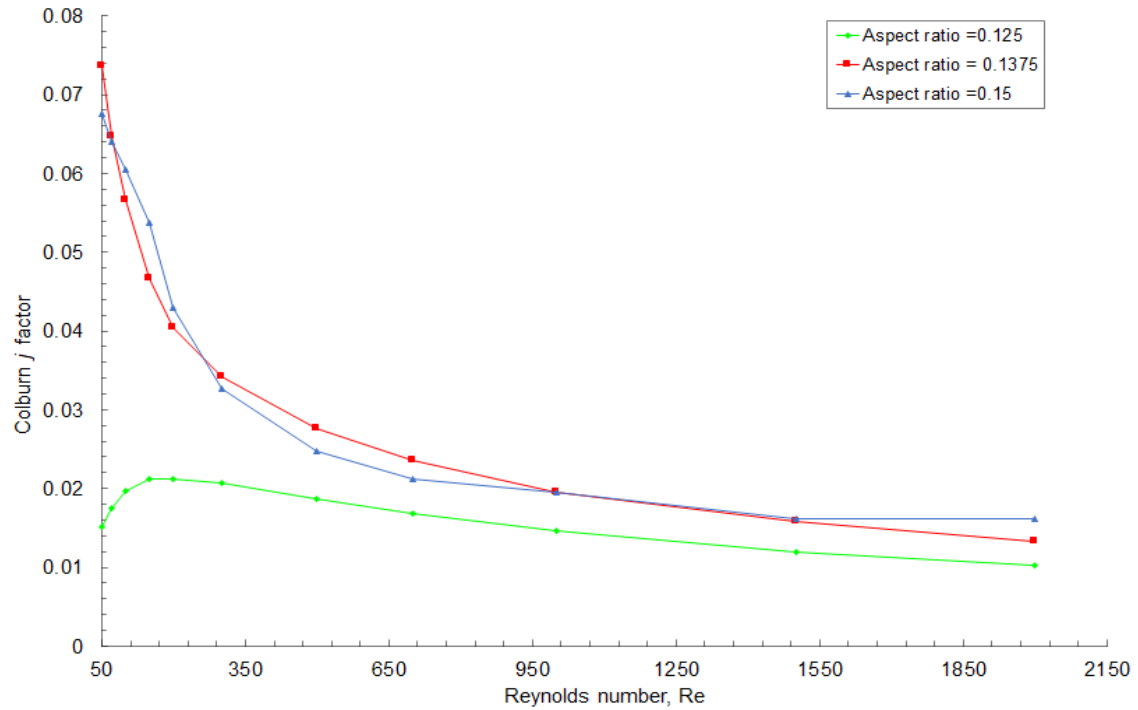
the increase of fin spacing at 1.2 mm, the magnitudes of  $j$  factor increase for fixed Reynolds numbers. The effects of fin amplitude on  $j$  factor, for increased fin amplitude of 2-2.5 mm, increases the  $j$  factor. Effect of  $s_{fs}/h_{fs}$  ratio on  $j$  factor indicates that the  $j$  factor decreases as Reynolds number increases, and  $j$  factor reduces as  $s_{fs}/h_{fs}$  ratio increases. Effects of the fin length on heat-transfer performance indicates that the Colburn factor increases with the increased fin length, at 130 mm.



-a-



-b-



-c-

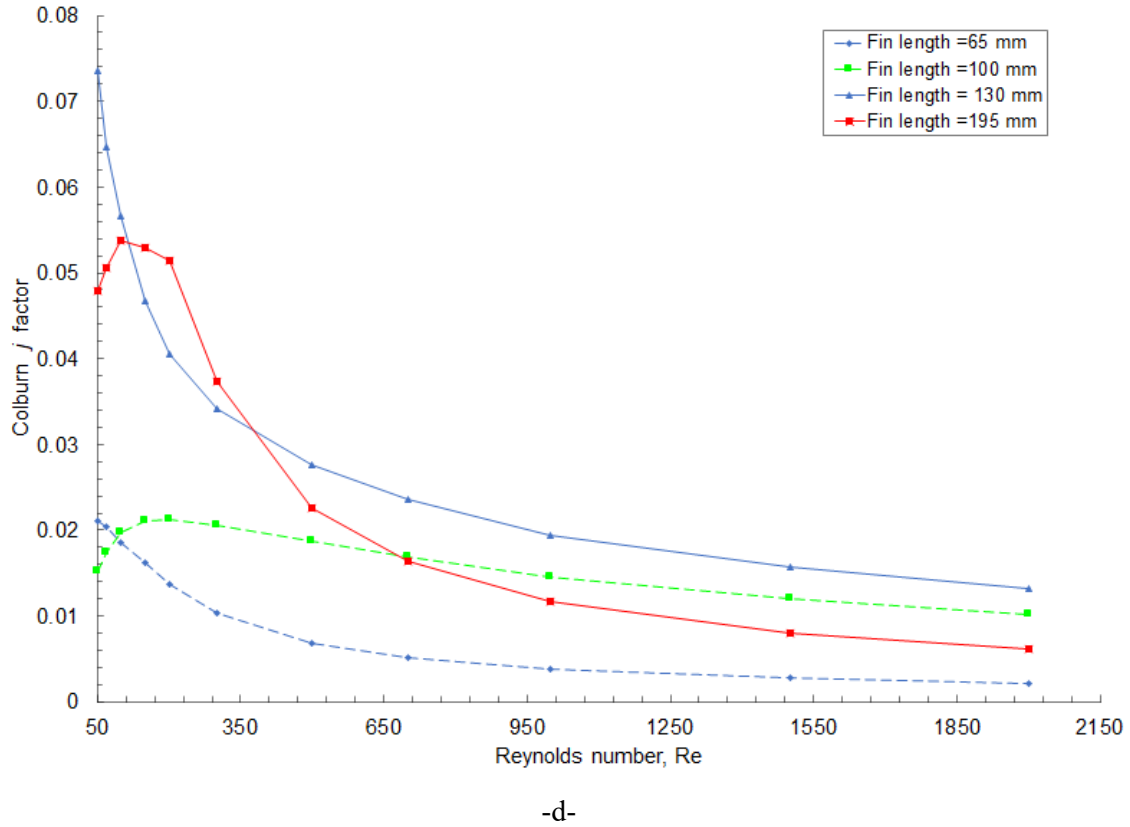


Figure 4.18 Shows the influence of the geometrical parameters on the heat transfer performance, (a) at varied fin spacing  $s_{fs}$ , (b) at varied fin amplitudes  $a_f$ , (c) at varied aspect ratios  $a_f = s_{fs}/h_{fs}$ , and (d) at varied fin lengths  $L$ .

The results revealed that increases to the value of the geometrical parameters, such as the fin spacing, fin amplitude, aspect ratio, and fin length, have a positive effect on the heat transfer. The reason is due to the characteristics of the wavy fin, which allow the interruption of gas flowing inside the channel and can induce the flow to become disturbed along the fin length. The corrugated surfaces have the ability to enhance the heat transfer area and thus enhance the heat transfer coefficients, more so than with other surface configurations.

The effectiveness plotted in Figure 4.19 illustrates the results for four fin amplitude ranges between (0, 1.5, 2.0, and 2.5 mm); for rectangular fin when the fin amplitude is zero and for wavy fin when the fin amplitude values range between (1.5, 2.0, and 2.5 mm).

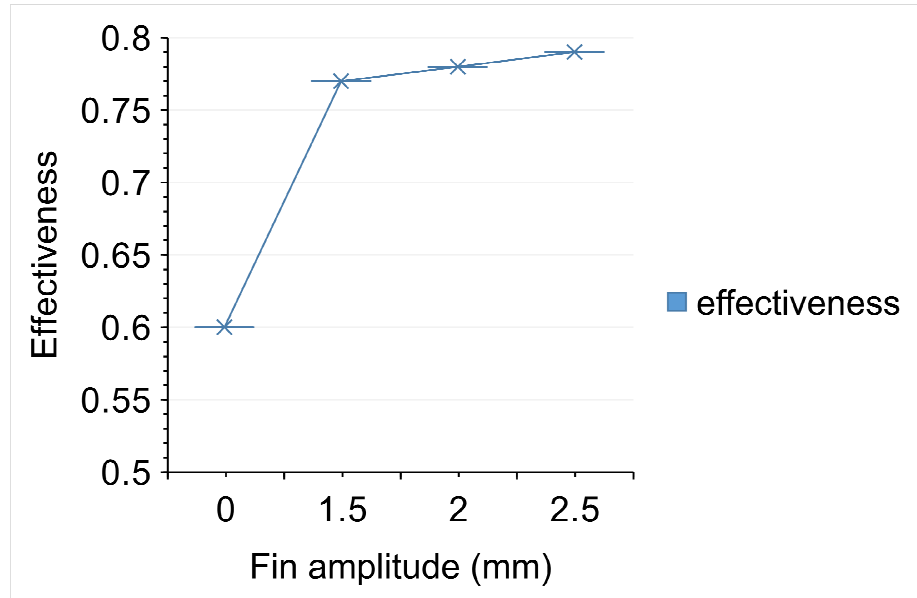


Figure 4.19: Effectiveness Vs fin amplitude.

The results that are plotted in the figure above were investigated at Reynolds number (300). This shows that the fin effectiveness was at its maximum of 78 % at fin amplitude 2.5 mm and the effectiveness was at its minimum of 60% at fin amplitude zero. Additionally, the heat transfer rate per fin is generally increased for wavy fin. The results show that in many applications, using a wavy fin in the plate-fin heat exchanger gives higher heat transfer and better performance than when using the plain or rectangular fin type.

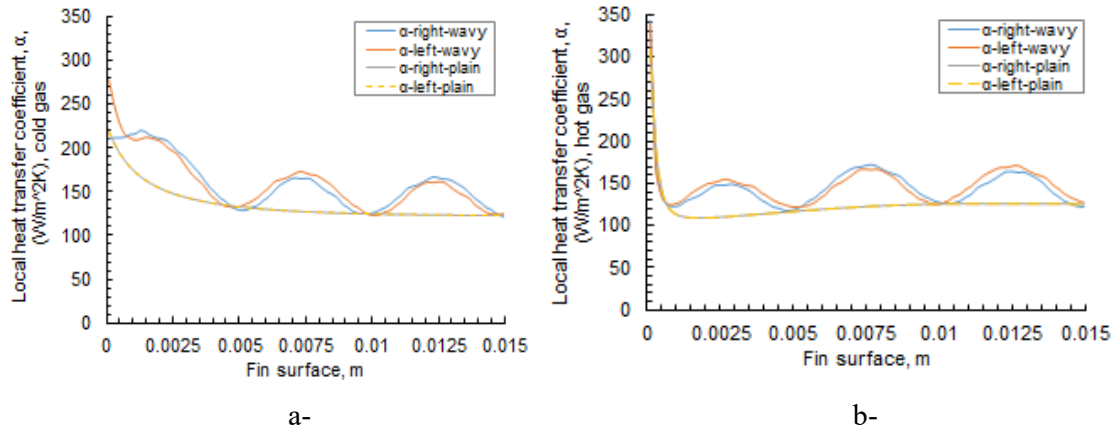
#### 4.5.4. FIN ANALYSIS

In this section, the fin analysis is discussed with various ranges of fin amplitude taken into account. One way to enhance the heat transfer on the air-side of the plate-fin heat exchanger is to modify the fin geometry. The wavy fin is considered one of the most popular fin types in PFHEs, particularly when superior heat transfer performance is required under a specific pressure drop allowance. The wavy fin has an uninterrupted surface, similar to that of the plain fin except for the undulations in the fluid flow direction.

The influence of both the fin surface and plate surface of wavy channel are investigated, to examine their effect on the heat transfer coefficient in a single pair channel in a PFHE.

The results are presented in the form of Colburn  $j$  factor and Fanning friction factor  $f$  for different geometrical parameters. Plain fin are set at (0, 1, 8, and 100 mm), and wavy fins at (1.5, 1, 8, and 100 mm) respectively denoting (fin amplitude  $a_f$ , fin space  $s_{fs}$ , fin height  $h_{fs}$ , and fin length  $L$ ). Numerical simulations have been conducted for wavy-fin type at Reynolds number (50) using OpenFOAM program.

Figure 4.20 (a, b) shows the local heat transfer coefficient in different directions in the fin surface for gases, for both fins types. For plain fins the fin amplitude is zero, and for wavy fins the fin amplitude is 1.5 mm. The effects of the fin surfaces on the heat transfer are the same for different fin amplitudes, with small differences in wavy fin where the local heat-transfer coefficient was higher for the cold gas at left position than at right position, especially at the entrance region of the fin surface. The behavior of the flow stream still fluctuates along the fin surface due to its corrugated shape. The heat transfer for the wavy fin was higher than with the plain fin. The trend line of the local heat transfer in the plain fin started at 230 W/m<sup>2</sup>K in the entrance region, and reduced with the gas flowing in the channel to 125 W/m<sup>2</sup>K. The trend line of the local heat transfer in the wavy fin started at 275 W/m<sup>2</sup>K at the entrance region, and reduced with the gas flowing in the channel to 130 W/m<sup>2</sup>K.



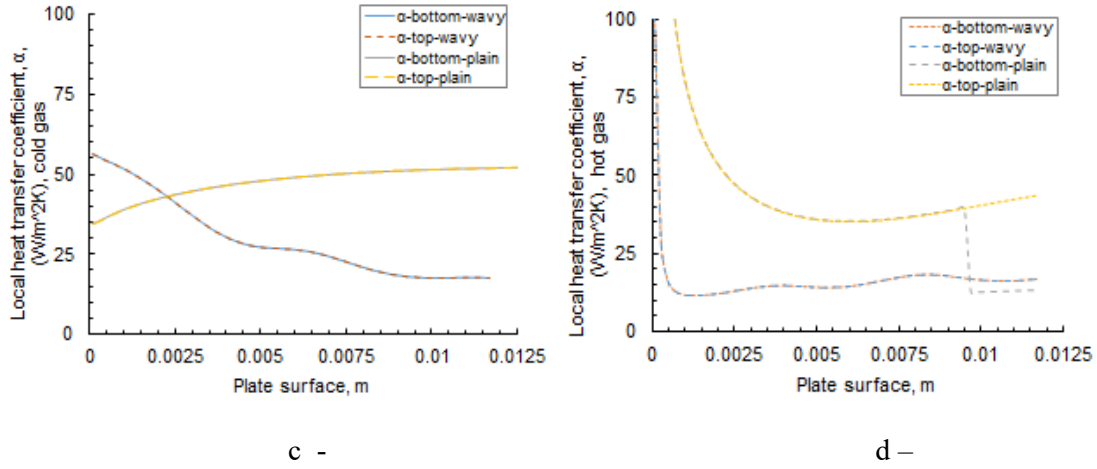


Figure 4.20: Local heat transfer coefficients in the fin and plate surfaces at different positions, (a b, c, d) for fin amplitude zero (plain fin), and for fin amplitude 1.5 mm (wavy fin), for both fluids.

Figure 4.20 (c, d) shows the behavior of gas at the top and the bottom of the plate surface for cold gas. For the plain fin, the local heat transfer coefficient increases along the surface of the plate from 35 to 53 W/m<sup>2</sup>K. In the wavy fin, the local heat transfer starts with a higher value, then reduces along the plate surface from 57 to 18 W/m<sup>2</sup>K. For hot gas, the local heat-transfer coefficient reduced from 300 to 15 W/m<sup>2</sup>K at the bottom of the plain fin, and at the top it reduced to 45 W/m<sup>2</sup>K. In the wavy fin, the trend line of the local heat transfer at the top and bottom of the plate surface had the same trend, reducing from 100 to 18 W/m<sup>2</sup>K. For the plain fin, the trend line of the local heat transfer at the top and bottom significantly affects the heat transfer. Regarding the top and bottom of the plate surface, the local heat transfer of the cold gas begins with a lower value at the entrance region of the channel, then increases due to the heat transfer taking part in the plate, which separates the hot and cold streams.

Figure 4.21 shows the mean heat transfer coefficient in the half-wave period, where the half wave is 0.004 m. The figure illustrates that the heat transfer for half wave at fin amplitude 1.5 m (wavy fin) is higher than for fin amplitude 0 (plain fin). For the wavy fin with the hot gas, the heat transfer is 118 W/m<sup>2</sup>K at the beginning of the wave, grows in value within the length of the wave ranging between 0.0008 and 0.001, whereafter the heat transfer is kept stable between the wave length range of (0.001-0.003 m).

The trend line of the hot gas goes down, which is reached at  $100 \text{ W/m}^2\text{K}$ . In contrast, for cold gas, it looked low at the beginning and increased to the level of heat transfer at  $120 \text{ W/m}^2\text{K}$ , at the end of the wave length.

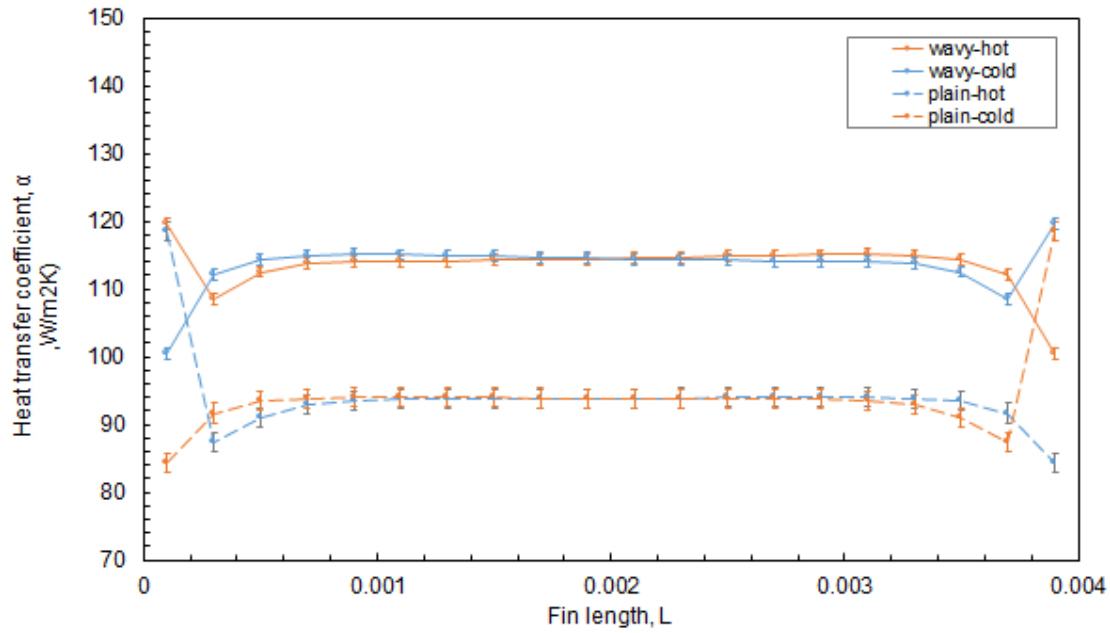


Figure 4.21: Mean heat transfer coefficient in the half wave period.

For the plain fin, the heat transfer for both fluids are the same at  $93 \text{ W/m}^2\text{K}$ , the difference occurs during the middle of the half wave period, as demonstrated in the figure above, and between the wave length ranges ( $0.001\text{-}0.003 \text{ m}$ ), the trend line of the cold gas goes up above the trend line of the hot gas. The results reveal that the flow distinction between plain and wavy fins has an significant influence on the heat transfer.

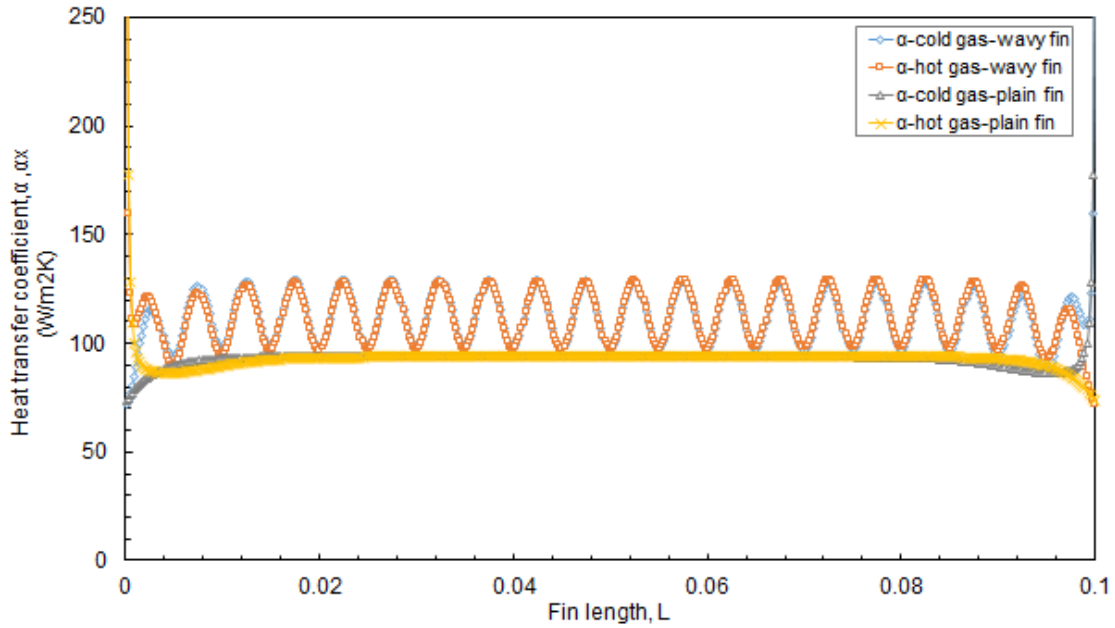


Figure 4.22: Local heat transfer coefficient along the flow direction.

Figure 4.22 shows the comparison of the local heat transfer between both fin types in the fin channel length. At the entrance of the fin length is zero, regardless of the fin geometry, the local heat transfer is a higher value, then it is reduced with the gas flowing along the fin length to  $90 \text{ W/m}^2 \text{ K}$ . At the end of the fin length, the trend line of the heat transfer goes down. The same behavior is shown for both fin types. For the wavy fin, the heat transfer fluctuation along the fin length depends on the corrugation of the fin surface geometry, which ranges between  $(90\text{--}130 \text{ W/m}^2 \text{ K})$ .

Figure 4.23 shows the comparison of the Colburn  $j$  factor and Fanning friction factor  $f$  for both fin shapes. The heat transfer performance in terms of Colburn  $j$  factor and Fanning fraction factor  $f$  have been presented for both fin types for cold gas and hot gas. For the plain fin in Figure (a), the heat transfer of the hot and cold gas reached the fully developed region at 0.145, starting at fin length 0.01 m and continuing to length 0.08 m. The hot gas line then goes down and the cold gas line goes up at the end of the fin length (0.1 m). For the wavy fin, the fluid flow fluctuates along the fin length due to the fin's surface undulations; in a wavy fin the heat transfer is more enhanced than with the plain fin.

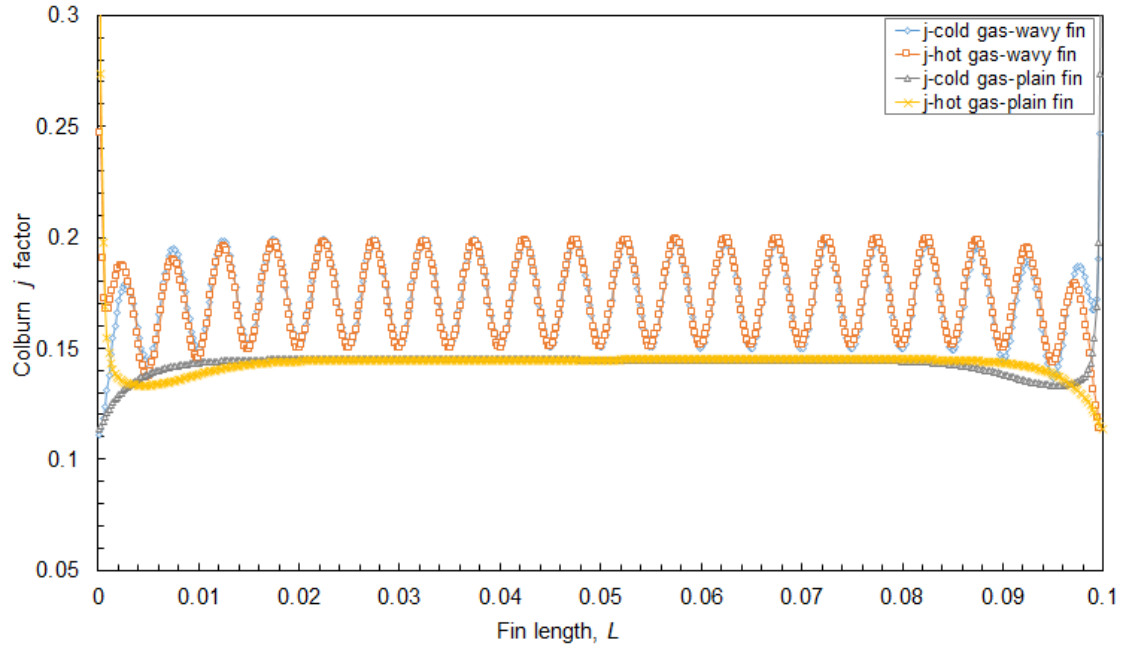
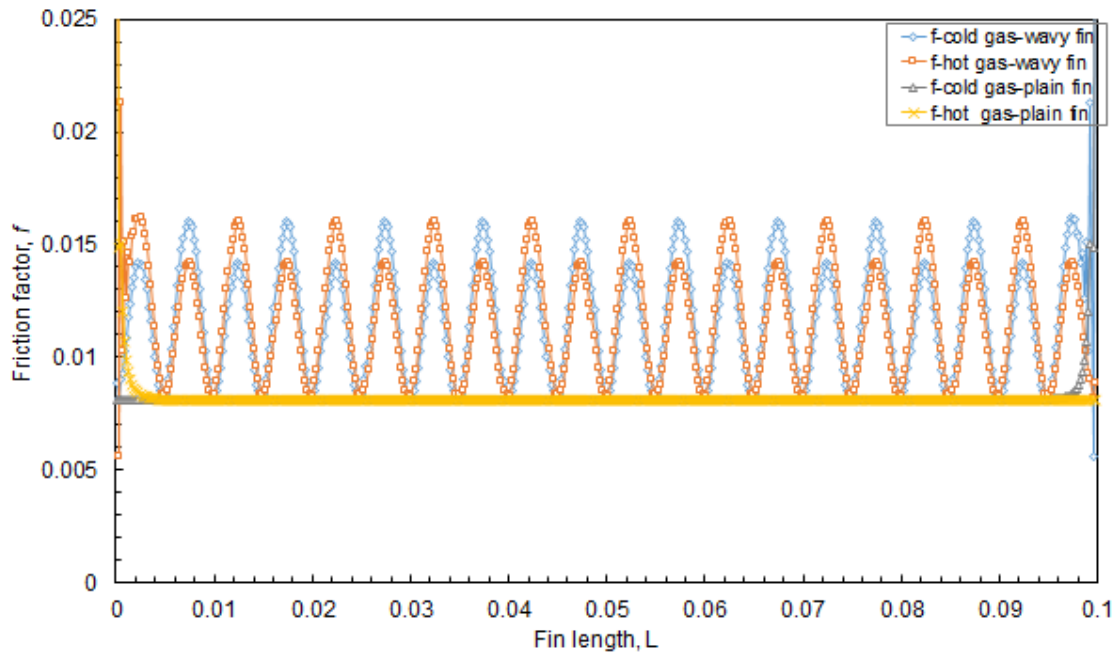
a- Colburn  $j$  factorb-Fanning friction factor  $f$ 

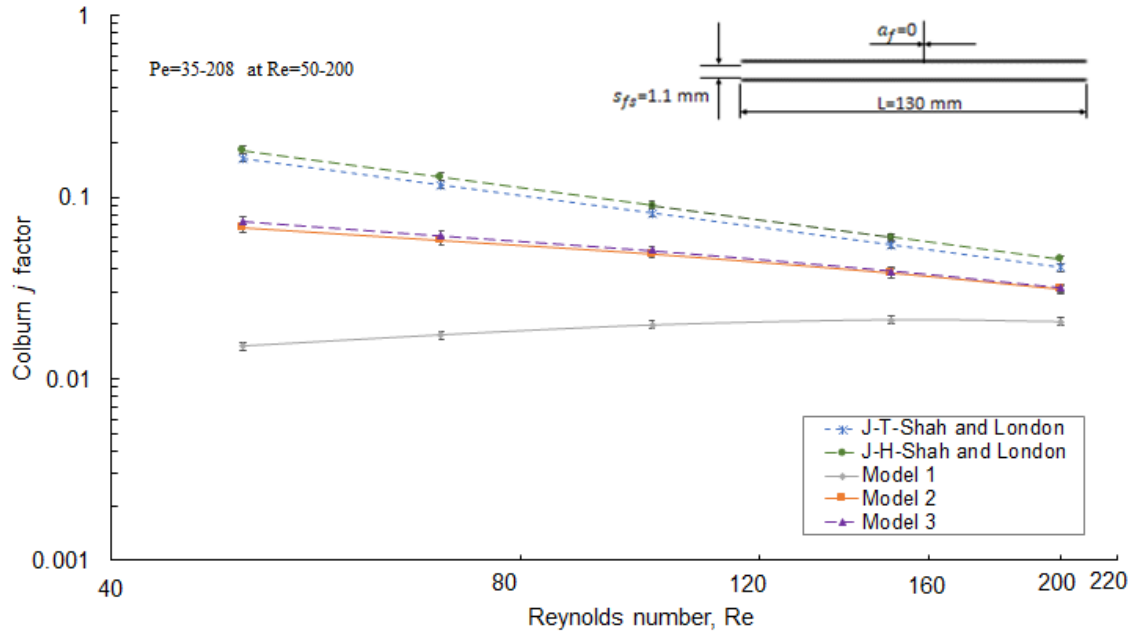
Figure 4.23: Heat transfer performance along the flow direction.

Figure (b) shows the comparison of Fanning friction factors  $f$  for both fin shapes. For the plain fin, the friction factor of the hot gas started at a higher value at the beginning of the fin length, then maintained stability along the fin length at friction factor 0.4. For cold gas, the friction factor started at a constant value until the fin length 0.096 m, and then the friction value increased to 0.8. For the wavy fin, the friction factor was higher at fin length zero, then it fluctuated along the fin length (0.4-0.8).

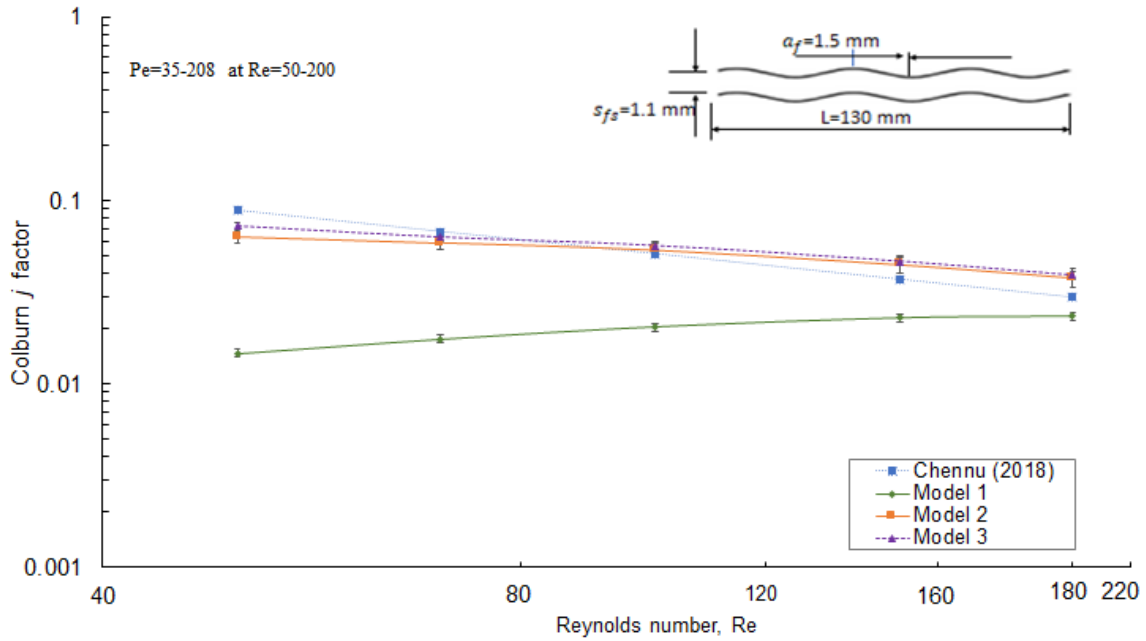
#### 4.5.5. MODELS VALIDATION

In this section, we will compare the three models. They have been described in previous sections as follows: Model (1) is the simple or traditional model. The efficiency of the fin takes the effect of the lateral heat conduction in fins into account, and neglects the longitudinal heat conduction in a solid wall. Model (2) is the analytical model based on the ordinary differential equation (ODE) method. This model takes into account the longitudinal heat conduction in the plate and fin. Model (3) is the numerical model based on the finite difference (FDM) method. This model takes into account the effect of 3D heat conduction in the plate and fin.

Obviously from Figure 4.24, Model (2) and Model (3) are the best models; both can increase the effect of the heat-transfer coefficients due to the addition of the effects of heat conductivity within their calculations. The three models were calculated in the MATLAB program through the assumptions specified for each model. To validate our models, a comparison with open literature for both of [1] and [11] has been undertaken. These comparisons are shown in Figure 4.24. (a, b, c, and d) at a range of different fin amplitudes.



a- At  $a_f=0$ , and Reynolds numbers ranging between (50-200)



b- At  $a_f=1.5$ , and Reynolds numbers ranging between (50-200)

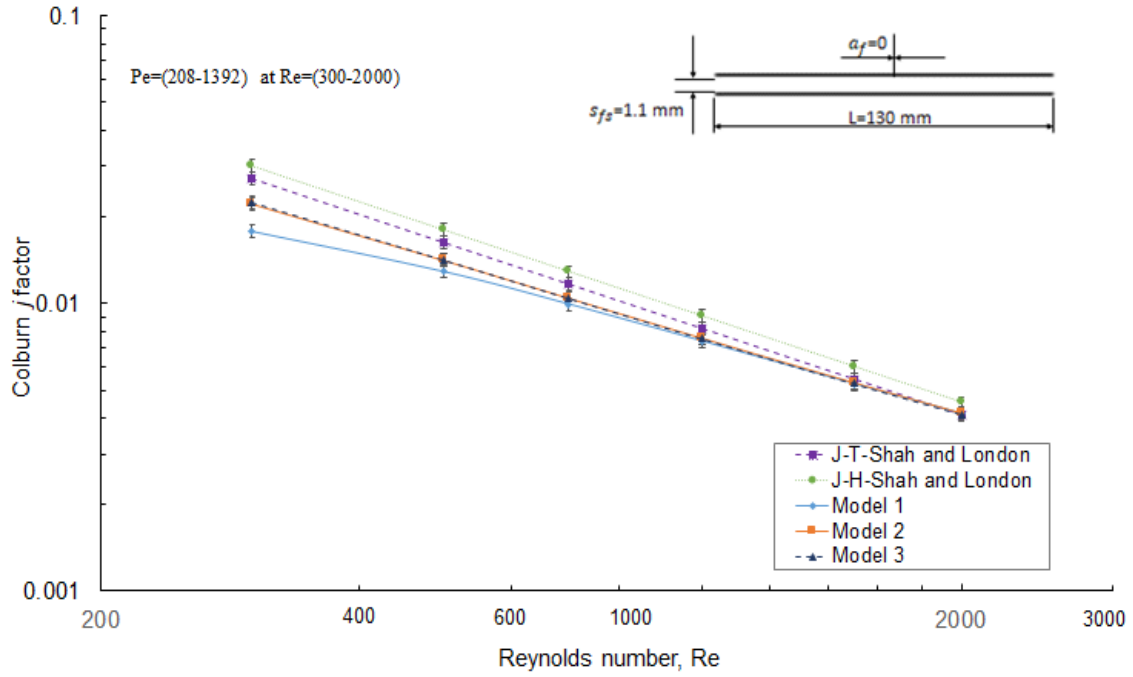
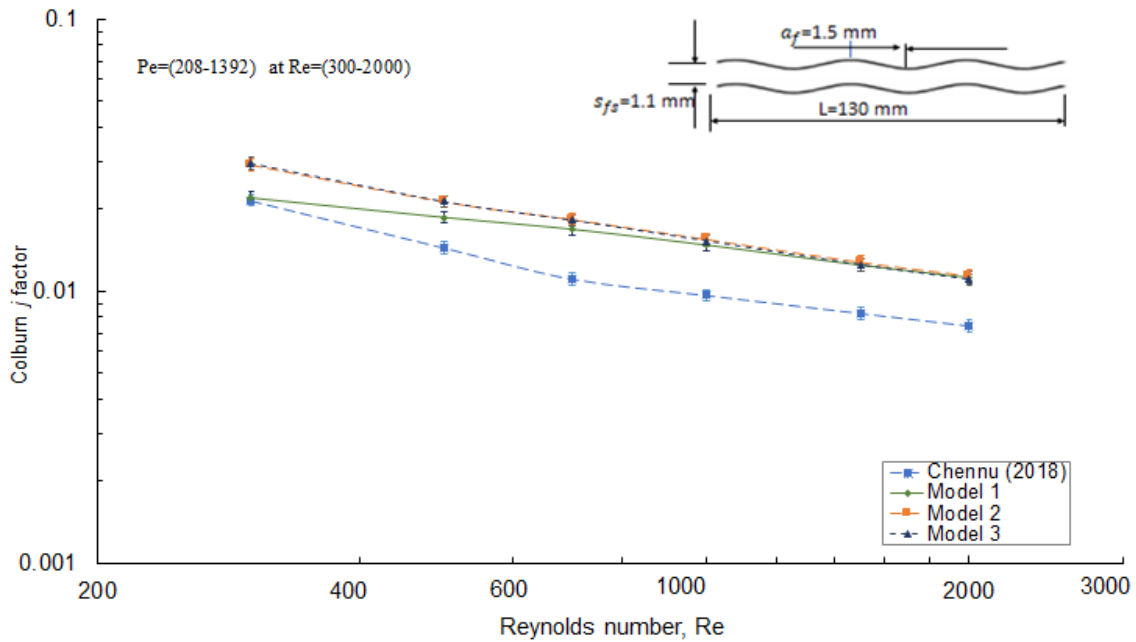
c- At  $a_f=0$ , and Reynolds numbers ranging between (300-2000).d- At  $a_f=1.5$ , and Reynolds numbers ranging between (300-2000).

Figure 4.24: Comparison between available literature with the developed models (1, 2, 3), Figures (a, and c) are for plain fin at geometrical parameters ( $a_f=0$ ,  $s_{fs}=1.1$  mm, and  $L_f=130$  mm), and Figures (b, and d) are for wavy fin at geometrical parameters ( $a_f=1.5$  mm,  $s_{fs}=1.1$  mm, and  $L_f=130$  mm).

Figures (a, c) show the comparison between the three models and the available literature, for the rectangular fin at fin amplitude 0, with different boundary conditions, as follows:

1- At constant heat flux  $j_H$ , and Reynolds numbers ranging between 50-200, the deviations ranged between (150-11%), (90-4%), and (80-4%). For Reynolds numbers ranging between 300-2000, the deviations ranged between (20-0.5%), (14-0.3%), and (12-0.2%) for the three models, respectively.

Figures (b, d) show the deviation ratios between the models and the available literature, as follows:

2- At constant heat flux  $j_H$ , the deviation found in the case of Reynolds numbers between 50-200 ranged between (74-3%), (30-3%), and (1-2%) for three models, respectively .

The results revealed that the extent of the longitudinal heat conduction has a significant influence on the heat transfer performance. Models (2 and 3) have a good agreement with the available literature, particularly for the wavy fin and Reynolds numbers ranging between (70-2000).

The results show that the trend line in the developing-region flow goes above that which is found in literature, which makes sense and should happen. The correlation with the literature has been proposed in the case of the fully developed region, but our case has been developed in the developing region. It is clear that for the wavy fin, the trend line in the developing region rises above the fully developed trend line found in the literature, except at low Reynolds numbers (specifically, it goes down at  $Re=50$ ). The deviation found in both the wavy fin and the rectangular fin is due to several reasons, listed below:

- 1- In our models' calculations, we have adopted aspect ratios between (0.125, 0.1375 and 0.15), while in the available literature the aspect ratios range is between (0.25, 0.5, and 1).
- 2- The developed models still require more assumptions for their development, such as the thermal conductivity of the fluid flow. The Peclet number is greater than  $Pe > 10$ , and the thermal conductivity of the fluid is neglected [Shah and London 1978].

In the present work, the Peclet number varies: for Re ranges between (50-2000), the  $Pe$  ranges between (35-1392), respectively. Therefore, the thermal conductivity of the fluid is negligible in the models' calculations.

3- The longitudinal heat conduction through the solid material of the heat exchanger had a detrimental effect on its thermal performance, hence the increasing deterioration of the exchanger. The thermal performance of the heat exchanger is strongly governed by losses, such as the longitudinal conduction in the separating solid wall, whereby loss of effectiveness in the heat exchanger has occurred in the wall's heat conduction. The low thermal conductivity of the fin causes an overall decrease in fin efficiency from about 98% to only 70%. The larger the factor of the longitudinal heat conduction, the greater the deterioration of the exchanger's effectiveness [2]. The results revealed that the thermal conduction has a greater effect than the thermal convection, particularly at Reynolds number 50, the ratio of  $\Delta Q = Q_{cond.}/Q_{conv.}$  was 10%. In contrast, at Reynolds number 2000, the ratio of  $\Delta Q = Q_{cond.}/Q_{conv.}$  was 0.24%. There is a feature to calculate model (2), that we should mention: The time required to calculate the second model in the MATLAB program is only one second (relative to no more than two hours), which is much faster than the time required for model (3).

The results revealed that the change in the flow direction induced by the fins caused boundary-layer separation with effects similar to complete fin interruption. The plate-fin surfaces are useful when both fluids in the heat exchanger are gases since the extended surface can be effectively employed on both fluid sides. The expressions provided for the heat transfer coefficient in terms of Colburn  $j$  factor and friction factor  $f$  allow the computation for all values of Reynolds number for the laminar flow regime. The heat transfer performances for the cases with wavy fins are better than those with plain fins, indicating that the enhancement of heat transfer is more significant with the wavy fin. Wavy fins are one of the most popular heat exchanger surfaces since they can lengthen the airflow inside the heat exchanger and improve mixing of the airflow.

#### 4.5.6. PROPOSED NEW CORRELATIONS

The thermal performance of the plate-fin heat exchanger depends heavily on the numerical simulation. In this thesis, the main goal is to develop a new correlation for wavy fin at various fin amplitudes, ranging between (0,1.5, 2, 2.5). Three models were developed based on the

simulation results, using OpenFOAM. The new, non-linear correlation has been proposed based on the proposed (Model (2) and Model (3)). In this section, we will describe the proposed non-linear correlation formula. The proposed correlation (as described below) contains many unknown constraints that will be optimized to minimize the objective function  $f(i)$ . The basic optimization problem is expressed mathematically by the following:

$$\min f(i) = \sum_{i=1}^n \left[ m \left( \frac{j}{j_i} - 1 \right) \right]^2 \quad (4.59)$$

Here,  $n$  is the number of specified operating conditions. The term  $j$  represents the new correlation to be calculated after substituting all geometrical parameters. The new correlations form has been proposed below with all unknown constraint variables specified as  $i = (c, m, n_1, n_2, n_3, n_4)$ , which are then defined and assumed in our MATLAB program. The unknown constraint variable values are assumed, depending on our experience. The  $j_i$  represents the heat transfer that will be calculated depending on the individual model.

$$j = C Re^m \left( \frac{S_{f-s}}{h_{f-s}} \right)^{n_1} \left( \frac{l_w}{h_{f-s}} \right)^{n_2} \left[ 1 + \left( \frac{a_f}{h_{f-s}} \right)^{n_3} Re^{n_4} \right] \quad (4.60)$$

$$f = C Re^m \left( \frac{S_{f-s}}{h_{f-s}} \right)^{n_1} \left( \frac{l_w}{h_{f-s}} \right)^{n_2} \left[ 1 + \left( \frac{a_f}{h_{f-s}} \right)^{n_3} Re^{n_4} \right] \quad (4.61)$$

The new correlation model contained six unknown parameters. All results of the two approved models were used to suggest the new correlation.

The results of the heat-transfer performance  $j_i$  were arranged for Reynolds numbers ranging between (50,70,100,150,200,300,500,500,700,100,1500,2000), in addition to the geometric parameters of the wavy fins for the fin amplitude variables, in order to calculate the heat transfer in terms of Colburn factor  $j$ . We then tested the MATLAB `fmincon` (minimum constrained nonlinear multivariate function) and PSO (particle swarm optimization), after which two optimization functions to optimize the constrained variables were proposed, which are included in the new correlations. The optimization results from the PSO solver were better because they are closer to the default values:

$$C = (2.41), m = (-0.732), n_1 = (0.0101), n_2 = (-1.215), n_3 = (0.6215), n_4 = (0.0777)$$

By applying the same method, we can get a set of unknown parameters for the  $f$  correlation:

$$C = (13.7), m = (-0.728), n_1 = (0.498), n_2 = (0.4233), n_3 = (1.017), n_4 = (0.227)$$

The results of the eight unknown constrained parameters were determined using the optimization methods referred to above. Now we have the final formula of the new proposed correlations to predict the performance of heat transfer in terms of Colburn factor  $j$  and Fanning friction factor  $f$ . New correlations have thus been developed, according to laminar flow regimes and accurate models. The final form of the new correlations are represented, as follows:

$$j = 2.41 \text{Re}^{-0.732} \left( \frac{S_{f-s}}{h_{f-s}} \right)^{0.0101} \left( \frac{l_w}{h_{f-s}} \right)^{-1.215} \left[ 1 + \left( \frac{a_f}{h_{f-s}} \right)^{0.6215} \text{Re}^{0.0777} \right] \quad (4.62)$$

$$f = 13.7 \text{Re}^{-0.728} \left( \frac{S_{f-s}}{h_{f-s}} \right)^{0.498} \left( \frac{l_w}{h_{f-s}} \right)^{0.4233} \left[ 1 + \left( \frac{a_f}{h_{f-s}} \right)^{1.017} \text{Re}^{0.227} \right] \quad (4.63)$$

Figure 4.25 shows the comparison between the new correlations with the best of the developed models. It illustrates that the new correlations have a strong function with Reynolds numbers, and good agreement with the trend line of the models. Two codes of optimization procedures are adopted to obtain the unknown constraint variables, they are `fmincon` and Particle Swarm Optimization PSO. In each optimization method there is a particular code to define functions as `x = fmincon(@(x) fun3(x, a, N, M, Re, JJ), x, A, b, Aeq, beq, rlb, rub);`  
`optionsPSO = optimoptions('particleswarm', 'SwarmSize', 200, 'HybridFcn', @fmincon);`  
`[x, fval, exitflag, output] = particleswarm(@(x)ObjectiveFunction(x, a, N, M, Re, JJ), nvars, lb, ub, optionsPSO);`

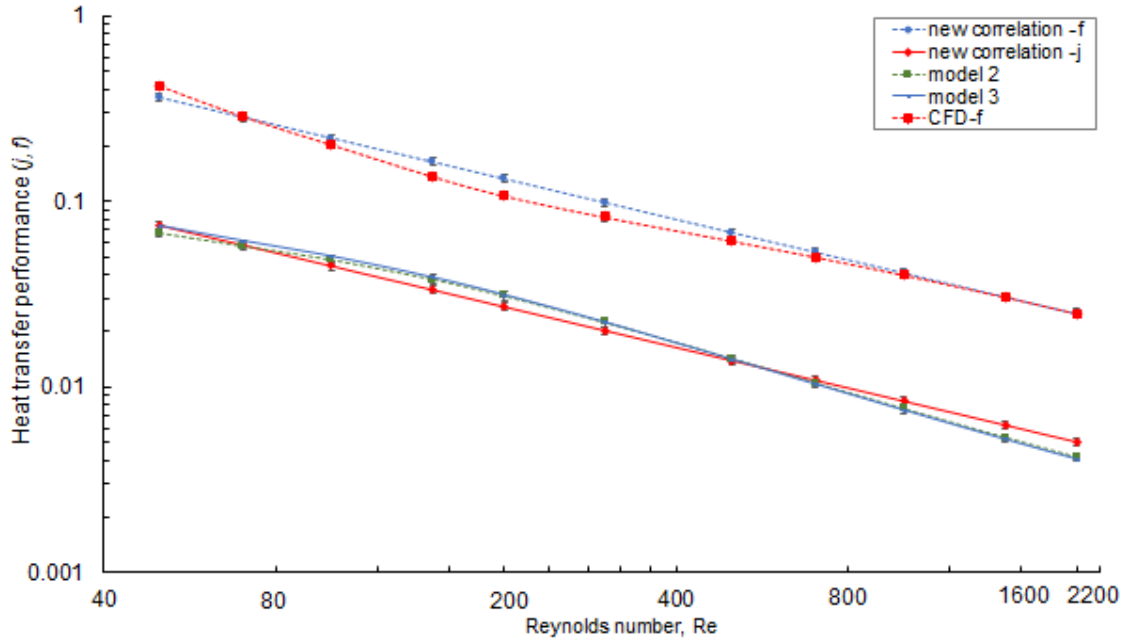
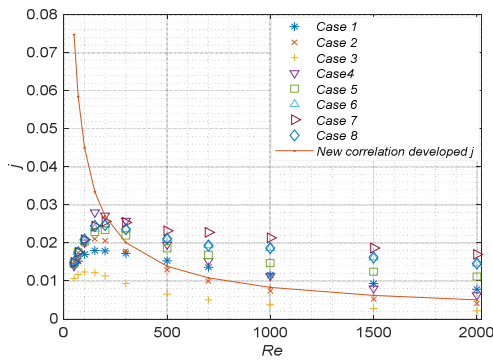
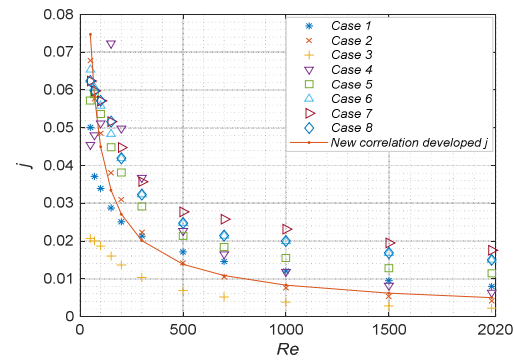


Figure 4.25: Comparisons between new correlations with the modified models, at geometrical parameter  $a_f=0$ ,  $s_{fs}=1.1$  mm, and  $l_w=130$  mm.

Figure 4.26: (a, b, c, d) shows the comparison of the Colburn factor  $j$  between the developed models and the new correlation proposed for all geometrical parameters, as listed in Table 4.1. The deviations for Reynolds numbers ranging between (50-200) were: Model (1) = 18%, Model (2) = 1.6% and Model (3) = 0.1%, and for Reynolds numbers ranging between (300-2000), the rate of deviation was as follows: Model (1) = 8%, Model (2) = 8%, and Model (3) = 1.6%. The deviation for Fanning friction factor  $f$  at Reynolds numbers ranging between (50-200) was 1.1%, and at Reynolds numbers ranging between (300-2000) was 1.6%, which can be neglected.



a- Colburn Factor  $j$ , Model 1



b- Colburn Factor  $j$ , Model 2

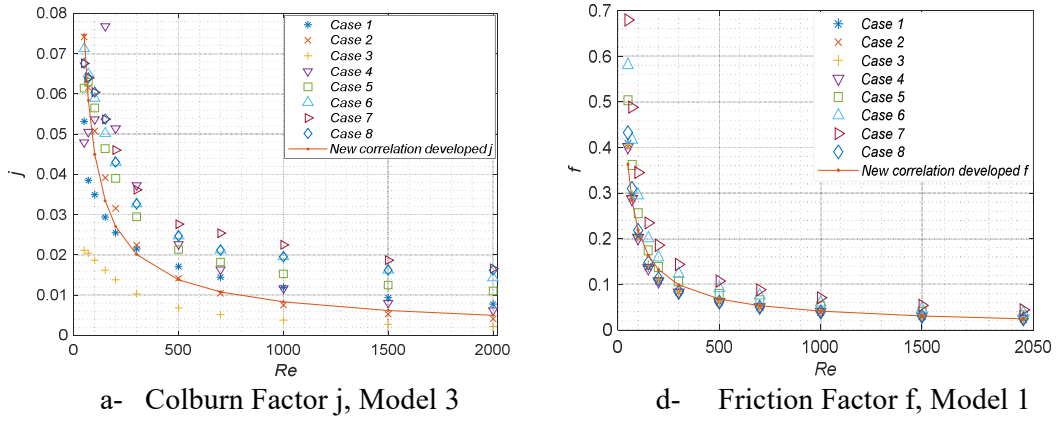


Figure 4.26: (a, b, c and d) Comparison between all cases and models developed.



## 5 HEAT EXCHANGER DESIGN PROCEDURES

---

The design methodology for a 3D-printed plate-fin heat exchanger is now proposed. The selection of fin types and imposed constraints can be considered simultaneously in PFHE design to enhance the heat-transfer performance through some geometrical parameters of the basic fin configuration, namely the fin height  $h_{f-s}$ , fin pitch  $s_{f-s}$ , fin length  $L$  and fin amplitude  $a_f$ . The methodology of our PFHE is based on the identical fin category for wavy fin type, with the same geometrical parameters for both sides of the gas flow. The design of the heat exchanger determines the heat transfer and pressure drop performance. The accurate prediction of heat transfer performance is specified in terms of Colburn  $j$  factor and Fanning friction factor  $f$ , which are important aspects of heat exchanger design, along with the strong function of the surface geometry. An increase in heat transfer is associated with an increased drop in pressure. The design procedure of the heat exchanger led us to investigate the hydraulic performance with the known geometrical dimensions of the heat exchanger and the fin dimensions. The outlet temperatures for cold and hot fluids are not known, the mean temperatures have, at first, been estimated while designing the heat exchanger. The fluid temperatures are calculated and then the physical properties of the fluid have been obtained at varying temperatures. The density, specific heat, viscosity and thermal conductivity for hot and cold fluids were also obtained. The heat transfer performance is estimated depending on the different correlations available. There are a few correlations available in the literature to determine the Colburn and Fanning factors for wavy fin. Our heat exchanger is designed based on the correlations developed by [11].

### 5.1. PFHE GEOMETRICAL PARAMETERS

Design calculations are based on the hot-fluid and cold-fluid sides of the heat exchanger. The maximum size has been adopted for the current plate-fin heat exchanger design, which are ( $L=0.225$  m,  $B=0.2$  m and  $H_0=0.2$  m). Complete details of the geometrical parameters of the plate-fin heat exchanger and the wavy fin are listed in Table 5.1 and table 5.2. The heat exchanger and fins were made of stainless steel.

Table 5.1: Dimensions of the heat exchanger.

Item	Hot side	Cold gas
Number of the gas layers $N$	5	6
Number of the flow channels (without channels near sidebars) $n_f$	100	100

Height of the exchanger $H$ (mm)	200	200
Length of distributor $L_d$ (mm)	12	12

Table 5.2: The basic dimensions of fins.

Item	Hot side	Cold gas
Fin spacing in width, $s_{fs}$ , mm	1.2	1.2
Fin spacing in height, $h_{fs}$ , mm	8	8
Wavelength, $l_w$ , mm	10	10
Wave amplitude, $a_f$ , mm	1.5	1.5
Fin thickness, $\delta_f$ , mm	0.7	0.7
Plate thickness, $\delta_p$ , mm	0.7	0.7
length enlargement of sine wave curve, $\psi$	1.1945	1.1945

## 5.2. PFHE DESIGN PROCEDURE

The heat exchanger consists of a restricted passage, meaning that the pressure drop will be high due to the flow rate of gas passing through the heat exchanger. For this reason, the cross-sectional area of the heater passages should be high, as it helps in distributing a uniform flow in the wavy fin channels. The outlet temperature and pressure were calculated for the heat exchanger, and the estimated calculation is based on the effectiveness  $\mathcal{E}$  and the number of transfer units NTU. These determine the given mass-flow rate and the desired inlet temperatures of the fluid, by using the available correlations for wavy fins developed by [11].

### 5.2.1. HYDRAULIC DIAMETER PARAMETER

The heat transfer area has been calculated separately for each region in the heat exchanger, namely the inlet section, inlet distributor, main section, outlet distributor and outlet section for gas flow through both sides of the channel. We have determined the physical properties for each fluid side, depending on the varying temperatures.

A- Hydraulic diameter for wavy fin:

$$D_h = \frac{2 \times h_{fs} \times (s_f - \delta_f)}{(h_{fs} + (s_f - \delta_f))} \quad (5.1)$$

B- Area ratio for wavy fin:

$$\frac{A_f}{A} = \frac{h_{fs} \times \psi}{(h_{fs} \times \psi + (s_f - \delta_f))} \quad (5.2)$$

C- Heat transfer area in the main section:

$$A = 2 \times N_{\text{layer}} \times A_{\text{m.p}}(h_{\text{fs}} \times \psi + (s_{\text{f}} - \delta_{\text{f}}))/s_{\text{f}} \quad (5.3)$$

### 5.2.2. HEAT TRANSFER COEFFICIENT

The mass velocity is calculated for the specified geometry parameters of the PFHE at the inlet or outlet section, main section, and inlet-outlet distributor as the following:

$$G = \frac{\dot{m} \times s_{\text{f}}}{N_{\text{layer}} \times B_{\text{m.eff}} \times (s_{\text{f}} - \delta_{\text{f}})} \quad (5.4)$$

The Reynolds number is calculated for the different regions in the heat exchanger, namely the inlet and outlet section, main section, and for the inlet-outlet distributor for single-pair channels.

$$\text{Re} = \frac{G \times D_{\text{h}}}{\mu} \quad (5.5)$$

The heat transfer coefficient is calculated depending on the available correlations specifically for the wavy fin category, as described in chapter three. The frictional pressure drop has been calculated for each section in the PFHE.

$$\Delta P = \frac{2 \times f \times G^2 \times L_{\text{eff}}}{\rho \times D_{\text{h}}} \quad (5.6)$$

The overall heat transfer coefficient  $KA$ .

$$KA = \frac{1}{1/(\eta_0 \times A \times \alpha)_h + R_w + 1/(\eta_0 \times A \times \alpha)_c} \quad (5.7)$$

The thermal resistance of the plate.

$$R_w = \frac{\delta_p + (\delta_{\text{f-h}} + \delta_{\text{f-c}}/2)}{\lambda_w \times 2 \times N_{\text{layer}} \times A_{\text{m-p}}} \quad (5.8)$$

The design of the heat exchanger based on the Number of Transfer Units method.

$$\text{NTU} = \frac{(KA_{\text{in-section}} + KA_{\text{main-section}} + KA_{\text{out-section}})}{\dot{m}_h \times c_{\text{p,h}}} \quad (5.9)$$

The effectiveness  $\mathcal{E}$  of the heat exchanger.

$$\varepsilon = \frac{(1 - \exp(NTU \times (R - 1)))}{(1 - R \times \exp(NTU \times (R - 1)))} \quad (5.10)$$

Heat capacity flow rate ratio  $R$  .

$$R = \frac{(\dot{m}c_p)_h}{(\dot{m}c_p)_c} \quad (5.11)$$

The outlet temperature of hot gas.

$$T_{\text{out-hot}} = T_{\text{in-hot}} - \varepsilon \times (T_{\text{in-hot}} - T_{\text{in-cold}}) \quad (5.12)$$

The heat load capacity for the hot side.

$$Q = \dot{m} \times c_p \times (T_{\text{in-hot}} - T_{\text{out-hot}}) \quad (5.13)$$

Now, the energy balance of the hot and cold gases is applied to calculate the outlet temperature of the cold gas.

### 5.3. GEOMETRICAL CHARACTERISTICS OF WAVY FIN

The geometrical parameters calculated for the PFHE are as follows:

A- Number of layer pairs:

$$N_{\text{-layer}} = \frac{(H_0 - h_{f-h} - 2 \times \delta_{sp})}{(h_{f-h} \times h_{f-c} + 2 \times \delta_p)} \quad (5.14)$$

B- Number of layers:

$$N_{\text{-channel}} = ((B - 2 \times (a_f + \delta_{s-b}) - \delta_f / s_{fs})) \quad (5.15)$$

C- Exchanger height:

$$H = (h_{f-s-h} + h_{f-s-c} + 2 \times \delta_p) \times N_{\text{-layer}} + h_{f-s-c} + 2 \times \delta_{sp} \quad (5.16)$$

D- Width of main flow section:

$$B_m = B - 2 \times \delta_{sp} \quad (5.17)$$

E- Width of flow inlet-outlet:

$$B_{i-o} = (B_m - \delta_{sp}) \quad (5.18)$$

F- Distributor angle 1:

$$\theta_1 = \arctan\left(\frac{L_d}{(B_m - B_{io})}\right) \quad (5.19)$$

G- Distributor connecting width:

$$B_d = \sqrt{(L_d)^2 + (B_{io})^2} \quad (5.20)$$

H- Effective distributor width:

$$B_{d,eff} = B_d \times \sin(\theta_1 + \theta_2) \quad (5.21)$$

I- Effective inlet-outlet length:

$$L_{io,eff} = \frac{\delta_{sb} + L_d}{2} \quad (5.22)$$

J- Effective distributor width:

$$L_{d,eff} = \frac{L_d}{2 \times \sin(\theta_1)} \quad (5.23)$$

K- Main section length:

$$L_m = L - 2 \times (\delta_{sb} + L_d) \quad (5.24)$$

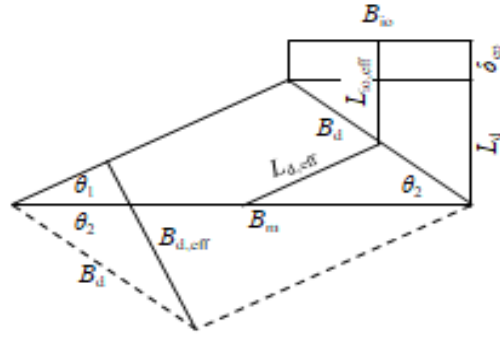


Figure 5.1: The geometrical parameters for one side of the inlet in the PFHE.

#### 5.4. DETERMINATION OF HEAT TRANSFER

The heat-transfer performance is investigated for the hot and cold gases for a single pair of the wavy channels. The following design procedures have been adopted for each part of the plate-fin heat exchanger. The pressure drop is calculated in terms of friction factor  $f$  for the hot and cold gases of the heat exchanger. All parts of the exchanger are calculated (such as the inlet section, inlet distributor, main section, outlet distributor, outlet section).

Thereafter, the heat-transfer coefficient in terms of Colburn factor  $j$  is calculated for both sides of the fluid flow channel. The calculations have been written for each part of the exchanger. Obviously, it seems like almost the same calculation procedure for each part of the exchanger. For additional clarification it has been written below. The physical properties for air were taken from the REFPROP program, according to the boundary condition for each gas; for hot gas the inlet temperature was 750 °C, and inlet pressure was 1.025 bar, and for cold gas the inlet temperature was 40 °C, and inlet pressure was 1.07 bar. The procedure for calculating the heat transfer coefficients for hot and cold gases are similar. The available correlation was applied to estimate the heat transfer in a single pair channel [11].

### 5.4.1. HOT GAS

#### a- At Inlet Section

- Fanning friction factor:

$$f_h = 9.827 \times 105^{-0.705} \left( \frac{0.008}{0.0012} \right)^{0.322} \left( \frac{2 \times 0.0015}{0.0012} \right)^{-0.394} \left( \frac{0.01}{2 \times 0.0015} \right)^{-0.603} = 0.23$$

- Pressure drop:  $\Delta p_h = \left( \frac{2 \times 0.23 \times 5.6^2 \times 0.009}{0.34 \times 0.0021} \right) \div 100000 = 0.0018 \text{ bar}$

#### At Inlet Distributor

- Fanning friction factor:

$$f_h = 9.827 \times 427^{-0.705} \left( \frac{0.008}{0.0012} \right)^{0.322} \left( \frac{2 \times 0.0015}{0.0012} \right)^{-0.394} \left( \frac{0.01}{2 \times 0.0015} \right)^{-0.603} = 0.087$$

- Pressure drop:  $\Delta p_h = \left( \frac{2 \times 0.087 \times 22.7^2 \times 0.05}{0.34 \times 0.0021} \right) \div 100000 = 0.064 \text{ bar}$

- Colburn factor:

$$j_h = 2.348 \times 427^{-0.786} \times \left( \frac{0.008}{0.0012} \right)^{0.312} \times \left( \frac{2 \times 0.0015}{0.0012} \right)^{-0.192} \times \left( \frac{0.01}{2 \times 0.0015} \right)^{-0.432} = 0.018$$

- Nusselt number:  $Nu_h = 0.018 \times 427 \times 0.76^{(1/3)} = 7$

- Heat transfer coefficient:  $\alpha_h = \frac{7 \times 0.069}{0.0021} = 235 \text{ W/m}^2 \cdot \text{K}$

#### b- At Main Section

- Fanning friction factor:

$$f_h = 9.827 \times 67^{-0.705} \left( \frac{0.008}{0.0012} \right)^{0.322} \left( \frac{2 \times 0.0015}{0.0012} \right)^{-0.394} \left( \frac{0.01}{2 \times 0.0015} \right)^{-0.603} = 0.32$$

- Pressure drop:  $\Delta p_h = \left( \frac{2 \times 0.32 \times 1.12^2 \times 0.23}{0.51 \times 0.00082} \right) \div 100000 = 0.0043 \text{ bar}$
- Colburn factor:

$$j_h = 2.348 \times 67^{-0.786} \times \left( \frac{0.008}{0.0012} \right)^{0.312} \times \left( \frac{2 \times 0.0015}{0.0012} \right)^{-0.192} \times \left( \frac{0.01}{2 \times 0.0015} \right)^{-0.432} = 0.078$$

- Nusselt number:  $Nu_h = 0.078 \times 67 \times 0.74^{(1/3)} = 4.7$
- Heat transfer coefficient:  $\alpha_h = \frac{4.7 \times 0.05}{0.00082} = 287 \text{ W/m}^2 \cdot \text{K}$

c- At Outlet Distributor

- Fanning friction factor:

$$f_h = 9.827 \times 954^{-0.705} \left( \frac{0.008}{0.0012} \right)^{0.322} \left( \frac{2 \times 0.0015}{0.0012} \right)^{-0.394} \left( \frac{0.01}{2 \times 0.0015} \right)^{-0.603} = 0.05$$

- Pressure drop:  $\Delta p_h = \left( \frac{2 \times 0.05 \times 22.7^2 \times 0.05}{1.05 \times 0.0021} \right) \div 100000 = 0.012 \text{ bar}$
- Colburn factor:

$$j_h = 2.348 \times 954^{-0.786} \times \left( \frac{0.008}{0.0012} \right)^{0.312} \times \left( \frac{2 \times 0.0015}{0.0012} \right)^{-0.192} \times \left( \frac{0.01}{2 \times 0.0015} \right)^{-0.432} = 0.01$$

- Nusselt number:  $Nu_h = 0.01 \times 954 \times 0.741^{(1/3)} = 8.3$
- Heat transfer coefficient:  $\alpha_h = \frac{8.3 \times 0.028}{0.0021} = 110 \text{ W/m}^2 \cdot \text{K}$

d- At the Outlet Section

- Pressure drop:  $\Delta p_h = \frac{2 \times 0.13 \times 5.6^2 \times 0.009}{1.05 \times 0.0021} \div 100000 = 0.00034 \text{ bar}$
- The total pressure drop has been calculated for each part of the parallel plates as follows:

$$\Delta P = 0.0018 + 0.064 + 0.0043 + 0.012 + 0.00034 = 0.083 \text{ bar}$$

## 5.4.2. COLD GAS

a- At Inlet Section

- Fanning friction factor:

$$f_h = 9.827 \times 181.46^{-0.705} \left( \frac{0.008}{0.0012} \right)^{0.322} \left( \frac{2 \times 0.0015}{0.0012} \right)^{-0.394} \left( \frac{0.01}{2 \times 0.0015} \right)^{-0.603} = 0.16$$

- Pressure drop:  $\Delta p_h = \left( \frac{2 \times 0.16 \times 4.27^2 \times 0.009}{1.179 \times 0.0021} \right) \div 100000 = 0.0002 \text{ bar}$

b- At Inlet Distributor

- Fanning friction factor:

$$f_h = 9.827 \times 736^{-0.705} \left( \frac{0.008}{0.0012} \right)^{0.322} \left( \frac{2 \times 0.0015}{0.0012} \right)^{-0.394} \left( \frac{0.01}{2 \times 0.0015} \right)^{-0.603} = 0.06$$

- Pressure drop:  $\Delta p_h = \left( \frac{2 \times 0.06 \times 17.35^2 \times 0.0514}{1.2 \times 0.0021} \right) \div 100000 = 0.007 \text{ bar}$

- Colburn factor:

$$j_h = 2.348 \times 736^{-0.786} \times \left( \frac{0.008}{0.0012} \right)^{0.312} \times \left( \frac{2 \times 0.0015}{0.0012} \right)^{-0.192} \times \left( \frac{0.01}{2 \times 0.0015} \right)^{-0.432} = 0.012$$

- Nusselt number:  $Nu_h = 0.012 \times 736 \times 0.71^{(1/3)} = 7.7$

- Heat transfer coefficient:  $\alpha_h = \frac{7.7 \times 0.03}{0.0021} = 102 \text{ W/m}^2 \cdot \text{K}$

c- At Main Section:

- Fanning friction factor:

$$f_h = 9.827 \times 52^{-0.705} \left( \frac{0.008}{0.0012} \right)^{0.322} \left( \frac{2 \times 0.0015}{0.0012} \right)^{-0.394} \left( \frac{0.01}{2 \times 0.0015} \right)^{-0.603} = 0.39$$

- Pressure drop:  $\Delta p_h = \left( \frac{2 \times 0.39 \times 2.05^2 \times 0.23}{0.58 \times 0.00082} \right) / 100000 = 0.02 \text{ bar}$

- Colburn factor:

$$j_h = 2.348 \times 52^{-0.786} \times \left( \frac{0.008}{0.0012} \right)^{0.312} \times \left( \frac{2 \times 0.0015}{0.0012} \right)^{-0.192} \times \left( \frac{0.01}{2 \times 0.0015} \right)^{-0.432} = 0.095$$

- Nusselt number:  $Nu_h = 0.095 \times 52 \times 0.706^{(1/3)} = 4.4$

- Heat transfer coefficient:  $\alpha_h = \frac{4.4 \times 0.0483}{0.00082} = 102 \text{ W/m}^2 \cdot \text{K}$

d- At Outlet Distributor:

- Fanning friction factor:

$$f_h = 9.827 \times 336^{-0.705} \left( \frac{0.008}{0.0012} \right)^{0.322} \left( \frac{2 \times 0.0015}{0.0012} \right)^{-0.394} \left( \frac{0.01}{2 \times 0.0015} \right)^{-0.603} = 0.1$$

- Pressure drop:  $\Delta p_h = \left( \frac{2 \times 0.1 \times 17.4^2 \times 0.05}{0.39 \times 0.0021} \right) \div 100000 = 0.039 \text{ bar}$

- Colburn factor:

$$j_h = 2.348 \times 336^{-0.786} \times \left( \frac{0.008}{0.0012} \right)^{0.312} \times \left( \frac{2 \times 0.0015}{0.0012} \right)^{-0.192} \times \left( \frac{0.01}{2 \times 0.0015} \right)^{-0.432} = 0.022$$

- Nusselt number:  $Nu_h = 0.022 \times 336 \times 0.73^{(1/3)} = 6.6$

- Heat transfer coefficient:  $\alpha_h = \frac{6.6 \times 0.066}{0.0021} = 209 \text{ W/m}^2 \cdot \text{K}$

e- At Outlet Section:

- Fanning friction factor:

$$f_h = 9.827 \times 82.83^{-0.705} \left( \frac{0.008}{0.0012} \right)^{0.322} \left( \frac{2 \times 0.0015}{0.0012} \right)^{-0.394} \left( \frac{0.01}{2 \times 0.0015} \right)^{-0.603} = 0.28$$

- Pressure drop:  $\Delta p_h = \left( \frac{2 \times 0.28 \times 4.3^2 \times 0.009}{0.39 \times 0.0021} \right) \div 100000 = 0.0011 \text{ bar}$

- The total pressure drop has been calculated for each part of the parallel plates as follows:

$$\Delta P = 0.0002 + 0.007 + 0.02 + 0.039 + 0.0011 = 0.063 \text{ bar}$$

It's clear that the above calculation for the heat-transfer coefficient increases with an increase of Reynolds number, and that the pressure drop (as a function of flow velocity) also increases.

## 5.5. FIN EFFICIENCY

Fins are mainly used to increase the surface area and enhance the heat transfer coefficient through both the thermal-conductivity and the heat-connectivity of the surface area, in order to transfer heat from hot to cold fluid. Furthermore, the surface temperature of the fin is generally considered to be lower than the base temperature if the fin convicts heat to the fluid. This is described by the fin temperature effectiveness or fin efficiency  $\eta_f$ . The heat will transfer from the surface to the fin by conduction and from the fin to the surrounding medium by convection, with the same heat transfer coefficient. The temperature gradually decreases from the base of the fin to the tip of the fin. Convection from the fin surfaces causes the temperature at any cross section to drop from the midsection toward the outer surfaces. Nevertheless, the cross-section area of the fins is usually very small, and thus the temperature at any cross section can be considered to be uniform. In limit cases at zero thermal resistance or at infinite thermal conductivity, the temperature of the fin will be uniform at the base values  $T_b$ . The heat transfer from the fin will be maximum in the case as the expressed  $Q_{\text{fin max}} = \alpha A_{\text{fin}}(T_b - T_{\infty})$ .

Here,  $A_{\text{fin}}$  denotes of the total surface area of the fin,  $T_b$  denotes the temperature of the plane wall surface and  $T_\infty$  denotes the temperature of the medium.

We can use the relation to determine the heat transfer from a fin when its efficiency is known. In reality, the temperature of the fin will drop along the length of the fin, and thus the heat transfer from the fin will be less toward the fin tip ( $T_b - T_\infty$ ). The fin efficiency ratio  $\eta_f = \dot{q}_{\text{fin}} / \dot{q}_{\text{fin max}}$  is defined as the ratio of the actual heat transfer  $\dot{q}_{\text{fin}}$  through the fin, to the ideal heat-transfer rate from the fin, if the entire fin were at the base temperature of the metal  $\dot{q}_{\text{fin max}}$ . This has been utilized for plate-fin surfaces in heat exchanger designs in the literature from Kays and London [28] and Shah and London [1]. The effectiveness would be determined through the hot gas and cold gas, as the following:

- Fin parameter is calculated as:  $m_h = \sqrt{\frac{2 \times \alpha \times P}{\lambda_t \times A_c}} = 0.94$  and the cold gas  $m_c = 0.6$

- Fin effectiveness for hot gas:  $\eta_{f-h} = \frac{\tanh[m]}{m} = 0.8$ , for cold gas  $\eta_{f-c} = 0.9$

- Overall fin efficiency:  $\eta_{0-h} = 1 - (1 - \eta_h) \times \left( \frac{h_{fs} \times \psi_h}{h_{fs} \times \psi_h + s_{fs}} \right)$

$$\eta_{0-h} = 1 - (1 - 0.8) \times \left( \frac{0.008 \times 1.194}{0.008 \times 1.19 + 0.0012} \right) = 0.8, \text{ for the cold gas is } \eta_{0-c} = 0.9$$

### 5.5.1. OUTLET TEMPERATURE AND PRESSURE ESTIMATION

Basically, for each part of the heat exchanger, the overall heat transfer coefficient  $KA$  should be calculated:

- Thermal resistance calculation:

$$R_w = \frac{(0.0007 + (0.0007 + 0.0007) / 2)}{(15 \times 2 \times 10 \times 0.043)} = 0.000054 \text{ W/K}$$

- Overall heat transfer coefficient  $\times$  area  $KA$  for the main section:

$$KA = \frac{1}{\left( \frac{1}{(287 \times 0.488 \times 0.8)} \right)_h + 0.0005 + \left( \frac{1}{(102 \times 0.488 \times 0.9)} \right)_c} = 318 \text{ W/K}$$

- Number of transfer units:  $NTU = \frac{(318 + 1.6 + 0.4)}{0.011 \times 1123} = 26$

- Rate ratio of the heat capacity flow:  $R = \frac{0.0108 \times 1123}{0.0091 \times 1061} = 1.3$

- The effectiveness: 
$$\varepsilon = \frac{(1 - \text{EXP}(26 \times (1.3 - 1)))}{(1 - 1.3 \times \text{EXP}(26 \times (1.3 - 1)))} = 0.8$$
- The outlet temperature of hot gas:  $T_{\text{out-hot}} = 750 - 0.7938 \times (750 - 43) = 189^\circ\text{C}$
- The heat load:  $Q = 0.0108 \times 1123 \times (750 - 189) = 7 \text{ kW}$

By applying the energy balance equation, we find the outlet temperature of the cold gas:  $T_{\text{out-cold}} = 750^\circ\text{C}$ . The outlet pressures of the hot gas and the cold gas are easily calculated by compensating for both inlet pressure and pressure drop as calculated above, in the relation of  $\Delta P = P_2 - P_1$ . All data for both the cold and hot gas is written in Table 5.3. The outlet pressure for hot gas is  $P_{2\text{-hot}} = 0.9321 \text{ bar}$ , and the outlet pressure for the cold gas is  $P_{2\text{-cold}} = 0.942 \text{ bar}$ .



## 6 EXPERIMENTAL DATA ANALYSIS

---

The experimental setup used in this experiment consists of a real plate-fin heat exchanger with counter flow arrangements. In this chapter, the principles of measurement available to complete the practical aspect of the current thesis will be presented, and the layout of the experimental setup will be displayed, including the description of the various components of the setup, and the calibration of the tools used. We'll start with the experimental and practical setup. The experimental setup consists of the following details: The heating unit, the section testing, and the instruments of the measurement system, as shown in Figure 6.1. The hot air coming from the first path in the lowest direction of the heat exchanger will pass through the heating unit. The cold air will be provided through the second path in the upper side, in the counter-flow of the heat exchanger. Also, in the second path, the cold gas will also pass through the heating unit to obtain the desired gas temperature. The air supply required to carry out the experiment will be provided from a compressed air unit, available in the laboratory, to complete the practical aspect of the present work.

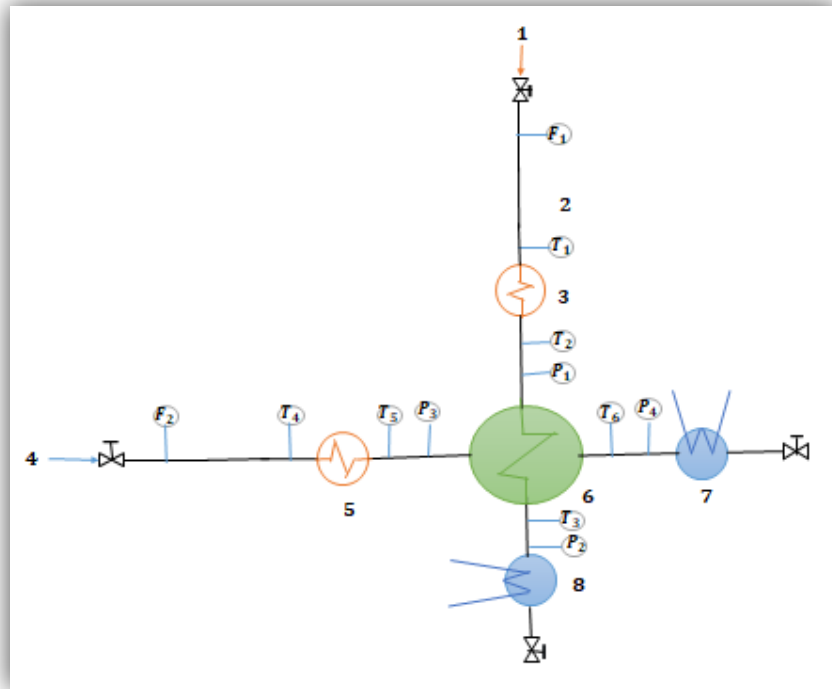


Figure 6.1: Schematic diagram of the experimental test rig with measurement position.

1: Compressed air–Hot path	3,5: Heater	4: Compressed air–Cold path	6: PFHE, Test section	7,8: Cooling unit
F1, F2: Mass flow rate	T1, T4: Thermocouples before the heater	T2, T5: Thermocouples before PFHE	T3, T6: Thermocouples Outlet of PFHE	P1, P2, P3, P4 Pressure Taps

The hot and cold air will be heated by passing the two paths through the heating unit to reach the required temperature before the gas flows into the heat exchanger. Mass-flow controllers are used to regulate the amount of gas entering the heat exchanger. The bypass valves will be closed when the mass-flow rates for both flows reach the required rate. Pressure gauges are provided to measure hot and cold air pressure and have been located before inlet and outlet in both gases' paths of the heat exchanger. These pressure taps are connected to the U tube pressure gauge to give the value of pressure drop. The temperature of the gases at the entrance and the exit of the heat exchanger are measured using thermocouples. The plate-fin heat exchanger (test section) is carefully insulated using layered insulation sheets with 50 mm thickness. This material is defined as microporous (silicon SiO<sub>2</sub>) and is used for high-temperature applications, as the separation of tiny particles is highly effective for heat exchanger insulation. Further, we are using another type of insulation material to insulate the pipes connected at the inlet and outlet for both gases: Stone wool sheets and white wool insulation. These are made of temperature-resistant wool, and are used to eliminate heat loss from the system to its surroundings, as shown in figure 6.2.

All the measurement instruments used in this experimental work are connected to the Lap View program on the computer, to report and read the outlet data. At first, the experimental rig is kept at a low value of flow rate, then it is gradually increased according to the desired rate of fluid-flow in both paths. The temperatures for hot and cold paths are maintained at the desired range by adjusting the power supply unit. The heat-transfer performance is calculated in terms of Colburn factor  $j$  and Fanning friction factor  $f$ , depending on our new correlations that were developed in this thesis. The experimental results are compared with the simulation results, through adopting the same operating conditions as used in the experimental work in the OpenFOAM program.



Figure 6.2: Photograph of the experimental setup

## 6.1. DESCRIPTION OF THE EQUIPMENT AND INSTRUMENTS

### 6.1.1. PLATE-FIN HEAT EXCHANGER

Our plate-fin heat exchanger utilizes the wavy fin with a counter flow arrangement. The design procedure has been explained in detail in chapter 5. Figure 6.3 shows an image of the heat exchanger, which was designed for and used in our experimental work.

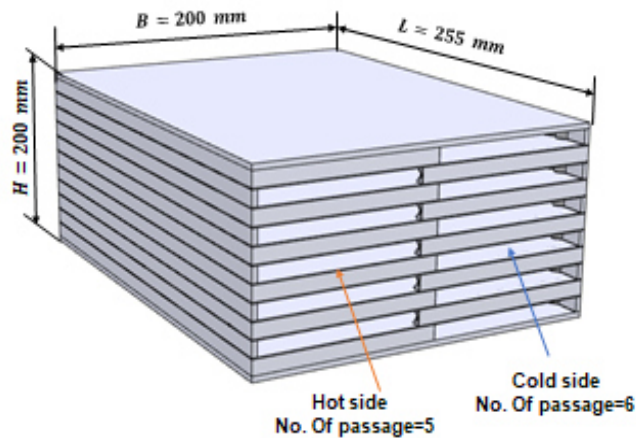


Fig. 6.3: The image of the plate-fin heat exchanger

The pressure setup at the hot fluid inlet is 1.025 bar and has 5 layers, whereas the pressure setup at the cold fluid inlet is 1.07 bar and has 6 layers. Tables 6.1 and 6.2 list the details of the PFHE dimensions and design data.

Table 6.1: The heat exchanger design data with flow arrangement.

Item	Hot Side	Cold Side
Fin	Wavy fin-type	Wavy fin-type
No. Of layer	5	6
No. Of channel	100	100
No. Of pass	1	1
Flow rate	Counterflow	Counterflow

Table 6.2: Polynomial physical properties.

Item	Hot side	Cold gas
$T_{in}$ , K	1023 - 840	523 - 476
$P_{in}$ , bar	1.025 - 1.025	1.07 - 1.07
$\dot{m}_{max}$ , kg/min	0.0391 - 0.098	0.033 - 0.0839
$\rho$ , kg/m <sup>3</sup>	0.349 - 0.425	0.712 - 0.782
$c_p$ , J/kg. K	1146 - 1108	1035 - 1025
$\mu$ , Pa.s	$4.4 \cdot 10^{-5}$ - $3.6 \cdot 10^{-5}$	$2.8 \cdot 10^{-5}$ - $2.8 \cdot 10^{-5}$
$\lambda$ , W/m. K	0.067 - 0.058	0.041 - 0.037
Pr	0.747 - 0.682	0.739 - 0.739

### 6.1.2. COMPRESSED AIR

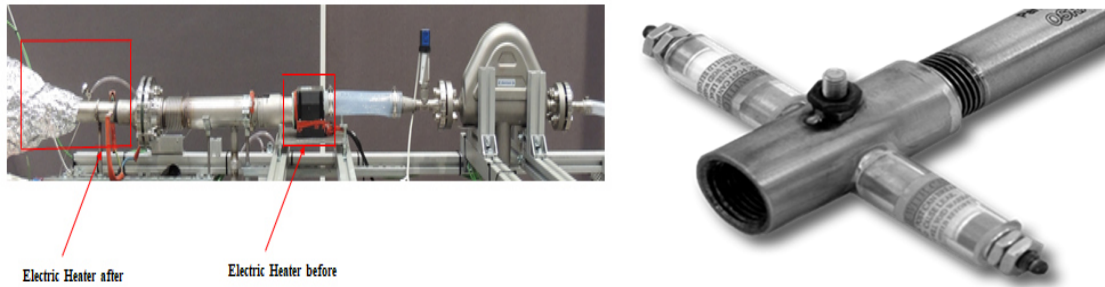
The Screw Compressed Air System is the device used to provide the required air supply in the experimental setup. It is manufactured by BOGE C9. This effectively delivers 1.06 kg/min, with a max pressure of 10 bar and motor power of 7.5 kW.



Figure 6.4: Screw Compressed Air System. [BOGE AIR. boge.com].

### 6.1.3. HEATING UNIT

The heaters used to achieve the desired temperature of the gas in this work are Threaded Inline air heaters. The Threaded Inline air heaters are installed on both compressed air supply line sides of the heat exchanger as shown in figure 6.5. The maximum inlet pressure for this product is 10 bar (150 psi), the maximum inlet air temperature of the heater can reach up to 482 C (900 F), the outlet temperature can reach up to 760 C (1400 F) and the maximum power is 8 kW.

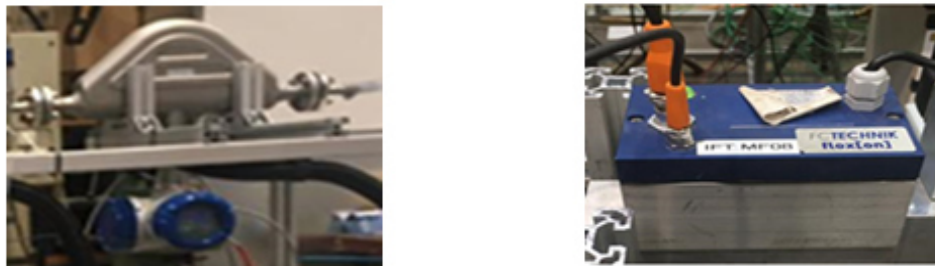


a- Experimental setup cold airflow line. b- Threaded Inline heater type [Tutco.com].

Figure 6.5: Heater unit used in the experimental setup.

### 6.1.4. MASS-FLOW MEASURING

This device is based on the principles of motion mechanics. Figure 6.6 shows the Coriolis device and mass control device which were used to measure the mass-flow meters. The Coriolis device is used to measure the force, which results from the acceleration caused by mass that is moving toward a center.



a- The Coriolis device

b- The mass-flow control device

Figure 6.6: Mass-flow measuring devices.

### 6.1.5. U-TUBE MANOMETER

The vertical U-Tube manometer is used in differential pressure measurement with flow meters like pitot tubes, orifices and nozzles. The pressure measuring devices use liquid columns in vertical tubes. The water-filled U-Tube manometer measures the pressure difference located in the airflow of the system.

### 6.1.6. THERMOCOUPLES

The temperature gradient along the length of an electrical conductor is a phenomenon known as the Seebeck effect. A thermocouple produces a temperature-dependent voltage as a result of the thermo-electric effect; this voltage can be interpreted to measure the temperature value. It is an electrical device consisting of two dissimilar electrical conductors forming an electrical junction, resulting in an electromotive force (emf). The emf is characteristic of the conductor materials used, and is also dependent upon the temperatures of the junctions. The main limitation with thermocouples is precision in achieving systematic errors of less than one degree Celsius °C. Different metals are joined at the ends and there is a temperature difference between the joints, the magnetic field is observed, the magnitude of the voltage depends on the types of wire being used.

## 6.2. EXPERIMENTAL DATA

In this study, the single pair wavy fin geometry has been studied. The radiative heat transfer ( $q_r$ ) was taken into account through considering the assumptions made: (1) Isothermal fins and not-radiating surrounding (2) The surrounding medium assumes that the enclosure is much larger and black-body, therefore the temperature of the surrounding medium can be assumed as equal to the ambient one; no reflection or transmission occurs. The heat that is dissipated by radiation has then been calculated by using the Stefan–Boltzmann equation. The radiant energy is transferred between two or more objects at different temperatures. The net rate of energy transfer depends on the geometric configuration of the wavy fin, which determines the amount of radiation emitted from one object to another. The net rate of radiant energy transfer from object 1 to object 2 is represented by:

$$\dot{q}_1 = \varepsilon \cdot \sigma_{SB} A \sum_{i=1}^N F_{1,i} (T_1^4 - T_2^4) \quad (6.1)$$

The radiative and convective coefficients can be combined to obtain a total heat-transfer coefficient. To find the radiation heat transfer coefficient  $\alpha_r$  is written as:

$$\dot{q}_{rad} = \alpha_r A \Delta T \quad (6.2)$$

$$\alpha_r = F_{1,2} \left[ \frac{\sigma_{SB} (T_1^4 - T_2^4)}{T_1 - T_2} \right] \quad (6.3)$$

Where,  $\varepsilon$  is the emissivity of the stainless-steel material (0.85),  $\sigma$  is the Stefan–Boltzmann constant ( $5.67 \cdot 10^{-8} \text{ W/m}^2 \text{ K}^4$ ),  $A$  is the area of the fin surface,  $F$  is the view factor between the fin surface and the ambient, and  $T_{fin}$  and  $T_{amb}$  are the temperatures of the fins and the ambient, respectively. Due to a lack of referenced methods to obtain the view factor for the wavy fin, we have assumed the view factor to be (0.85). As it is essential to validate the numerical with experimental results, we have adopted two cases' results, as written in Tables 6.3 and 6.4. The pressure at the inlet of both fluids should be high enough to overcome the pressure losses that will occur during the flow, through the heat exchanger. In this way, we can ensure that the flow channels are completely flooded and there is no starvation anywhere. The heat-transfer performance enhancement is associated with an increase in flow-friction and vice versa, so, Colburn factor  $j$  and Fanning friction factor  $f$  are strong functions of the surface geometry. The physical properties for both gases were taken with temperature dependent polynomial expressions:  $(C_p, \mu, \rho, \lambda) = \sum_{i=0}^7 a_i T^i$ . The experimental data is conducted at different mass-flow rates at constant inlet temperatures to study the heat transfer performance at different Reynolds numbers. As mentioned, the amount of air entering the heat exchanger is regulated by the mass-flow control device placed at the inlets of both paths.

The mass-flow rate for each measurement in the experimental work is calculated depending on the number of layers for cold and for hot gas in the heat exchanger. For our case, we have divided the mass-flow rate for the gas entering into the test section by the number of layers, to obtain the mass-flow rate for the channel.

$$\dot{m}_{channel} = \frac{\dot{m}_{total}}{N_{layer}} \quad (6.4)$$

Where  $\dot{m}_{total}$  is the value of mass-flow rate, calculated for the entire heat exchanger.

Table 6.3: Experimentally observed data at different mass-flow rates for hot and cold air at constant inlet temperature.  $T_{\text{hot}}=1023 \text{ K}$ ,  $T_{\text{cold}}=523 \text{ K}$ .

Flow rate, hot air kg/min	Re, hot	Pressure drop at hot air, mbar	out temp. hot air, $T_3$ , K	Flow rate, cold air , kg/min	Re, cold	Pressure drop at cold fluid, mbar	Out temp. cold air, $T_6$ , K
0.1957	77	2.2	246	0.1996	102	3.8	715
0.1957	77	2.6	248	0.2019	103	4.0	724
0.1957	77	2.9	303	0.2022	104	2.6	654
0.2956	115	3.9	250	0.2993	153	6.1	728
0.3454	135	6.4	309	0.3396	174	5.4	685
0.3454	136	8.3	452	0.3507	180	3.5	527
0.3935	154	6.9	269	0.4150	213	7.9	720
0.4185	164	8.6	311	0.4241	217	7.1	692
0.4935	192	15.2	553	0.4962	254	7.2	642
0.4935	193	12.5	374	0.49931	256	6.1	544
0.4935	194	10.9	319	0.5018	257	5.2	452
0.4936	195	14.5	471	0.5035	258	9.0	700

Table 6.4: Experimentally observed data at different mass-flow rates for hot and cold air at constant inlet temperature.  $T_{\text{hot}}=840 \text{ K}$ ,  $T_{\text{cold}}=476 \text{ K}$ .

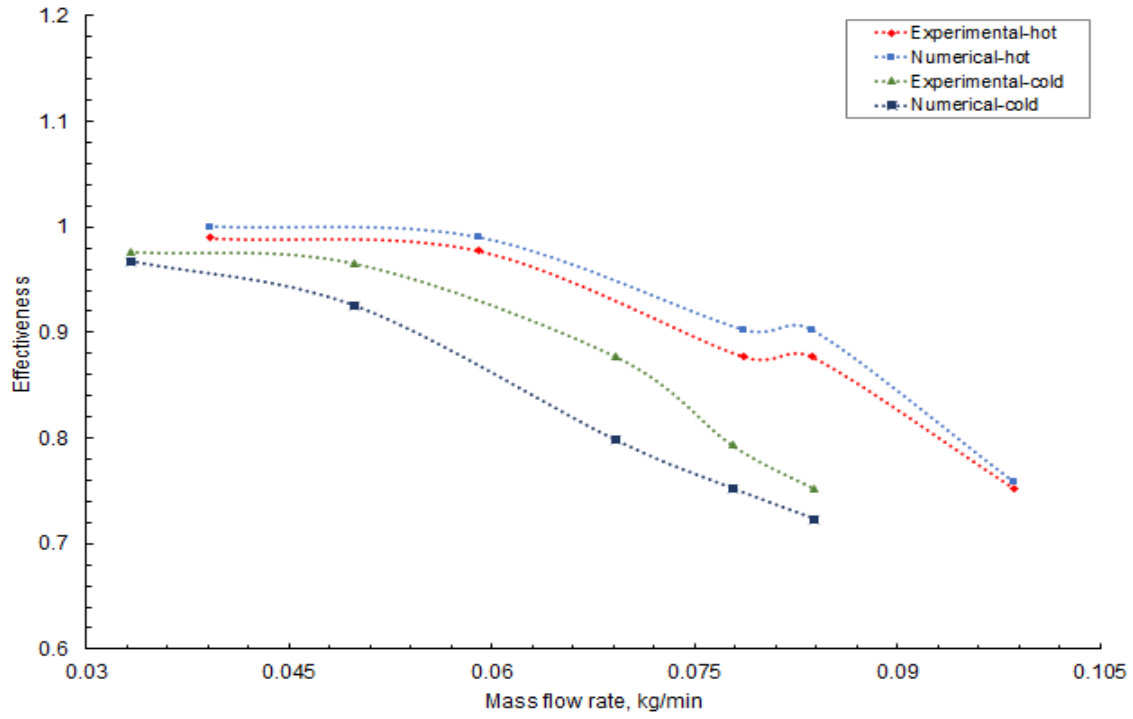
Flow rate, hot air kg/min	Re, hot	Pressure drop at hot air, mbar	out temp. hot air, $T_3$ , K	Flow rate, cold air , kg/min	Re, cold	Pressure drop at cold fluid, mbar	Out temp. hot air, $T_6$ , K
0.045	106	3.43	361	0.034	105	2.93	557

0.064	153	4.99	319	0.034	105	3.04	559
0.064	153	4.11	209	0.035	107	2.44	521
0.084	200	5.68	215	0.036	110	2.84	549
0.084	200	8.33	382	0.055	167	4.89	550
0.084	200	6.61	247	0.055	168	5.09	558
0.084	200	7.54	301	0.071	217	6.76	551
0.109	259	11.07	303	0.071	219	5.88	528
0.134	313	13.71	310	0.072	220	4.51	466
0.134	318	14.69	444	0.080	247	7.54	552
0.134	318	14.69	382	0.090	277	5.09	356
0.284	676	2.253	200	0.091	280	6.27	484

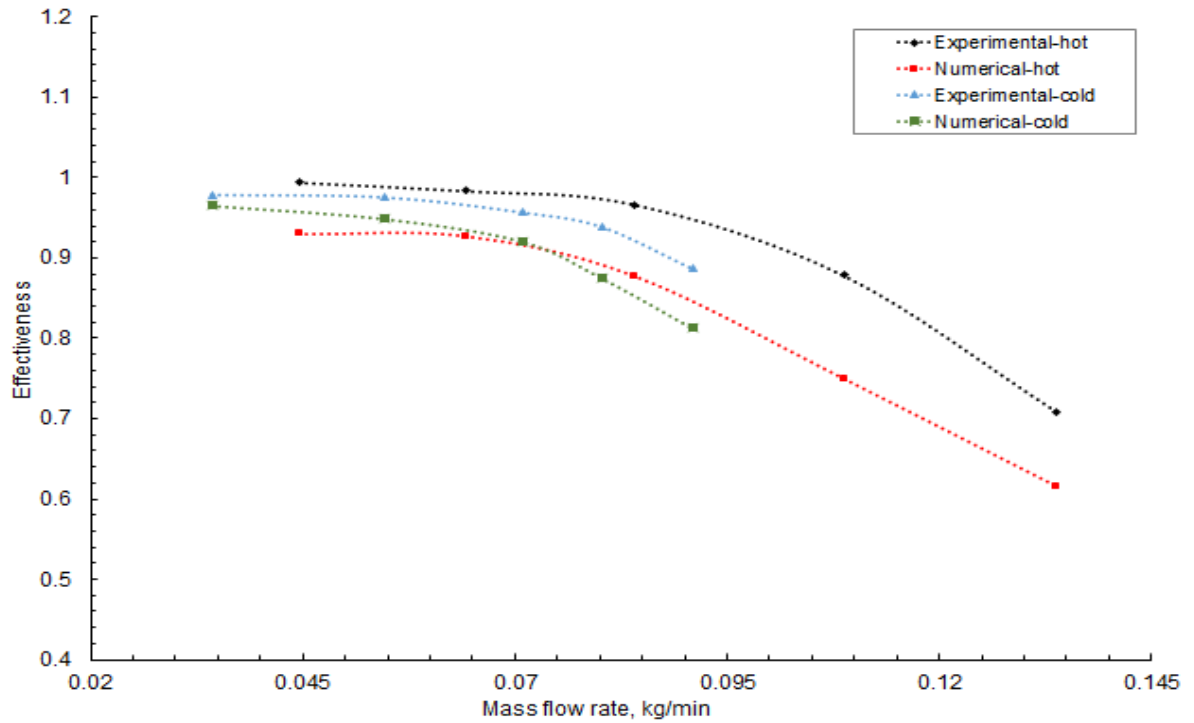
### 6.2.1 EFFECTIVENESS DIFFERENCES WITH MASS-FLOW RATE

The different outlet temperatures for hot gas and cold gas indicate a heat loss of energy. In an ideal situation without heat leak, the temperature drop in the hot stream channel should be equal to the temperature gain in the cold stream channel. Figure 6.7 shows the effectiveness comparison between the numerical and experimental results. The effectiveness is calculated at different mass-flow rates and at constant inlet temperatures for the hot gas and cold gas. The effectiveness of the hot gas ( $\varepsilon_h$ ) is based on the hot air, and the effectiveness of cold gas ( $\varepsilon_c$ ) is based on the cold air, for inlet and outlet temperatures. The figure illustrates the validation of results through comparison of the numerical and experimental data. Validation is obtained for the hot and cold effectiveness  $\varepsilon_h$ ,  $\varepsilon_c$ , as they increased with the reduction of the mass-flow rate. The experimental and numerical results for hot gas are in better agreement than the results of the cold gas within the specified range of deviation.

The effectiveness is directly related to the increase in Reynolds number, and thus the heat transfer coefficient increases when the mass-flow rate is increased. The numerical and experimental results have been calculated without taking heat loss to the surroundings into account.



a-Inlet Temperatures:  $T_{\text{hot}}=1023$  K,  $T_{\text{cold}}=523$  K



b- Inlet Temperatures:  $T_{\text{hot}}= 840$  K,  $T_{\text{cold}}= 476$  K

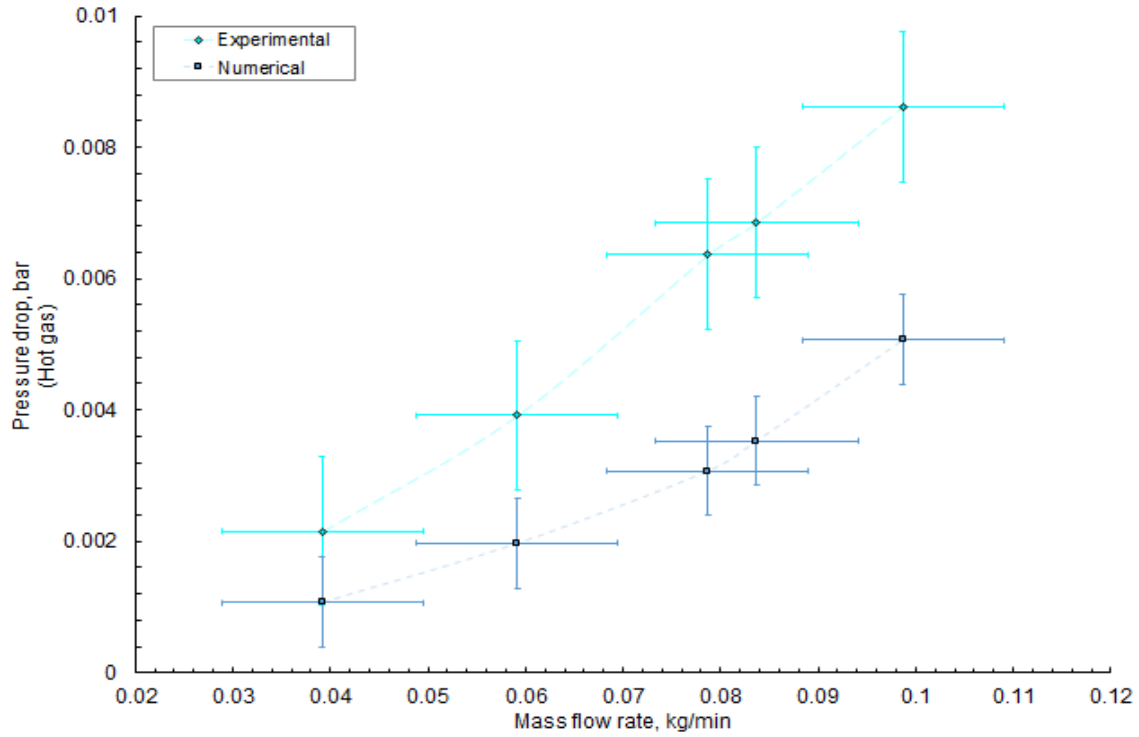
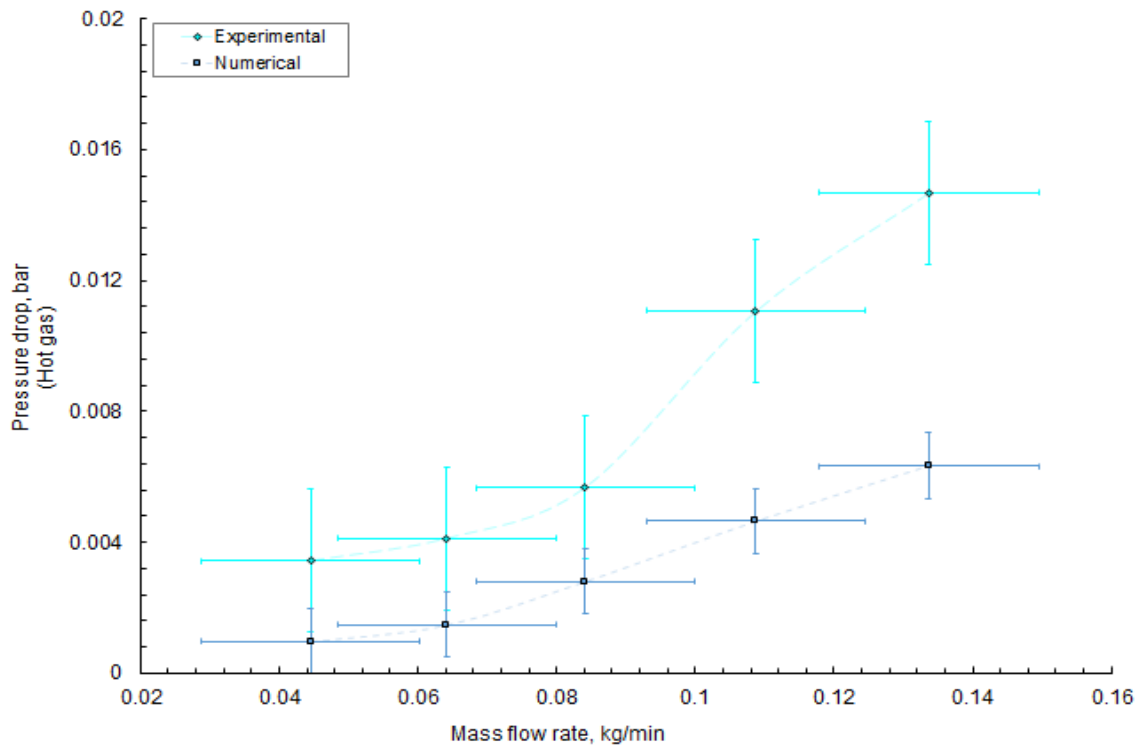
Figure 6.7: Effectiveness variation with mass-flow rate.

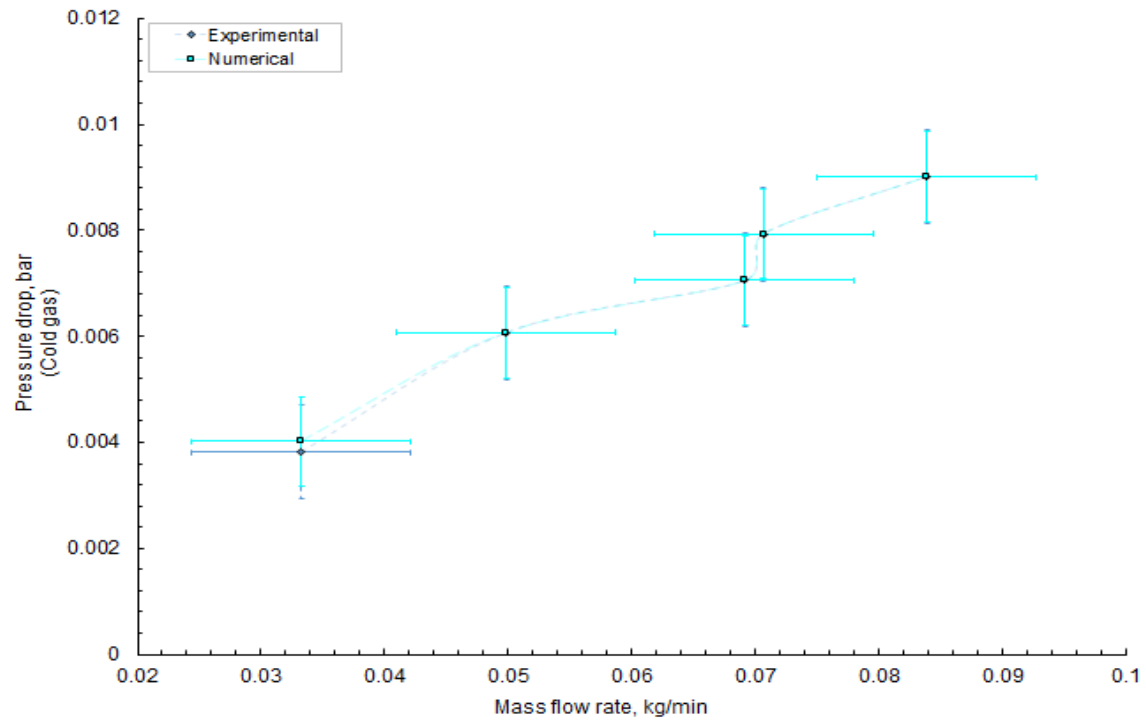
For the effectiveness, the percentage of deviation between the experimental values and the numerical simulation values is varied. For hot gas, the deviations range between  $\pm 5\%$  and  $\pm 6\%$  at inlet temperatures 1023 K and 840 K. For cold gas, the deviations range between  $\pm 20\%$  and  $\pm 8\%$  at inlet temperatures 523.15 K and 476 K. The uncertainties found between the results of the experiment and the simulation may be caused by the estimations being obtained without factoring heat loss into the calculations. The effectiveness is calculated at different mass-flow rates ranging between (0.0391-0.0986 kg/min) for hot gas, and (0.0332-0.0839 kg/min) for cold gas, which are applied for two cases.

### **6.2.2. VARIATION OF PRESSURE DROP WITH MASS-FLOW RATES**

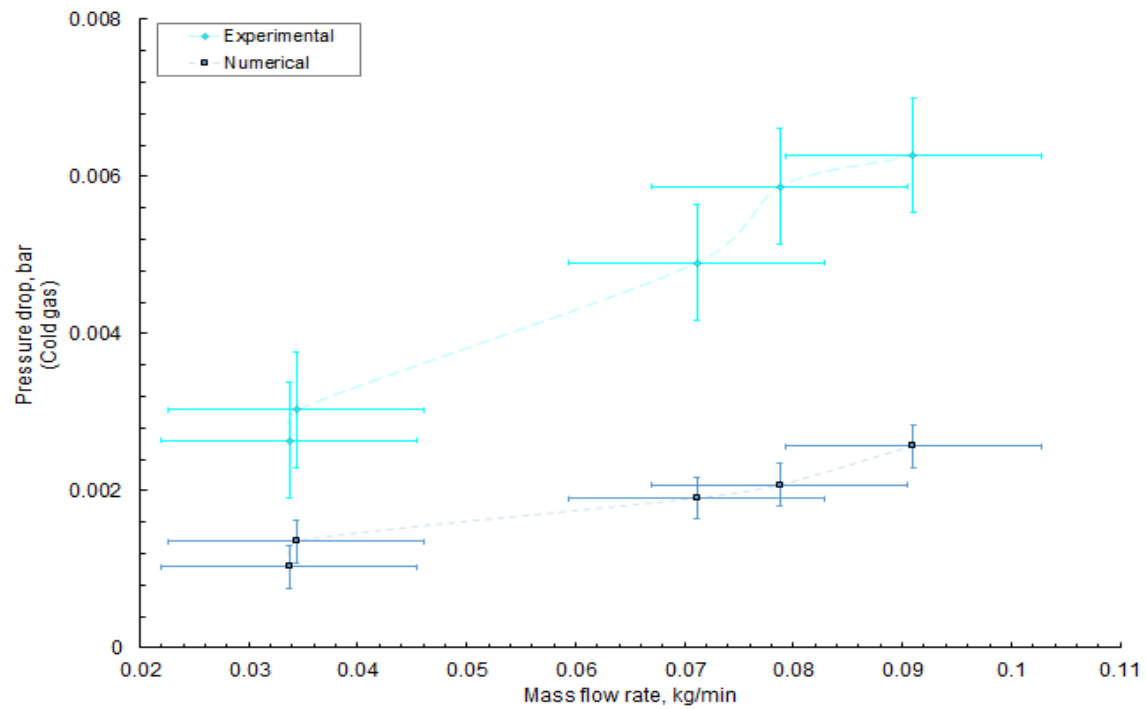
Figure 6.8 presents the pressures drop comparison for both the numerical simulation and experimental values, which are obtained with ranging mass-flow rates, and at constant hot- and cold-inlet gas temperatures for two cases. It can be observed that the pressure drop increases continuously with the increasing mass-flow rate.

The trend line of the simulation results for hot gas goes down below the allowable pressure drop, at 0.01 bar. The deviation is observed as significant between the pressure drop of the simulation and the experiment, specifically at high mass-flow rates. Nevertheless, the pressure drop is not a serious concern since it is within the allowable pressure drop limit. The pressure drop difference between the two fluids, the hot gas and the cold gas, are noted in Table 6.3.

a-  $T_{\text{hot}} = 1023 \text{ K}$  (inlet temp.)b-  $T_{\text{hot}} = 840 \text{ K}$  (inlet temp.)



c-  $T_{\text{cold}} = 523 \text{ K}$  (inlet temp.)



d-  $T_{\text{cold}} = 476 \text{ K}$  (inlet temp.)

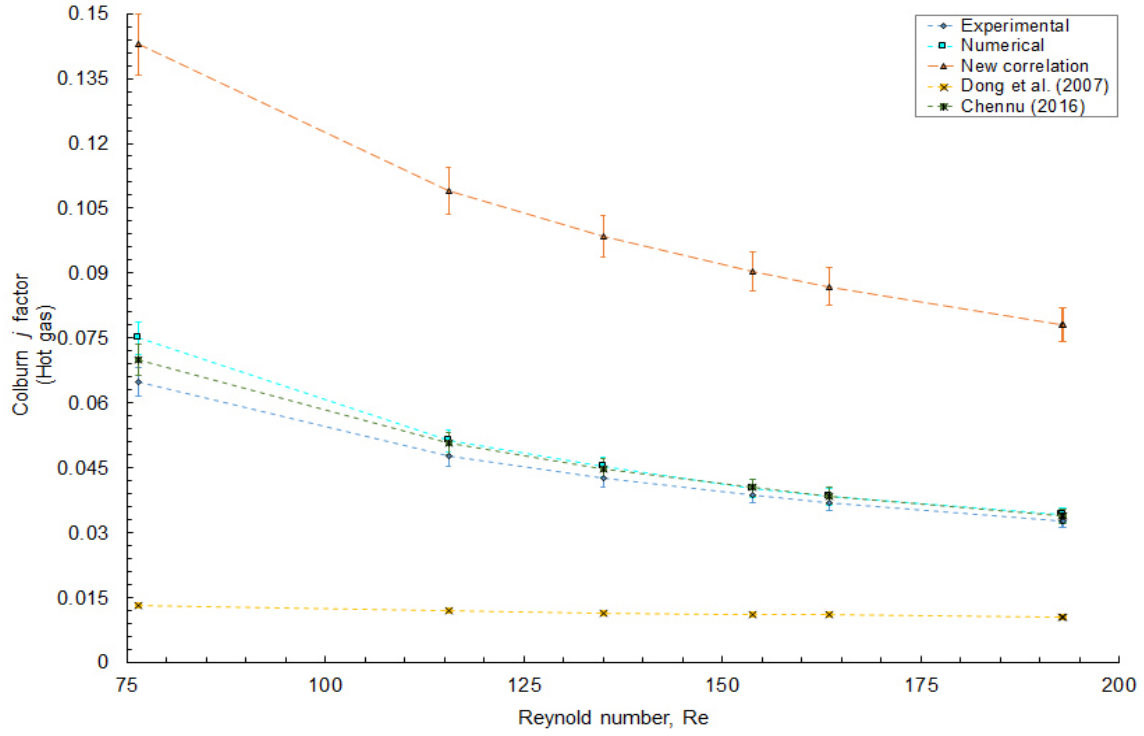
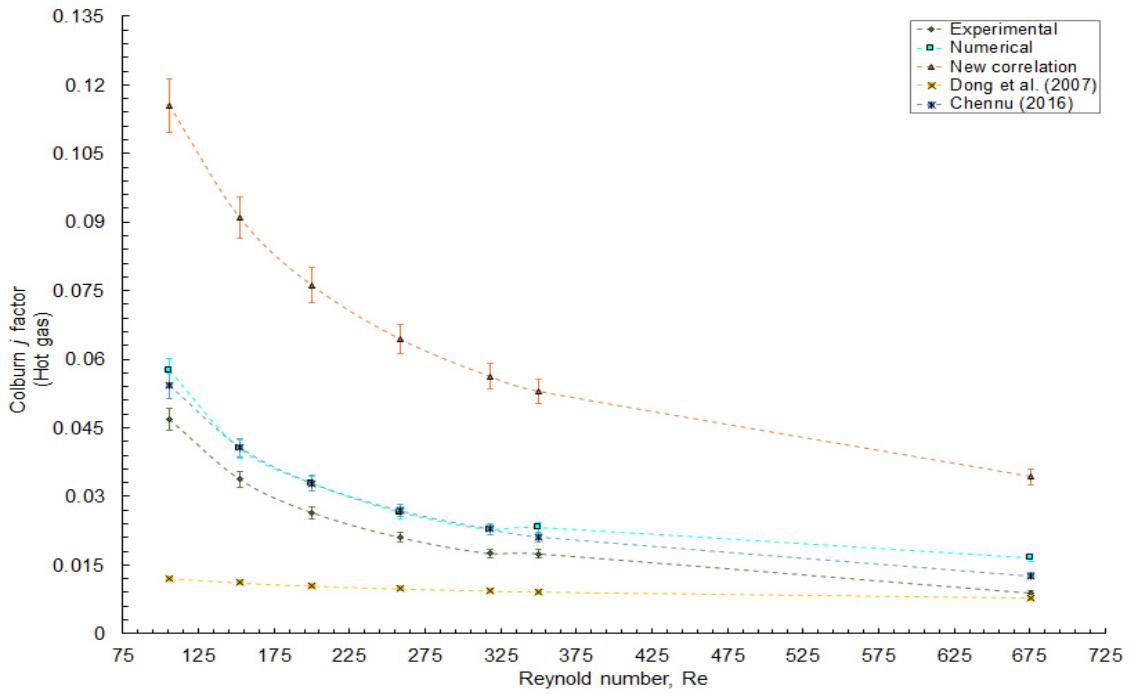
Figure 6.8: Variation of pressure drop with mass-flow rates.

Figure 6.8 illustrates that the trend line of the experimental pressure drop exceeds the allowable pressure drop, at 0.01 bar. The reason for this is that the surfaces of the plate used to manufacture the fins and the plate in the real plate-fin heat exchanger (test section) is rough, and not smooth as was assumed in the simulation. In addition, during the experiment, at the entrance of the hot and cold air we used a plate that contains holes that are equally distributed to ensure that the fluid is distributed uniformly inside the heat exchanger. These two aspects influence the increasing pressure drop in the experimental work.

### **6.2.3. SIMULATION RESULTS VALIDATION WITH EXPERIMENTAL**

The CFD data of the single pair of wavy channels in the plate-fin heat exchanger were validated with the experimental data. The heat-transfer performance data for both the experimental and CFD numerical results were obtained at the inlet gas temperature, ranging (1023-840 K) for hot gas, and for cold gas ranging between (523-476 K). Figure 6.9 shows the comparison between the experimental and numerical simulation results with the available literature. The deviation found ranges between (0.8% -12%) and (22%-85%) for hot-gas inlet temperatures ranging between (1023 K-840 K), and deviation ranging between (2%-21%) and (3%-25%) for cold-gas inlet temperatures ranging between (503 K-476 K) respectively. The numerical results are larger than the experimental results for hot gas, particularly for high Reynolds numbers. This was one of the conclusions of this thesis: The numerical simulation results indicate that the flow uniformity in the channels is affected by the flow structures. In addition, the simulated gas temperatures will be relatively sensitive inside the channels in laminar flow.

The heat transfer coefficient is calculated without the heat loss for each mass-flow and the hot end of the PFHE channel is more effected by heat loss to its surroundings. The values obtained from the experiment and the numerical simulation are in acceptable agreement.

a-  $T_{hot} = 1023$  K (inlet temp.)b-  $T_{hot} = 840$  K (inlet temp.)

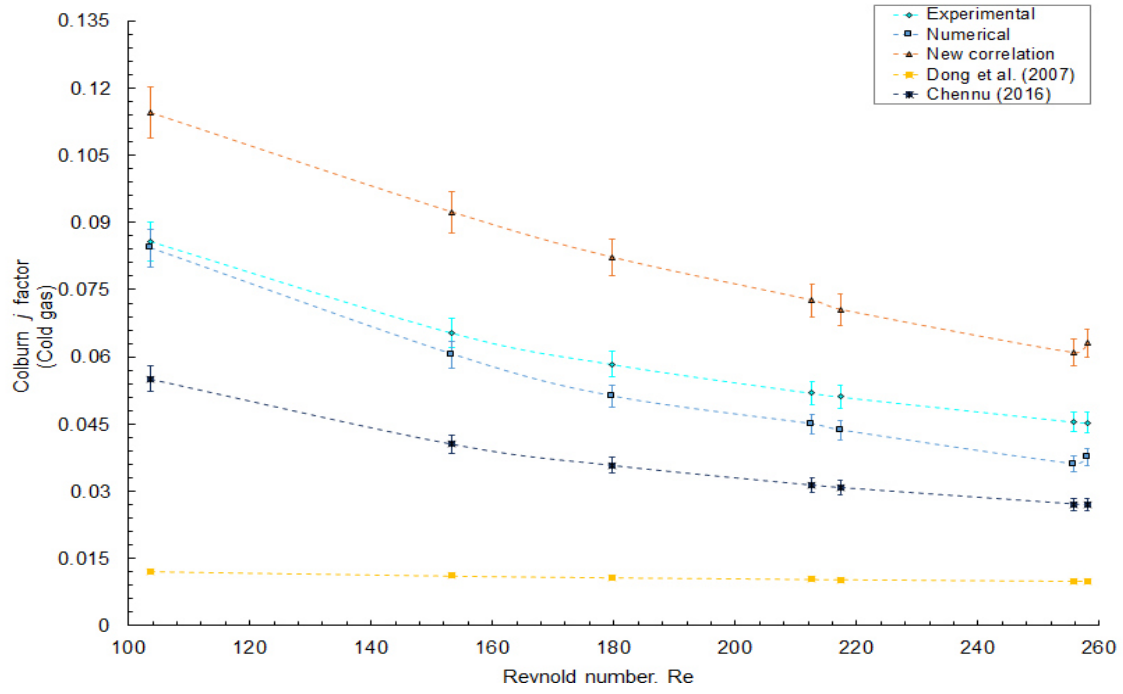
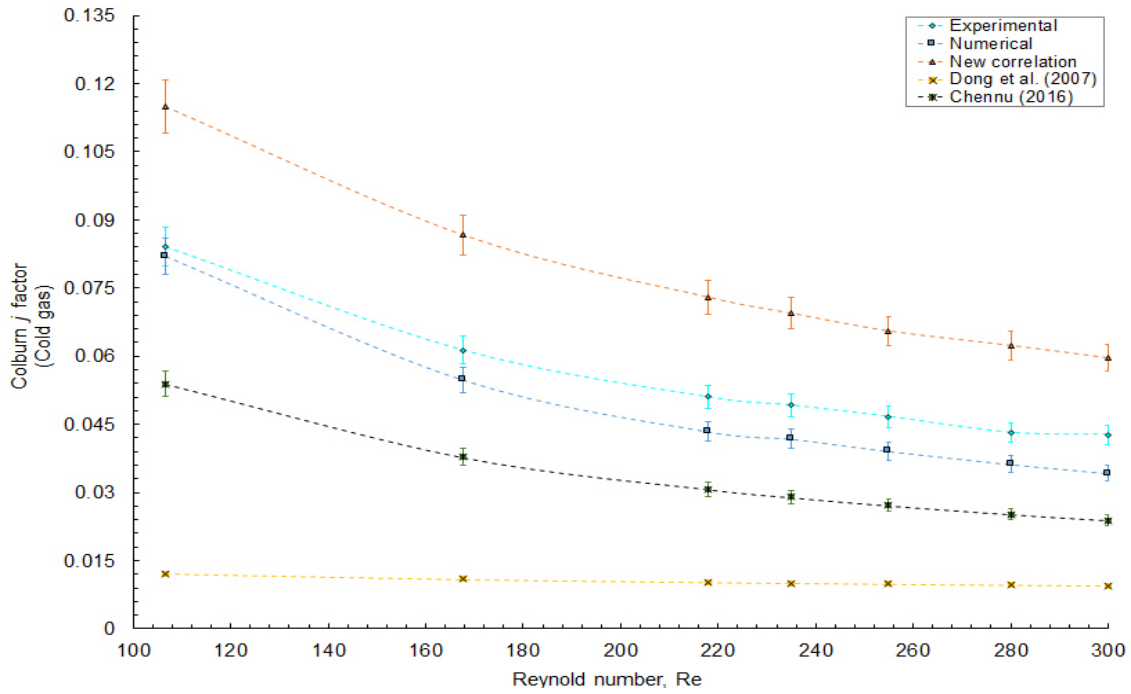
c-  $T_{cold} = 523$  K (inlet temp.)d-  $T_{cold} = 476$  K (inlet temp.)

Figure 6.9: The heat transfer comparison between numerical, experimental, new correlation, and the available literatures.

Additionally, the experimental and numerical results are validated by the available literature from Chennau [11], which illustrates a sufficiently good agreement with our results, than can be found with other correlations. Many assumptions have been made during the aforementioned numerical analysis. This may have led to uncertain results that are less reflective of the experimental data and other correlations in the available literature.

The deviation between the experimental data and the new correlation are due to adopting the radiation heat transfer in this part of the thesis, and the new equation is adopted the longitudinal heat conduction for both of the fin and the plate.

#### 6.2.4. ERROR ESTIMATION IN HEAT TRANSFER

The deviation in the heat transfer coefficient for each fluid has been estimated for the experimental and numerical results. Tables 6.5 and 6.6 include the heat transfer coefficients for the experimental and numerical data.

Table 6.5: Heat transfer coefficient results for the inlet temperature for hot gas  $T_{\text{hot}}=1023$  K, and for cold gas  $T_{\text{cold}}=523$  K.

Re	$\alpha_{\text{hot, experimental}}$	$\alpha_{\text{hot, numerical}}$	Uncertainty, %	Re	$\alpha_{\text{cold, experimental}}$	$\alpha_{\text{cold, numerical}}$	Uncertainty, %
77	170	167	2	103	158	162	3
115	189	174	9	153	177	165	7
135	197	179	10	179	186	157	19
154	203	181	12	180	195	170	15
164	207	184	13	213	197	167	18
192	216	195	11	217	207	164	26
193	217	193	12	257	207	172	20

Table 6.6: Heat transfer coefficient results for the inlet temperature for hot gas  $T_{\text{hot}}=840$  K, and for cold gas  $T_{\text{cold}}=476$  K.

Re	$\alpha_{\text{hot}}$ , experimental	$\alpha_{\text{hot}}$ , numerical	Uncertainty, %	Re	$\alpha_{\text{cold}}$ , experimental	$\alpha_{\text{cold}}$ , numerical	Uncertainty, %
106	123	151	23	107	146	143	2
153	127	153	21	168	167	152	10
200	131	163	24	217	181	154	18
259	134	170	27	235	182	151	21
318	137	168	23	255	188	154	19
350	137	182	33	280	195	164	19
675	148	276	87	300	195	157	24



## 7 CONCLUSION AND OUTLOOK FOR FUTURE WORK

---

### 7.1. CONCLUSIONS & REMARKS

The present work presents a numerical simulation for a plate-fin heat exchanger with wavy fin. These internally finned surfaces are widely used in many engineering fields to enhance heat-transfer capacity. The special requirements for such heat exchangers involve high compactness, long lifetime, low thermal strain and low pressure drop. Some of the typical applications include electrical and electronic equipment cooling, compact heat exchangers, and gas turbine blade cooling.

Numerical simulations were carried out for a 3D-printed plate-fin heat exchanger in the OpenFOAM program. In order to reduce the thermal strain, we used the counter-flow type of exchanger rather than the commonly used cross-flow exchanger, in order to investigate the heat-transfer and fluid-flow behaviors in a single pair of wavy channels. Therefore, the main temperature gradient occurs only in one direction. In a counter-flow heat exchanger, the pressure drop found in a traditional plate-fin heat exchanger would be relatively large, due to the half-free flow area in the distributor section. Therefore, there are no fins in the distributor sections; the hot fluid and cold fluid enter through two separate parallel channels, in opposite directions. Our study is performed at laminar flow, with various geometrical parameters of fin, such as the fin amplitude  $a_f$ , fin space  $s_{fs}$ , wave fin length  $l_w$ , and fin length  $L$ , and air is used as the working fluid.

There are a few correlations available to predict the heat-transfer performance and pressure-drop for the wavy fin type. However, these correlations were not applicable to the cases in this research, especially for the small fin amplitudes required. Therefore, the main objective was to propose a new correlation based on the developed models, to predict the heat-transfer performance in terms of the Colburn factor  $j$  and the friction factor  $f$ , particularly at small values of wavy fin amplitude, ranging between (0, 1.5, 2, and 2.5 mm). The ratio of  $j/f$  is taken as a measure of the adequateness of a finned surface. The ideal fin geometry should have a high value of  $j/f$ . The selection of particular fin geometry is primarily governed by the process requirements.

New correlations are proposed depending on the accurate analytical models, which were developed by investigating the effect of longitudinal heat conduction in the solid wall for both fin and plate thickness. The lower thermal conductivity of the fins resulted in a decrease in the overall efficiency of the fins, ranging between 98% to 70%.

In this work, we conducted numerical simulations and experimental work to achieve our objective. New correlations will help to facilitate the work of researchers in their future endeavors, and could be a starting point for a plate-fin heat exchanger design with a focus on the wavy fin. This fin type gives competitive performance with other types of fin. The waviness was introduced based on two hypotheses: (a) The waviness of the fins might interrupt the boundary layers, and (b) The flow between the fins may deflect and impinge on other fin surfaces. Both hypotheses suggest the possibility of higher heat-transfer rates. The advantages of a corrugated fin are that they provide an effective flow, the induction of turbulent flows that enhance the heat transfer, and they allow for breaking the boundary layer. Wavy fins are often a better option to increase the heat-transfer coefficient, but at the same time they increase the friction factor. The results revealed that the heat transfer performance in terms of Colburn factor,  $j$  and Fanning friction factor  $f$  are strong functions of the surface geometry.

In the second part of the present thesis, high temperatures were applied in OpenFOAM. The radiative heat flux (computed using the radiosity method and view factors) proved highly sensitive to the precision of the view factors. The method currently used in OpenFOAM can lead to errors on coarser grids. However, due to the nature of the view factor calculation used, the view factor converges to the correct value when the cell size goes towards 0.

## 7.2 SCOPE OF FUTURE WORK

In future research, many areas of study may benefit from the expansion of the current work. The following are some of the proposed activities:

- 1- In the current work, the calculation of the heat-transfer performance was carried out on one single pair of wavy fins within the main section of the heat exchanger. This could be extended to include the work of all sections in the heat exchanger, such as the inlet distributor and outlet distributor.
2. It is necessary to try mixing different fin categories in the design of a plate-fin heat exchanger.
3. The analytical and numerical models were developed to predict the heat transfer performance in terms of Colburn factor  $j$ . The same method could be used to develop models of the Fanning friction factor  $f$ .
4. It has been shown that due to the flow of vortex and the effective mixing of liquids, the heat transfer would be promoted by corrugated surfaces structures. A similar approach could be used

to create a new correlation that predicts the performance of heat transfer for the other three types of corrugated plate fins, namely perforated wavy fin, staggered wavy fin, and discontinuous wavy fin, as shown in Figure 7.1. The key design parameters in the construction of the three fins are the fin height  $h_{fs}$ , fin spacing  $s_{f-s}$ , perforation radius  $r$ , and breaking distance in discontinuous wavy fin  $S$ .

5-The heat loss could not be eliminated; the wavy plate-fin heat exchanger presents a large surface area, through which the heat gets dissipated into its surroundings. So, it is necessary to include this in the calculations.

Currently, wavy fins are not widely used, but in the near future the wavy fins should be more regularly utilized in a variety of different applications. As the fin's surface enhancement leads to high heat-transfer coefficients in passive methods, and due to the simplicity of its construction and its economic benefits, it would be particularly appropriate for industrial applications.

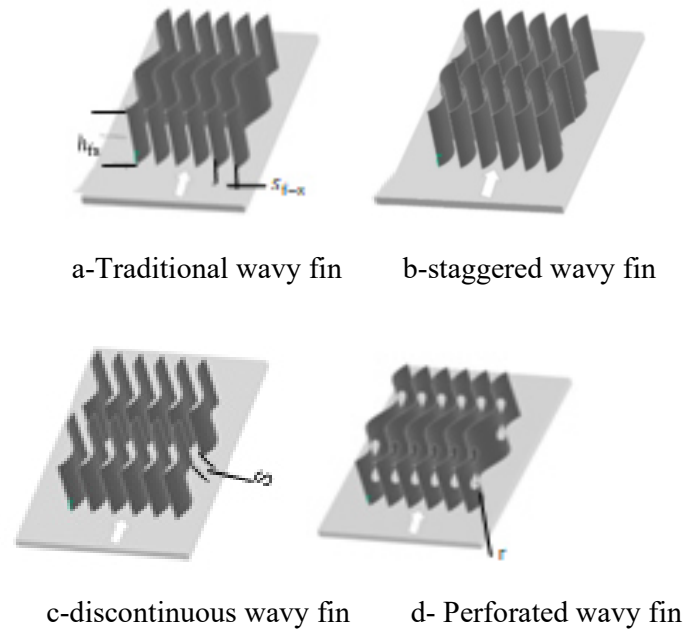


Fig. 7.1. The shape of (a) continuous wavy fin; (b) staggered wavy fin; (c) discontinuous wavy fin; (d) perforated wavy fin [54].



## REFERENCES

---

- [1] R. K. Shah and A. L. London 1978. Laminar flow forced convection in ducts. A source book for compact heat exchanger Analytical data, Advances in heat transfer (1978), ISBN 0-12-020051-1.
- [2] C. Ranganayakulu, and K.N. Seetharamu 2018. Compact Heat Exchangers, Analysis. Design and Optimization using FEM and CFD Approach. This edition first published of this book (2018). DDC 621.402/2–dc23.
- [3] Ketan C. Prasadi, A.M. Patil 2016. Heat Transfer Enhancement using Herringbone wavy & Smooth Wavy Fin Heat Exchanger for Hydraulic Oil Cooling. International Research Journal of Engineering and Technology (2016), ISSN: 2395-0056.
- [4] Ahmed F. Khudheyer, and Mahmoud Sh. Mahmoud 2011. Numerical analysis of fin-tube plate heat exchanger by using CFD technique. Journal of Engineering and Applied Sciences (2011) ISSN 1819-6608.
- [5] Xiao Wei Zhu, Yun Han Fu, Jing Quan Zhao, and Lei Zhu 2015. Three-dimensional numerical study of the laminar flow and heat transfer in a wavy-finned heat sink filled with Al<sub>2</sub>O<sub>3</sub>/ethylene glycol-water nanofluid. International Journal of Computation and Methodology (2015), ISSN: 1040-7782.
- [6] Sepehr Sanaye, and Hassan Hajabdollahi 2010. Thermal-economic multi-objective optimization of plate-fin heat exchanger using a genetic algorithm. Applied Energy 87 (2010) 1893–1902.
- [7] M. el Abbassia, D.J.P. Lahaye, and C. Vuik 2017. Modelling turbulent combustion coupled with conjugate heat transfer in OpenFoam. Conference Paper · September (2017). [online]
- [8] D.A. Jones, M. Chapuis, M. Liefvendahl, D. Norrison, and R. Widjaja 2016. RANS Simulations using OpenFOAM Software. (2016). [online]
- [9] Christopher J. Greenshields 2018]. The OpenFOAM Foundation. User Guide version 6. [https:// openfoam.org](https://openfoam.org) (2018). [online]
- [10] Raj M. Manglik, and Arthur E. Bergles 1995. Heat Transfer and Pressure Drop Correlations for the Rectangular Offset Strip Fin Compact Heat Exchanger. Experimental Thermal and Fluid Science, Elsevier Science Inc. (1995) 10:171-180.
- [11] BOGE compressed air systems. [BOGE Kompressoren](#).
- [12] L. Sheik Ismail, and C. Ranganayakulu, 2007. Heat Transfer and Flow Friction correlations for Compact Wavy Plate Fin Heat Exchangers. [online] Aeronautical

- 
- Development Agency, Bangalore –560 017, and Sree Nidhi Institute of Science and Technology, Hyderabad (2007)–501 301.
- [13] Dong Junqi, Chen Jiangping, Chen Zhijiu, Zhou Yimin, and Zhang Wenfeng 2007. Heat transfer and pressure drop correlations for the wavy fin and flat tube heat exchangers. *Applied Thermal Engineering*, (2007) 27:2066–2073.
- [14] Yinhai Zhu, and Yanzhong Li 2008. Three-Dimensional Numerical simulation on the laminar flow and heat transfer in four basic fins of plate-fin heat exchangers (2008) Vol. 130 / 111801.1.
- [15] Xing Luo, Guo-Yan Zhou, Long-Wei Cong, Marco Fuchs, Stephan Kabelac 2019. Numerical Simulation of Heat Transfer and Fluid Flow in 3D-Printed High-Temperature Plate-Fin Heat Exchangers with OpenFoam. *Proceedings of the 25th National and 3rd (2019) International ISHMT-ASTFE, Heat and Mass Transfer Conference*.
- [16] Weiping Zhu, Xiujuan Xie, Huihui Yang, Laifeng Li, and Linghui Gong 2015. Analytical study on multi-stream heat exchanger includes longitudinal heat conduction and parasitic heat loads. *Physics Procedia* (2015) 67:667 – 674.
- [17] P. Konečný, and R. Ševčík 2016. Comparison of Turbulence Models in OpenFOAM for 3DSimulation of Gas Flow in Solid Propellant Rocket Engine. *Advances in Military Technology*, (2016) ISSN1802-2308.
- [18] Ramesh K. Shah, and Dus̃an P. Sekulic 2003. *Fundamentals of Heat Exchanger Design*, Published by JOHN WILEY & SONS, (2003) INC. ISBN 0-471-32171-0.
- [19] Hamid Nabati 2012. *Numerical Analysis of Heat Transfer and Fluid Flow in Heat Exchangers with Emphasis on Pin Fin Technology*. Printed by Mälardalen University, Västerås, Sweden, (2012) ISSN 1651-4238.
- [20] Pandey Mukesh Kumar, and Gaur Anurag 2014. An Optimized Plate Fin Type Heat Exchanger. *International Journal of Engineering Research and Development*, Volume 10, Issue 9, (2014) PP.01-06.
- [21] Hannah Ritchie, and Max Roser 2017. *Fossil Fuels*. Published online at OurWorldInData.org. <https://ourworldindata.org/fossil-fuels>
- [22] Arafat A. Bhuiyan, R. I. Zaman, and A K M Sadrul Islam 2010. Numerical Analysis of Thermal and Hydraulic Performance of Fin and Tube Heat Exchangers. *Proceedings of the 13th Asian Congress of Fluid Mechanics*, 17-21 December (2010), Dhaka, Bangladesh. [online]
-

- 
- [23] G. N. Xie, B. Sunden, and Q. W. Wang 2008. Optimization of compact heat exchangers by a genetic algorithm. *Applied Thermal Engineering*, (2008) 28 895–906.
- [24] L. Sheik Ismail, and R. Velraj 2009. Studies on Fanning Friction ( $f$ ) and Colburn ( $j$ ) Factors of Offset and Wavy Fins Compact Plate Fin Heat Exchanger—A CFD Approach. Part A: Applications, (2009), ISSN: 1040-7782.
- [25] Yuri Stephan Muzychka 1999. Analytical and Experimental Study of Fluid Friction and Heat Transfer in Low Reynolds Number Flow Heat Exchangers. A thesis presented to the University of Waterloo, (1999). [online]
- [26] Peter Renze, and Kevin Akermann 2019. Simulation of Conjugate Heat Transfer in Thermal Processes with Open Source CFD. *ChemEngineering*, (2019)3,59; doi: 10.3390-chemengineering 3020059.
- [27] Weiping Zhu, Xiujuan Xie, Huihui Yang, Laifeng Li, and Linghui Gong 2014. Analytical study on multi-stream heat exchanger includes longitudinal heat conduction and parasitic heat loads. *Physics Procedia*, (2014), 67 (2015) 667 – 674.
- [28] W.M. Kays, and A. L. London 1984. *Compact heat exchangers*, Third Edition (1984).
- [29] Morteza Khoshvaght Aliabadi, and Faramarz Hormozi 2013. Performance Analysis of Plate-Fin Heat Exchangers: Different Fin Configurations and Coolants. *JOURNAL OF Thermophysics and heat transfer*, (2013), Vol. 27, No. 3.
- [30] Tianyi Gao, James Geer, and Bahgat Sammakia 2015. Review and Analysis of Cross-Flow Heat Exchanger Transient Modeling for Flow Rate and Temperature Variations, (2015), Vol. 7 / 041017-1.
- [31] M. Khoshvaght Aliabadi, M. Gholam Samani, F. Hormozi, and A. Haghighi Asl 2011. 3D-CFD Simulation and neural network model for the  $j$  and  $f$  factors of the wavy fin and flat tube heat exchangers  $j$  and  $f$  factors of the wavy fin and flat tube heat exchangers, (2011), Vol. 28, No. 03, pp. 505 – 520.
- [32] Y.L He, W.Q. Tao, F. Q. Song, and W. Zhang 2004. Three-dimensional numerical study of heat transfer characteristics of plain plate-fin and tube heat exchangers from viewpoint of field synergy principle. *International Journal of Heat and Fluid Flow*, (2004), 26 (2005) 459–473.
- [33] Pradeep Shinde, and Cheng-Xian Lin 2017. A heat transfers and friction factor correlation for low air-side Reynolds number applications of compact heat exchangers (1535-RP). *Science and Technology for the Built Environment*, (2017), ISSN: 2374-4731.
-

- 
- [34] Dawid Taler 2004. Determination of heat transfer correlations for plate-fin-and-tube heat exchangers. *Heat and Mass Transfer*, (2004), 40: 809–822.
- [35] A. R. Wieting 1975. Empirical Correlations for Heat Transfer and Flow Friction Characteristics of Rectangular Offset-Fin Plate-Fin Heat Exchangers, (1975). [online].
- [36] F. V. TINAUT, A. MELGAR, and A. A. RAHMAN AL 1992. Correlations for heat transfer and flow friction characteristics of compact plate-type heat exchangers. (1992), Vol. 35, No. 7, pp. 1659-1665.
- [37] Masoud Asadi, and Dr Ramin Haghighi Khoshkhoo 2014. Study on Heat Transfer Area of a Plate-Fin Heat Exchanger with Wavy surfaces. *IJTE*, (2014), Volume 1, Issue1, Pages 15-29.
- [38] Sundaresan Subramanian, valery Ponyavin, Clayton Ray Delosier, Yitung Chen, and Anthony E. Hechanova 2005. Design considerations for compact ceramic offset strip fin high temperature heat exchangers. *Proceedings of fifth international conference on enhanced, compact and Ultra-compact heat exchangers, engineering and technology*, (2005), compact and Ultra CHE, Hoboken, NJ, USA. [ online]
- [39] Morteza Khoshvaght-Aliabadi, and Faramarz Hormozi 2013. Performance Analysis of Plate-Fin Heat Exchangers: Different Fin Configurations and Coolants. *Journal of thermophysics and heat transfer*, (2013), Vol. 27, No. 3, July–September.
- [40] Hamid Reza Seyf, and Mohammad Layeghi 2010. Numerical Analysis of convective heat transfer from an Elliptic pin fin heat sink with and without metal foam insert. *Journal of Heat Transfer*, (2010), Vol. 132 / 071401-1.
- [41] Ramisetty Bala Sundar Rao, Gurappa Ranganath, and Chennu Ranganayakulu 2016]. Development of Colburn  $j$  Factor and Fanning Friction Factor  $f$  Correlations for Compact Surfaces of the Triangular Perforated Fins Using CFD. *Heat Transfer Engineering*, (2016), ISSN, 0145-7632.
- [42] Kunpeng Guo, Nan Zhang, and Robin Smith 2015. Optimization of fin selection and thermal design of counter-current plate-fin heat exchangers. *Applied Thermal Engineering*, 78 (2015) 491-499.
- [43] Y. Sui, C.J. Teo, and P.S. Lee 2012. Direct numerical simulation of fluid flow and heat transfer in periodic wavy channels with rectangular cross-sections. *International journal of heat and Mass transfer*, 55 (2012) 73-88.
-

- 
- [44] A. Diani, S. Mancin, C. Zilio, and L. Rossetto 2012. Experimental and numerical analyses of different extended surfaces. 6th European Thermal Sciences Conference (2012), Journal of Physics: Conference Series 395: 012045.
- [45] K. M. Stone, and S. P. Vanka 1997. Numerical Study of Flow and Heat Transfer in Wavy Passages. Conditioning and Refrigeration Center in the University of Illinois, (1997), (217) 333-3115. [online]
- [46] M. Khoshvaght Aliabadi, M. Gholam Samani, F. Hormozi, and A. Haghighi Asl 2011. 3D-CFD Simulation and Neural Network Model for The  $j$  and  $f$  Factors of the Wavy Fin and Flat Tube Heat Exchangers. Brazilian Journal of Chemical Engineering, (2011), ISSN 0104-6632.
- [47] R. L. WEBB 1981. Performance Evaluation Criteria for Use of Enhanced Heat Transfer Surfaces in Heat Exchanger Design. International Journal Heat Mass Transfer. (1981), Vol. 24, No. 4, pp. 715-726.
- [48] S M Sohel Murshed, and Manuel L Matos Lopes 2017. Advanced Features and Applications of Heat Exchangers an Outline, (2017). [online]
- [49] L. Sheik Ismail, C. Ranganayakulu, and Ramesh K. Shah 2009]. Numerical study of flow patterns of compact plate-fin heat exchangers and generation of design data for offset and wavy fins. International Journal of Heat and Mass Transfer, (2009), 52: 3972–3983.
- [50] M.R. Shaeri, and M. Yaghoubi 2009. Numerical analysis of turbulent convection heat transfer from an array of perforated fins. International journal of heat and fluid flow, 30: (2009) 218-228.
- [51] Jeanette Cobian-Iniguez, Angela Wu, Florian Dugast and Arturo Pacheco-Vega 2015. Numerically based parametric analysis of plain fin and tube compact heat exchangers. Journal Applied thermal engineering, 86 (2015) 1-13.
- [52] Nur Rohmaha, Ghalya Pikraa, Andri Joko Purwantoa, and Rakhmad Indra Pramanaa 2014. The effect of plate spacing in plate heat exchanger design as a condenser in an organic Rankine cycle for a low-temperature heat source. Energy Procedia 68 (2015) 87 – 96. [online]
- [53] Amaranatha Raju. Muppala, Ashok Babu T. P. and Ranganayakulu.Chennu 2015. Development of Single-Phase Heat Transfer Correlations for Water & R134a in Rectangular Channel with Smooth Wavy Fin. Journal of Physical Science and Application 5 (2015) (3)199-208.
-

- 
- [54] Yuan Xue, Zhihua Ge, Xiaoze Du, and Lijun Yang 2018. On the Heat Transfer Enhancement of Plate Fin Heat Exchanger. [online] Journal Energies, (2018)11, 1398.
- [55] Dong Junqi, Zhang Yi, Li Gengtian, and Xu Weiwu 2012. Experimental Study of Wavy Fin Aluminum Plate Fin Heat Exchanger. Experimental Heat Transfer, (2013), 26:384–396. ISSN: 0891-6152. [online]
- [56] Alexey Vdovin, and Andreu Oliver González 2009] Alexey Vdovin 2009. Radiation heat transfer in OpenFOAM. [online]
- [57] Manel Bosch Hermosilla 2016. Study of Heat and Mass Transfer Applications in The Field of Engineering by using OpenFoam. School of Industrial and Aeronautic Engineering of Terrassa Universitat Politècnica de Catalunya (2016), [online], Escola Tecnica Superior d Enginyeries Industrial I Aeronautica de Terrassa.
- [58] Prandtl, L 1904 Prandtl, L 1904. Fluid movement with very little friction. Int. Mathematiker kongress, heidelberg, P.484-491.
- [59] K. Comakli, F. Simsek, O. Comakli, and B. Sahin 2009. Determination of optimum working conditions R22 and R404A refrigerant mixtures in heat pumps using Taguchi method. Applied Energy 86 2451–2458.
- [60] Ya-Ling He, and Yuwen Zhang 2009. Advances and Outlooks of Heat Transfer Enhancement by Longitudinal Vortex Generators. Department of Mechanical and Aerospace Engineering, University of Missouri, Columbia (2009), MO 65211.
- [61] Vipin B. Gawande, Abhishek G. Ramgadga and Arun K. Saha 2010. NUMERICAL STUDY OF FLOW AND HEAT TRANSFER IN A WAVY CHANNEL. Proceedings of the 20th National and 9th International, ISHMT-ASME Heat and Mass Transfer Conference, January 4-6, 2010, Mumbai, India.
- [62] Kunpeng Guo 2015. Optimisation of Plate-Plate-Fin Heat Exchanger Design. A thesis submitted to The University of Manchester for the degree of Doctor of Philosophy (2015) [online]
- [63] Sidramappa Alur 2012. Experimental Studies on Plate Fin Heat Exchangers. Mechanical Engineering Department National Institute of Technology Rourkela. A Thesis Submitted for Award of the Degree of Doctor of Philosophy (2012). [online]
- [64] Nabou Mohamed, Biara Ratiba Wided, El Mir Mohamed, Missoum Abd el karim, and Bouanini Mohameda 2013. Numerical Investigation on the Fluid Flow and Heat Transfer in the Entrance Region of Wavy Channel. Energy Procedia 36 (2013) 76 – 85. [online]
-

- 
- [65] Ma, X M Wu, F Chu, and B Zhu 2017. Numerical Simulation of Frosting on Wavy Fin-and-tube Heat Exchanger Surfaces. *Journal of Physics: Conference Series*, (2017) J. Phys.: Conf. Ser. 891 012052.
- [66] T. A. Rush, A. M. Jacobi, and T. A. Newell 1997. An Experimental Study of Flow and Heat Transfer in Wavy Passages. Air Conditioning and Refrigeration Center University of Illinois Mechanical & Industrial Engineering Dept. Prepared as part of ACRC Project 65 Investigation of Wavy Fins for Heat Transfer Augmentation in Refrigeration/Air Conditioning Systems Thesis, (1997).
- [67] F. Oviedo-Tolentino, R. Romero-Méndez, A. Hernández-Guerrero, and B. Girón-Palomares 2008. Experimental study of fluid flow in the entrance of a sinusoidal channel. *International Journal of Heat and Fluid Flow* 29 (2008) 1233–1239.
- [68] Dong Junqi, Chen Jiangping, Chen Zhijiu, Zhou Yimin, and Zhang Wenfeng 2007. Heat transfer and pressure drop correlations for the wavy fin and flat tube heat exchangers. *Applied Thermal Engineering* 27 (2007) 2066–2073. [online]
- [69] Process- Cooling 2021. Plate-fin heat exchanger. [www.process-cooling.com/](http://www.process-cooling.com/brazed-aluminum-plate-fin-heat-exchanger) brazed-aluminum-plate-fin heat exchanger.
- [70] M.A. Ahmed, N.H. Shuaib, and M.Z. Yusoff 2012. Numerical investigations on the heat transfer enhancement in a wavy channel using nanofluid. *International Journal of Heat Transfer* 55 (2012) 5891-5898.
- [71] M. Yousefi, R. Enayatifar, and A.N. Darus 2012. Optimal design of plate-fin heat exchangers by a hybrid evolutionary algorithm. *International Communication in Heat and Mass Transfer* 39 (2012) 258-263.
- [72] Jiin-Yuh Jang, Ling-Fang Hsu, and Jin-Sheng Leu 2013. Optimization of the span angle and location of vortex generators in a plate-fin and tube heat exchanger. *International Journal of Heat and mass Transfer* 67(2013) 432-444.
- [73] Kunpeng Guo, Nan Zhang, and Robin Smith 2015. Optimisation of fin selection and thermal design of counter-current plate-fin heat exchangers. *Applied thermal Engineering* 78(2015) 491-499.
- [74] Qingfeng JIANG, Zhigang ZHU, Qiyong ZHANG, Ming ZHUANG, and Xiaofei LU 2018. Optimal design of the first stage of the platefin heat exchanger for the EAST cryogenic system. *Plasma Sci. Technol.* 20 (2018) 035601 (9pp).
-

- 
- [75] Evren Bayraktar 2011. Numerical and Experimental Studies on PBEs in OpenFOAM Environment. Institute of Applied Mathematics (LS III), TU Dortmund Vogelpothsweg 87, D-44227, Dortmund, Germany. [online]
- [76] Mitranvanu Sahoo 2015. Experimental and Numerical Studies on Plate Fin Heat Exchanger. Thesis. Department of Mechanical Engineering National Institute of technology India. [online], 2015.
- [77] Tao Wen, Hongbo Zhan, Yimo Luo, and Dalin Zhang 2018. Experimental Study on the Flow Boiling Heat Transfer Characteristics in a Mini-Channel with Offset Fins. (2018), 2, 1376; doi:10.3390/proceedings2221376. [www.mdpi.com/journal/proceedings](http://www.mdpi.com/journal/proceedings).
- [78] Hamed Bazdar, Davood Toghraie, Farzad Pourfattah, Omid Ali Akbari, Hoang Minh Nguyen, and Amin Asadi 2020. Numerical investigation of turbulent flow and heat transfer of nanofluid inside a wavy microchannel with different wavelengths. Journal of Thermal Analysis and Calorimetry (2020) 139:2365–2380.
- [79] H.A. Mohammed, P. Gunnasegaran, and N.H. Shuaib 2011. Numerical simulation of heat transfer enhancement in wavy microchannel heat sink. International Communications in Heat and Mass Transfer 38 (2011) 63-68.
- [80] Ali Reza Anvari, and Koroush Javaherdeh 2019. Experimental Investigation of Newtonian and Non-Newtonian Liquid Flow in Wavy and Straight Mini-Channel Cross-Flow Plate Heat Exchangers. Strojniški vestnik - Journal of Mechanical Engineering 65(2019)1, 41-49.
- [81] John E. Hesselgreaves, Richard law, and David A. Reay 2017. Compact Heat Exchangers Selection. Design and Operation, Book, Second Edition. Butterworth-Heinemann is an imprint of Elsevier. The Boulevard, Langford Lane, Kidlington, Oxford OX5 1GB, (2017) United Kingdom.
- [82] Caihang Liang, Xiaoman Tong, Tengyue Lei, Zhenxing Li, and Guoshan Wu 2017. Optimal Design of an Air-to-Air Heat Exchanger with Cross-Corrugated Triangular Ducts by Using a Particle Swarm Optimization Algorithm. Applied Sciences, Appl. Sci. 2017, 7, 554; doi:10.3390/app7060554.
- [83] Yin Hai Zhu, and Yan Zhong Li 2008. Three-Dimensional Numerical Simulation on the Laminar Flow and Heat Transfer in Four Basic Fins of Plate-Fin Heat Exchangers. Journal of Heat Transfer, [online], NOVEMBER (2008), Vol. 130 / 111801-1.
-

- 
- [84] M. yousefi, and A.N. Darus 2011. Optimal Design of Plate-fin Heat Exchangers by Particle Swarm Optimization. Proceedings of International Conference on Fuzzy Information and Engineering, ISBN 998-1-84926. Singapore, December 9-10, (2011).
- [85] Brahim Selma, Martin Désilets, and Pierre Proulx 2014. Optimization of an industrial heat exchanger using an open-source CFD code. Applied thermal Engineering 69 (2014) 241-250.
- [86] Tubular-Heaters. Heating Solutions Group. <https://www.tutco.com/tubular-heaters>.
- [87] Latife Berrin Erbay, Mehmet Mete Öztürk, and Bahadır Doğan 2017. Comprehensive Study of Compact Heat Exchangers with Offset Strip Fin. Heat Exchangers– Advanced Features and Applications. <http://dx.doi.org/10.5772/66749>.
- [88] K. M. Stone, and S. P. Vanka 1997. Numerical Study of Flow and Heat Transfer in Wavy Passages. Air Conditioning and Refrigeration Center University of Illinois Mechanical & Industrial Engineering Dept. 1206 West Green Street Urbana, IL 61801. (1997), (217) 333-3115.
- [89] B.V. Babu, and S.A. Munawar 2007. Differential evolution strategies for optimal design of shell-and-tube heat exchangers. Elsevier Ltd, Chemical Engineering Science 62 (2007) 3720 – 3739.
- [90] José M. Ponce-Ortega, Medardo Serna-González, and Arturo Jiménez-Gutiérrez 2009. Use of genetic algorithms for the optimal design of shell-and-tube heat exchangers. Applied Thermal Engineering 29 (2009) 203–209.
- [91] Renan Hilbert, Ga'bor Janiga, Romain Baron, and Dominique The'venin 2006. Multi-objective shape optimization of a heat exchanger using parallel genetic algorithms. International Journal of Heat and Mass Transfer 49 (2006) 2567–2577. [online]
- [92] Ibrahim Ozkol, and Guven Komurgoz 2005. Determination of The Optimum Geometry of the Heat Exchanger Body Via a Genetic Algorithm. Numerical Heat Transfer, Part A, 48: 283–296, (2005). ISSN: 1040-7782 print=1521-0634. [online]
- [93] Resat Selbas, Onder Kızılkkan, and Marcus Reppich 2006. A new design approach for shell-and-tube heat exchangers using genetic algorithms from economic point of view. Chemical Engineering and Processing 45 (2006) 268–275. [online]
- [94] Amin Hadidi 2015. A robust approach for optimal design of plate fin heat exchangers using biogeography based optimization (BBO) algorithm. Applied Energy Journal 150 (2015) 196-210.
-

- [95] Xiaofeng Liu 2013. Modeling of Earth Surface Dynamics and Related Problems Using OpenFOAM. CSDMS 2013 Meeting, Department of Civil and Environmental Engineering University of Texas at San Antonio, Texas (2013). <http://engineering.utsa.edu/~xiaofengliu>.
- [96] Antonio Gómez, Carlos Montañés, Miguel Cámara, Ana Cubero, Norberto Fueyo, and José Manuel Muñoz 2018. An OpenFOAM-based model for heat-exchanger design in the Cloud. *Applied thermal Engineering* 139 (2018) 239-255.
- [97] David P. Hawn 2009. Development of a Dynamic Model of a CounterFlow Compact Heat Exchanger for Simulation of the Gt-Mhr Recuperator Using matlab and Simulink. Thesis. The Ohio State University (2009). [online]
- [98] Ajit Rajesh Desai 2015. Computational Model for Steady State Simulation of a Plate – Fin Heat Exchanger. Thesis. The University of Texas at Arlington in Partial Fulfillment (2015). [online].
- [99] Vladimir Kriventsev, Hiroyuki Oshima, Akira Yamaguchi, and Hisashi Ninokata 2003. Numerical Prediction of Secondary Flows in Complex Areas Using Concept of Local Turbulent Reynolds Number. *Journal of Nuclear Science and Technology*, Vol. 40, No. 9, p. 655–663 - September (2003).
- [100] J. Richard Culham, Member, IEEE, and Yuri S. Muzychka 2001. Optimization of Plate Fin Heat Sinks Using Entropy Generation Minimization. *IEEE Transactions On Components and packaging Technologies*, VOL. 24, NO. 2, June (2001).
- [101] A.K. Gupta, P. Kumar, R.K. Sahoo, A.K. Sahu, and S.K. Sarangi 2017. Performance measurement of plate fin heat exchanger by exploration: ANN, ANFIS, GA, and SA. *Journal of Computational Design and Engineering* 4 (2017) 60–68. [online]
- [102] R.V. Rao, and V.K. Patel 2010. Thermodynamic optimization of cross flow plate-fin heat exchanger using a particle swarm optimization algorithm. *International Journal of Thermal Sciences* 49 (2010) 1712-1722.
- [103] Su Thet Mon Than, Khin Aung Lin, and Mi Sandar Mon 2008. Heat Exchanger Design. *World Academy of Science, Engineering and Technology* 46, (2008).
- [104] Joel David Lindstrom 2005. Design and Evaluation of Compact Heat Exchangers for Hybrid Fuel Cell and Gas Turbine Systems. Thesis. Montana State University Bozeman, Montana (2005).

- 
- [105] Jing-cheng LIU, Shu-you Zhang, Xin-yue Zhao, Guo-dong YI, and Zhi-yong Zhou 2015. Influence of fin arrangement on fluid flow and heat transfer in the inlet of a plate-fin heat exchanger. Liu et al. / J Zhejiang Univ-Sci A (Appl Phys & Eng), (2015) 16(4):279-294.
- [106] Mehdi Nasrabad 2008. Design of fin plate heat exchanger for increasing micro turbine efficiency and introduction of fin plate heat exchanger design software (KhoshNasr) for this purpose. Proceedings of 2008 ASME Summer Heat Transfer Conference HT2008 August 10-14, (2008), Jacksonville, HT2008-56114, Florida USA.
- [107] Daniël Walraven, Ben Laenen, and William D'haeseleer 2013. Optimum configuration of plate-type heat exchangers for the use in ORCs for low-temperature geothermal heat sources. European Geothermal Congress 2013 Pisa, Italy, 3-7 June (2013).
- [108] Prabhat Kumar Gupta, Vivek Nema, and P. Kush 2015. Comparative Design Evaluation of Plate Fin Heat Exchanger, and Coiled Finned Tube Heat Exchanger for Helium Liquefier in The Temperature Range of 300-80 K. Preprint of Indian Journal of Cryogenics Vol 40, (2015).
- [109] José M. Ponce-Ortega, Medardo Serna-González, and Arturo Jiménez-Gutiérrez 2009. Use of genetic algorithms for the optimal design of shell-and-tube heat exchangers. Applied Thermal Engineering 29 (2009) 203–209.
- [110] K. Comakli, F. Simsek, O. Comakli, and B. Sahin 2009. Determination of optimum working conditions R22 and R404A refrigerant mixtures in heat-pumps using Taguchi method. Journal of Applied Energy 86 (2009) 2451–2458.
- [111] Lieke Wang, and Bengt Sunden 2003. Optimal design of plate heat exchangers with and without pressure drop specifications. Applied Thermal Engineering 23 (2003) 295–311. [online]
- [112] Jin-Sheng Leu, Ying-Hao Wu, and Jiin-Yuh Jang 2004. Heat transfer and fluid flow analysis in plate-fin and tube heat exchangers with a pair of block shape vortex generators. International Journal of Heat and Mass Transfer 47 (2004) 4327–4338. [online]
- [113] Robert H. Perry, Don W. Green, and James O. Maloney 1997. Perry's Chemical Engineers Handbook. Seventh Edition. Chemical engineering—Handbooks. I. Perry, Robert H., date. II. Green, Don W. III. Maloney, James O. TP151.P45 1997 660—dc21 96-51648.
-

- 
- [114] Lu Shen 2017. Modeling and simulation for Particulate Heat Exchanger. Thesis, George W. Woodruff School of Mechanical Engineering - Georgia Institute of Technology, (2017).
- [115] Noah Yakah 2012. Heat Exchanger Design for a Solar Gas-Turbine Power Plant. Thesis, KTH School of Industrial Engineering and Management Energy Technology EGI, (2012), 110MSC EKV925 Division of Heat and Power SE-100 44 STOCKHOLM.
- [116] Waqar Ahmed Khan 2004. Modeling of Fluid Flow and Heat Transfer for Optimization of Pin-Fin Heat Sinks. Thesis- Mechanical Engineering, Waterloo, Ontario, Canada- (2004).
- [117] C.D. Argyropoulos, and N.C. Markatos 2015. Recent advances on the numerical modelling of turbulent flows. *Applied Mathematical Modelling* 39 (2015) 693-732.
- [118] Paulo Eduardo Batista de Mello, Sérgio Scuotto, Fernando do Santos Ortega, and Gustavo Henrique Bolognesi Donato 2013. Heat transfer and Pressure Drop in a Plate and Fin Ceramic Heat Exchanger. 8th World Conference on Experimental Heat Transfer, Fluid Mechanics, and Thermodynamics (2013), Lisbon, Portugal. <https://www.researchgate.net/publication/262964277>.
- [119] Miloš Mihailović, Uroš Milovančević, Srbslav Genić, Branislav Jaćimović, Milena Otović, and Petar Kolendić 2019. Air side heat transfer coefficient in plate finned tube Heat exchangers, <https://doi.org/10.1080/08916152.2019.1656298>.
- [120] Björn Schilling 2016. Modeling a Turbulent Boundary Layer with OpenFOAM. <https://www.researchgate.net/publication/317416606>.
- [121] Jainender Dewatwal 2009. Design of Compact plate Fin Heat Exchanger. Thesis, Department of Mechanical Engineering National Institute of Technology Rourkela (2009).
- [122] Aklilu Gebremariam 2016. Gasketed Plate Type Heat Exchanger Design Software. Thesis, Turku University of Applied Sciences.
- [123] D.A. Jones, M. Chapuis, M. Liefvendahl, D. Norrison, and R. Widjaja 2016. RANS Simulations using OpenFOAM Software. Defense Security Systems Technology, Swedish Defence Research Agency - FOI, SE 147 25 – (2016)-Tumba, Stockholm, Sweden.
- [124] Jin-Sheng Leu, Ying-Hao Wu, and Jiin-Yuh Jang 2004. Heat transfer and fluid flow analysis in plate-fin and tube heat exchangers with a pair of block shape vortex
-

- generators. *International Journal of Heat and Mass Transfer* 47 (2004) 4327–4338. [online]
- [125] M. el Abbassia, D.J.P. Lahaye, and C. Vuik 2017. Modelling Turbulant Combustion Coupled with Conjugate Heat Transfer in OPENFOAM. (2017) <https://www.researchgate.net/publication/320012227>.
- [126] Qingfeng JIANG, Zhigang ZHU, Qiyong ZHANG, Ming ZHUANG, and Xiaofei LU 2018. Optimal design of the first stage of the platefin heat exchanger for the EAST cryogenic system. *Plasma Science and Technology, Plasma Sci. Technol.* 20 (2018) 035601 (9pp) <https://doi.org/10.1088/2058-6272/aa969f>.
- [127] OpenFOAM 2018. The OpenFOAM Foundation. User Guide version 6, 10th July (2018). <https://openfoam.org>.
- [128] Tao Wen, Hongbo Zhan, Yimo Luo, and Dalin Zhang 2018. Experimental Study on the Flow Boiling Heat Transfer Characteristics in a Mini-Channel with Offset Fins. (2018), 2, 1376; doi:10.3390/2221376 [www.mdpi.com/journal/proceedings](http://www.mdpi.com/journal/proceedings).
- [129] G.N. Xie, B. Sunden, and Q.W. Wang 2008. Optimization of compact heat exchangers by a genetic algorithm. *Applied Thermal Engineering* 28 (2008) 895–906. [online]
- [130] Bala Sundar Rao Ramisetty, Ranganath G., and Ranganayakulu C. 2015. Colburn ‘j’ factor and fanning friction factor ‘f’ correlations of triangular plain fin surface of a compact heat exchanger using CFD. *Applied Mechanics and Materials*, (2015), ISSN, 1662-7482, Vol. 787, pp 207-211.
- [131] F. V. Tinaut, A. Melgar, and A. A. Rahman Al 1992. Correlations for heat transfer and flow friction characteristics of compact plate-type heat exchangers. *Heat mass transfer*, vol. 35, (1992), No. 7, pp. 1659-1665.

## APPENDIX

### Appendix A: Coriolis Device Calibration

The flow calibration for coriolis device illustrated in the diagram bellow. The calibration graph and the measured values are shown in the figure A.1, and data listed in table A.1 and table A.2.

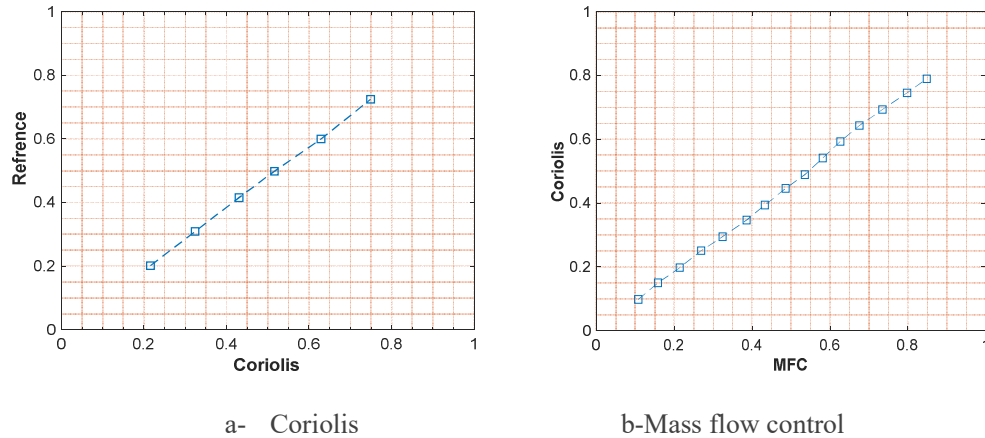


Figure A.1: Calibration graph

Table A.1: Calibration chart of the Coriolis device for hot gas.

Mass flow rate kg/min	Coriolis kg/min	Reference kg/min	Percent of deviation%
0.2155	0.2015	0.2158	7.1021
0.3233	0.3087	0.3239	4.9417
0.4310	0.4151	0.4302	3.6415
0.5388	0.4983	0.5161	3.5667
0.6465	0.5996	0.6288	4.8697
0.7543	0.7243	0.7490	3.4113
0.8620	0.8046	0.8254	2.5867

Table A.2: Calibration chart of mass flow control device for hot gas.

Mass flow kg/min	MFC kg/min	Coriolis kg/min	Per cent of deviation%
0.0959	0.0978	0.1078	9.3025
0.1452	0.1498	0.1580	5.2210
0.2005	0.1974	0.2144	7.8909
0.2542	0.2506	0.2691	6.8619
0.3083	0.2945	0.3241	9.1592
0.3689	0.3465	0.3858	10.1816
0.4150	0.3939	0.4329	9.0149
0.4674	0.4459	0.4862	8.2944
0.5157	0.4891	0.5354	8.6428
0.5610	0.5413	0.5816	6.9181

---

0.6053	0.5930	0.6266	5.3462
0.6534	0.6432	0.6756	4.8006
0.7114	0.6931	0.7347	5.6538
0.7735	0.7454	0.7979	6.5793
0.8231	0.7895	0.8484	6.9443

**Appendix B: Polynomials correlations at temperature-dependent properties**

The most common method to generate a polynomial equation from a given data set is the least squares method of temperature-dependent properties.

**a-For hot gas**

$$\rho = 1.1136E-17x^6 - 5.1556E-14x^5 + 9.9927E-11x^4 - 1.0494E-07x^3 + 6.4377E-05x^2 - 2.3039E-02x + 0.4476E+00 = 0.3491 \text{ kg/m}^3 .$$

$$c_p = -1.0829E-15x^6 + 4.6776E-12x^5 - 7.8906E-09x^4 + 6.2621E-06x^3 - 2.1060E-03x^2 + 2.8639E-01x + 9.9456E+02 = 1145.58 \text{ J/kg.K} .$$

$$\mu = -5.6186E-24x^6 + 2.9994E-20x^5 - 7.0168E-17x^4 + 9.6193E-14x^3 - 8.8953E-11x^2 + 8.2105E-08x - 1.4327E-07 = 0.00004 \text{ Pas} .$$

$$\lambda = -8.6887E-21x^6 + 4.40667E-17x^5 - 9.80906E-14x^4 + 1.2835E-10x^3 - 1.1369E-07x^2 + 1.1564E-04x - 1.2428E-03 = 0.675 \text{ W/m.K} .$$

$$Pr = 0.748.$$

**b-For cold gas**

$$\rho = 1.2288E-17x^6 - 5.6361E-14x^5 + 1.0827E-10x^4 - 1.1274E-07x^3 + 6.8611E-05x^2 - 2.4372E-02x + 4.6727E+00 = 1.1898 \text{ kg/m}^3 .$$

$$c_p = -1.0785E-15x^6 + 4.6204E-12x^5 - 7.7267E-09x^4 + 6.0585E-06x^3 - 1.9792E-03x^2 + 2.4752E-01x + 9.9923E+02 = 1007.3 \text{ J/kg.K} .$$

$$\mu = -6.2139E-24x^6 + 3.2542E-20x^5 - 7.4607E-17x^4 + 1.0021E-13x^3 - 9.0942E-11x^2 + 8.2612E-08x - 1.9453E-07 = 0.0000195 \text{ Pas} .$$

$$\lambda = -6.9503E-21x^6 + 3.7178E-17x^5 - 8.6977E-14x^4 + 1.1902E-10x^3 - 1.0939E-07x^2 + 1.1461E-04x - 1.1397E-03 = 0.02666 \text{ W/m.K} .$$

$$Pr = 0.7396.$$

**Appendix C: OpenFoam files**

OpenFoam files, which is presented the initial boundary condition in (0) directory for cold gas.

```
/*-----*- C++ -*-----*\
\\ / field | OpenFOAM: The Open Source CFD Toolbox
\\ / Operation | Version: dev
\\ / And | Web: www.OpenFOAM.org
\\ / Manipulation
OpenFOAM for Windows 18.06 (v1)
|* Built by CFD Support, www.cfdsupport.com (based on Symscape)
\*-----*/
FoamFile
{
    version 2.0;
    format ascii;
    class volScalarField;
    location "0/cold Gas";
    object T;
}
// *****
dimensions [0 0 0 1 0 0 0];
internalField uniform 283.15;
boundaryField
{
    x0
    {
        type inletOutlet;
        value uniform 293.15;
        inletValue uniform 293.15;
    }
    x1
    {
```

---

```

    type      fixed Value;
    value      uniform 283.15;
}
Cold Gas_to_solid Wall
{
    type      compressible: turbulent Temperature Coupled BaffleMixed;
    value      uniform 283.15;
    Tnbr      T;
    kappaMethod  fluidThermo;
}
}

// ***** //
/*-----*- C++ -*-----*\
|=====|
| \ \ / F i e l d | OpenFOAM: The Open Source CFD Toolbox |
| \ \ / O p e r a t i o n | Version: dev |
| \ \ / A n d | Web: www.OpenFOAM.org |
| \ \ M a n i p u l a t i o n |
|*-----*|
|* OpenFOAM for Windows 18.06 (v1) *|
|* Built by CFD Support, www.cfdsupport.com (based on Symscape). *|
\*-----*/

FoamFile
{
    version 2.0;
    format ascii;
    class volScalarField;
    location "0/coldGas";
    object p;
}

// ***** //

dimensions [1 -1 -2 0 0 0];

```

---

---

```

internalField uniform 100000;
boundaryField
{
    x0
    {
        type    calculated;
        value    uniform 100000;
    }
    x1
    {
        type    calculated;
        value    uniform 100000;
    }
    coldGas_to_solidWall
    {
        type    calculated;
        value    uniform 100000;
    }
}

// ***** //
-The thermophysical properties in Constant directory for cold is the same for hot fluid.
/*-----*- C++ -*-----*\
|=====|
|\\  / F ield   | OpenFOAM: The Open Source CFD Toolbox   |
| \\  / O peration | Version: dev                        |
| \\  / A nd      | Web:   www.OpenFOAM.org                |
|  \\  M anipulation |                                     |
\*-----*/

FoamFile
{
    version 2.0;
    format  ascii;

```

---

```

class    dictionary;
    object    thermophysicalProperties;
}
// ***** //
thermoType
{
    type        heRhoThermo; // includes heat transfer
    mixture      pureMixture;
    transport     polynomial; // const, polynomial
    thermo        hPolynomial; // hConst, hPolynomial
    equationOfState icoPolynomial; // perfectGas, icoPolynomial
    specie        specie;
    energy        sensibleEnthalpy; // form of energy
}
mixture
{
    specie
    {
        molWeight    28.965000;
    }
    equationOfState // rho(T)
    {
        // c_rho(1) + c_rho(2)T + c_rho(3)T^2 + ...
        rhoCoeffs<8> ( 1.200000e+00 0.000000e+00 0.000000e+00 0.000000e+00 0.000000e+00
            0.000000e+00 0.000000e+00 0.000000e+00);
    }
    thermodynamics
    {
        Hf        0; // Heat of formation
        Sf        0; // Standard entropy
        CpCoeffs<8> ( 1.005000e+03 0.000000e+00 0.000000e+00 0.000000e+00 0.000000e+00
            0.000000e+00 0.000000e+00 0.000000e+00);
    }
}

```

---

---

```

}
transport
{
    muCoeffs<8> ( 1.800000e-05 0.000000e+00 0.000000e+00 0.000000e+00 0.000000e+00
                  0.000000e+00 0.000000e+00 0.000000e+00);
    kappaCoeffs<8> ( 2.600000e-02 0.000000e+00 0.000000e+00 0.000000e+00 0.000000e+00
                     0.000000e+00 0.000000e+00 0.000000e+00);
}
// ***** //
-The ControlDict file in (system) directory to arrange the time.
/*-----*- C++ -*-----*\
|=====|
| \ \ / F i e l d | OpenFOAM: The Open Source CFD Toolbox |
| \ \ / O p e r a t i o n | Version: dev |
| \ \ / A n d | Web: www.OpenFOAM.org |
| \ \ M a n i p u l a t i o n |
\*-----*/
FoamFile
{
    version 2.0;
    format ascii;
    class dictionary;
    location "system";
    object controlDict;
}
// ***** //
application chtMultiRegionFoam;
startFrom latestTime; // startTime, firstTime, latestTime
startTime 0;
stopAt endTime; // endTime, writeNow, noWriteNow, nextWrite
endTime 20;
deltaT 0.001;

```

---

```
writeControl  timeStep; // timeStep, runTime, adjustableRunTime, cpuTime, clockTime
writeInterval 1000;
purgeWrite    0; // 0: deactivate the limit; n: keep the last n results
writeFormat   ascii; // ascii, binary
writePrecision 12; // 7
writeCompression uncompressed; // off, on // uncompressed, compressed
timeFormat    general;
timePrecision 10;
runTimeModifiable false; // true, false
adjustTimeStep no; // yes, no
maxCo         0.5; // Co < 1. For the phase fields, maxAlphaCo
maxDeltaT     1;
// ***** //
```